

# Aerodynamic Design of a Hyperloop Pod by Computational Fluid Dynamics Analysis

**Bachelor Thesis**

**Author(s):**

Nick, Nathalie

**Publication date:**

2019-05

**Permanent link:**

<https://doi.org/10.3929/ethz-b-000637809>

**Rights / license:**

[In Copyright - Non-Commercial Use Permitted](#)



Eidgenössische Technische Hochschule Zürich  
Swiss Federal Institute of Technology Zurich

PAUL SCHERRER INSTITUT



Nathalie Nick

# Aerodynamic Design of a Hyperloop Pod by Computational Fluid Dynamics Analysis

## Bachelor Thesis

Institute of Fluid Dynamics  
Swiss Federal Institute of Technology (ETH) Zurich

Laboratory for Scientific Computing and Modelling  
Paul Scherrer Institute (PSI)

## Supervision

Prof. Dr. Horst-Michael Prasser, ETH Zurich  
Dr. Bojan Niceno, Paul Scherrer Institute (PSI)  
Dr. Yohei Sato, Paul Scherrer Institute (PSI)

May 2019



# Preface

Mechanical engineering students at ETH Zurich can participate in an engineering project at the end of their bachelor or in their master studies. It provides the opportunity to apply their theoretical knowledge and gain hands-on experience and practical insight in an engineering process.

One of this projects is participating in the Hyperloop Pod Competition, which is organized and held by SpaceX in Los Angeles, California, USA. The engineering competition for student teams from all over the world was initiated by entrepreneur Elon Musk to accelerate the development of the Hyperloop. For a period of one year, each student engineering team designs, develops and manufactures a complete Hyperloop vehicle. After the testing phase, the teams travel to the headquarter of SpaceX to participate in the competition.

The Hyperloop team of ETH Zurich, Swissloop, was founded in 2016 and participates in the Hyperloop Pod Competition for the third time in July 2019. The various technical sections (structure, suspension, stability, brakes, wheels, aerodynamics, electronics, propulsion etc.) are covered within the team.

I am a part of this project in the year 2018/2019 and responsible for the aerodynamics. This package includes the complete design process, analysis and improvement of the Hyperloop vehicle's shell, proper interfaces to the chassis followed by the shell's manufacturing and testing.

The following thesis is written under this project. It covers the design approach, planning and creation of computational fluid dynamic simulations, its iterations, analysis and improvement of the shell geometry.





# Acknowledgements

Throughout my thesis, I gained new knowledge and fundamental insight in Computational Fluid Dynamics simulations and I would like to acknowledge the people who made this possible.

My acknowledgement goes to Prof. Dr. Horst-Michael Prasser, Professor for Nuclear Energy Systems at ETH Zurich and head of the Thermal Hydraulics Laboratory at Paul Scherrer Institute (PSI). He gave me the opportunity to perform my work in the Laboratory for Scientific Computing and Modelling (LSM) at Paul Scherrer Institute in Villigen, Switzerland.

I would like to acknowledge Dr. Bojan Niceno, Group Leader of the Computational Fluid Dynamics Group in the Laboratory for Scientific Computing and Modelling at PSI for enabling me to perform my work in his research group and supervising my thesis. His help and valuable support were greatly appreciated at all time of the project.

My further acknowledgement goes to Dr. Yohei Sato for his supervision of the thesis and professional support. His willingness to give his time has been very much appreciated. He provided me with very valuable and constructive inputs and advice in computational fluid dynamics and without his dedicated involvement, this work could not have been accomplished.

I would also like to extend my thanks to the LSM group members and employees for their help and support and for offering me the resources for performing this work.



# Contents

<b>Abstract</b>	<b>vii</b>
<b>List of Tables</b>	<b>viii</b>
<b>List of Figures</b>	<b>x</b>
<b>Nomenclature</b>	<b>xi</b>
<b>1 Introduction</b>	<b>1</b>
1.1 Hyperloop . . . . .	1
1.2 Hyperloop Pod Competition . . . . .	2
1.2.1 Preliminary Phase . . . . .	2
1.2.2 Competition Week . . . . .	2
1.3 Swissloop . . . . .	3
1.3.1 Active Team 2019 . . . . .	3
1.4 Objectives of Aerodynamics . . . . .	4
<b>2 Theoretical Background</b>	<b>5</b>
2.1 Fluid Dynamics Basics . . . . .	5
2.2 Aerodynamics . . . . .	10
2.3 Computational Fluid Dynamics (CFD) . . . . .	13
2.3.1 Basic Equations . . . . .	13
2.3.2 Discretization . . . . .	14
2.3.3 Turbulence Modeling . . . . .	14
2.3.4 Boundary Conditions . . . . .	14
<b>3 Goals</b>	<b>17</b>
<b>4 Concept</b>	<b>19</b>
4.1 Target Setting . . . . .	19
4.2 Implementation . . . . .	19
4.2.1 First Sketches . . . . .	19
4.2.2 Concept Decision . . . . .	22
<b>5 Simulation</b>	<b>23</b>
5.1 Introduction . . . . .	23
5.1.1 The CFD program STAR-CCM+ . . . . .	23
5.1.2 Calculation on Euler Cluster . . . . .	23
5.1.3 Development Procedure . . . . .	23
5.1.4 Sequence of a CFD-Simulation . . . . .	24
5.2 Preparation . . . . .	25
5.3 Environment in STAR-CCM+ . . . . .	26
5.4 Grid Generation . . . . .	28

5.4.1	Chosen Grid structure . . . . .	29
5.5	Physics Conditions . . . . .	36
5.5.1	Reference Values . . . . .	36
5.5.2	Boundary Conditions . . . . .	36
<b>6</b>	<b>Results</b>	<b>37</b>
6.1	First Results . . . . .	37
6.2	Design Iteration . . . . .	37
6.3	Comparison of two Versions . . . . .	38
6.3.1	Dimensions . . . . .	39
6.3.2	Geometries . . . . .	40
6.3.3	Forces . . . . .	44
6.3.4	Visualization of Flow Field . . . . .	48
6.3.5	Conclusion . . . . .	64
6.3.6	General Analysis of the Final Version . . . . .	65
6.4	Final Version . . . . .	67
6.4.1	Results in Open-Air (Atmospheric Pressure) . . . . .	68
6.4.2	Results at 0.01 bar . . . . .	70
6.4.3	Results at 0.001 bar (Hyperloop concept Condition) . . . . .	72
6.4.4	Influence of System Pressure on the total Drag Coefficient $C_{tot}$ for Version B . . . . .	74
<b>7</b>	<b>Conclusions</b>	<b>75</b>
7.1	Conclusions . . . . .	75
7.2	Outlook . . . . .	75
<b>A</b>	<b>Pod Competition Rules</b>	<b>77</b>

# Abstract

The rise in mobility and demand for fast movement brings the traditional modes of transport to their limits. A broader development of transport systems is crucial.

The Hyperloop pushes the boundaries and enables an efficient and safe way of transport. With the principle of a pneumatic tube, transport capsules, so-called pods, travel at high speeds through a low-pressure tube to minimize aerodynamic drag. To guarantee a solid development, aerodynamic phenomena need to be investigated and addressed.

In the present bachelor thesis, the aerodynamic design system for a pod participating in a Hyperloop Pod Competition is developed. The design-by-simulation system consists of three-dimensional (3D) computer-aided design (CAD) and the Computational Fluid Dynamics (CFD) simulations. The CFD simulation part is the main topic in this thesis.

Various three-dimensional CFD simulations at partial-vacuum condition were performed, analyzed and compared whereby the aerodynamic drag on the vehicle's surface could noticeably be reduced. Based on the design-by-simulation system, the pod's shell geometry was improved, drag reduction of 19 percent was achieved. Further, the optimized shape was simulated and analyzed for conditions with different system pressure.

The results build a firm foundation for further aerodynamic elaboration and investigation for the Hyperloop concept. On this basis, it is recommended to perform physical tests and measurements of the pod to validate the obtained CFD results.

# List of Tables

5.1	Prism Layer Layup Comparison . . . . .	29
6.1	Dimensions Version A . . . . .	39
6.2	Dimensions Version B . . . . .	39
6.3	Absolute differences from dimensions Version A and Version B . . . . .	39
6.4	Computed Results of Version A at 0.15 bar . . . . .	44
6.5	Grid Parameters, Prism Layers, and Flow Parameters of Version A at 0.15 bar . . . . .	45
6.6	Computed Results at 0.15 bar . . . . .	46
6.7	Grid parameters, Prism Layers, and Flow parameters of Version B at 0.15 bar . . . . .	47
6.8	Computed Forces and C-values at 1 bar . . . . .	68
6.9	Grid parameters, Prism Layers, and Flow parameters at 1 bar . . . . .	69
6.10	Computed Results at 0.01 bar . . . . .	70
6.11	Grid parameters, Prism Layers, and Flow parameters at 0.01 bar . . . . .	71
6.12	Computed Results at 0.001 bar . . . . .	72
6.13	Grid parameters, Prism Layers, and Flow parameters at 0.001 bar . . . . .	73

# List of Figures

2.1	Streamlines for attached (A) and separated (B) flow [5]	5
2.2	Reynolds number dependence of different flow states [4]	6
2.3	Streamlines for laminar and turbulent flow [5]	7
2.4	Typical $C_D$ and $C_L$ values [5]	11
2.5	Flow around an Airfoil with lift force $A$ . $\Gamma$ : circulation of the wing [1]	11
2.6	Governing equations for compressible flow	13
4.1	First Sketches	19
4.2	First Sketches	20
4.3	First Sketches	20
4.4	First Sketches	20
4.5	First Sketches	21
4.6	CAD Model Version 1	22
5.1	Imported geometry in STAR-CCM+	26
5.2	Overview	26
5.3	Three-dimensional Overview (mirrored at the symmetry plane)	27
5.4	Structured Grid [10]	28
5.5	Unstructured Grid [10]	28
5.6	Mesh of pod surface	30
5.7	Mesh of pod surface	30
5.8	Mesh of pod surface	31
5.9	Mesh of pod surface and tube	31
5.10	Mesh of pod surface and tube	32
5.11	Mesh of tube	32
5.12	Mesh of tube	32
5.13	Mesh of pod	33
5.14	Mesh of pod	34
5.15	Mesh of pod	34
5.16	Mesh of pod. Which stretching Factor 1.8	35
6.1	Different Versions	37
6.2	Sheer Plan Version A	40
6.3	Half-breadth Plan Version A	40
6.4	Body Plan Version A	40
6.5	Side View Version A	41
6.6	Top View Version A	41
6.7	Front View (right half) and Rear View (left half) of Version A	41
6.8	Sheer Plan Version B	42
6.9	Half-breadth Plan Version B	42
6.10	Body Plan Version B	42
6.11	Side View Version B	43
6.12	Top View Version B	43



6.13	Front View (right half) and Rear View (left half) of Version B . . . . .	43
6.14	Force Monitor Plot of Version A at 0.15 bar . . . . .	45
6.15	Force Monitor Plot of Version B at 0.15 bar . . . . .	47
6.16	Relative Pressure Side View Version A . . . . .	48
6.17	Relative Pressure Top View Version A . . . . .	48
6.18	Relative Pressure Front View (right) and Rear View (left) of Version A . . . . .	48
6.19	Relative Pressure 3D View Version A . . . . .	49
6.20	Relative Pressure 3D View Version A . . . . .	49
6.21	Relative Pressure 3D View Version A . . . . .	50
6.22	Relative Pressure 3D View Version A . . . . .	50
6.23	Relative Pressure Side View Version B . . . . .	51
6.24	Relative Pressure Top View Version B . . . . .	51
6.25	Relative Pressure Front View (right) and Rear View (left) of Version B . . . . .	51
6.26	Relative Pressure 3D View Version B . . . . .	52
6.27	Relative Pressure 3D View Version B . . . . .	52
6.28	Relative Pressure 3D View Version B . . . . .	53
6.29	Relative Pressure 3D View Version B . . . . .	53
6.30	Skin Friction Coefficient Side View Version A . . . . .	54
6.31	Skin Friction Coefficient Top View Version A . . . . .	54
6.32	Skin Friction Coefficient 3D View Version A . . . . .	54
6.33	Skin Friction Coefficient 3D View Version A . . . . .	55
6.34	Skin Friction Coefficient 3D View Version A - zoomed in . . . . .	55
6.35	Skin Friction Coefficient Side View Version B . . . . .	56
6.36	Skin Friction Coefficient Top View Version B . . . . .	56
6.37	Skin Friction Coefficient 3D View Version B . . . . .	56
6.38	Skin Friction Coefficient 3D View Version B . . . . .	57
6.39	Skin Friction Coefficient 3D View Version B - zoomed in . . . . .	57
6.40	Streamlines Version A . . . . .	58
6.41	Streamlines Version A . . . . .	58
6.42	Streamlines Version A . . . . .	59
6.43	Streamlines Version A . . . . .	59
6.44	Streamlines Version B . . . . .	60
6.45	Streamlines Version B . . . . .	60
6.46	Streamlines Version B . . . . .	60
6.47	Streamlines Version B . . . . .	61
6.48	Velocity Field Version A . . . . .	62
6.49	Velocity Field Version A . . . . .	62
6.50	Velocity Field Version B . . . . .	63
6.51	Velocity Field Version B . . . . .	63
6.52	Final Version . . . . .	65
6.53	Final Version . . . . .	65
6.54	Final Version . . . . .	65
6.55	Final Version . . . . .	66
6.56	Final Version . . . . .	66
6.57	Force Monitor Plot of Version B at 1 bar . . . . .	69
6.58	Force Monitor Plot of Version B at 0.01 bar . . . . .	71
6.59	Force Monitor Plot of Version B at 0.001 bar . . . . .	73
6.60	Influence of System Pressure on the total Drag Coefficient $C_{tot}$ for final Version . . . . .	74

# Nomenclature

CFD	Computational Fluid Dynamics
CAD	Computer Aided Design
$C_L$	Lift Coefficient
$C_D$	Drag Coefficient
DNS	Direct Numerical Simulation
LES	Large-Eddy Simulation
RANS	Reynolds Averaged Navier-Stokes
NS	Navier-Stokes
$F_{\text{total}}$ [N]	Total Force
$F_{\text{friction}}$ [N]	Friction Force
$F_{\text{pressure}}$ [N]	Pressure Force
Re	Reynolds Number
Ma	Mach Number
$\beta$	Blockage Ratio



# 1. Introduction

## 1.1 Hyperloop

In the Hyperloop concept, capsules, so-called pods, travel on a rail through a low pressure tube at low and high speeds. Thanks to the partial vacuum in the tube, aerodynamic drag is drastically reduced.

The Hyperloop is called the fifth mode of transport. Compared to ships, trains, cars and airplanes, there are huge advantages that a realization of the Hyperloop principle would provide. Transportation with a Hyperloop would be safer, cheaper, environmentally sound, more efficient and not depending on weather.

The idea of traveling at high speeds in air-evacuated tunnels goes back to the 19th century. Many years later, in the 1970s, there was a concept elaborated in Switzerland called Swissmetro. The idea is very similar to the common Hyperloop idea of today. Unfortunately, due to the immense costs, the Swissmetro project was never realized and no low pressure tube was built.

The Hyperloop concept has three main technological advances. The first is the vacuum tunnel, which minimizes the aerodynamic drag on transport pods. Second, magnetic hovering is used to reduce the rolling drag of the pod through contactless gliding. Furthermore, an ideal propulsion system must be realised and is crucial.

In 2013, the idea was reintroduced by entrepreneur Elon Musk. In his white paper Hyperloop Alpha he proposed the various benefits and technical concepts. His aim is to optimize long-distance travel by combining the efficacy of modern-day railway systems with the speed of air travel by transporting passengers and cargo in pods in near-vacuum tubes at speeds up to 1200 *km/h*. For the final concept, the capsules are supported on air cushions, with pressurized air and aerodynamic lift. They would be accelerated via a magnetic linear accelerator fixed to various stations. Passenger would enter and exit at Hyperloop stations located at the ends of the tubes. [8]

As elaborating a complete new mode of transport is extremely time consuming, Elon Musk left the development of the Hyperloop as an open source form. Four years after the paper Hyperloop Alpha was published, the first Hyperloop Pod Competition was held by SpaceX.

## 1.2 Hyperloop Pod Competition

The Hyperloop Pod Competition is an engineering contest involving students from universities all over the world. It is organized and held by the space company SpaceX and initiated by entrepreneur Elon Musk to accelerate the development of the Hyperloop concept. The competition, which takes place in Hawthorne, Los Angeles, California, USA, was first held in 2017. In July 2019, the fourth Hyperloop Pod Competition takes place.

For a period of one year, each participating university engineering team develops, builds and tests its own Hyperloop pod. At the beginning of each year, several hundred university teams enroll in the competition. The competition year includes different assessments where reports need to be submitted to SpaceX. Based on these reports, it is decided whether the team advances to the next stage.

### 1.2.1 Preliminary Phase

The project starts in September. The first report is the so-called Preliminary Design Briefing and needs to be submitted in November. First engineering concepts, ideas and solutions for the pod are thereby presented to SpaceX. Only 50 teams out of the several hundred who applied get on and stay in the competition.

The second report is called Final Design Package and is submitted in January. In a documentation of around 100 pages, the team presents its detailed mechanical and electrical development as well as the feasibility to build the pod. Thereafter, 20 teams advance to the next stage and are invited to the Pod Competition in Hawthorne, Los Angeles, USA.

In April, a safety-briefing is submitted to SpaceX. It contains a summary of general pod information, pod operations, pod transport, hazardous operations, software and navigation systems, to only name a few.

### 1.2.2 Competition Week

In July, the competition takes place at the headquarter of SpaceX in Hawthorne, Los Angeles and lasts for one week. During competition week, every team's pod is tested on-site and has to pass the analyses and inspections. The tests include a pressure system investigation, a mechanical fit check, a structural inspection, a battery inspection, a functional test, a vacuum test, a navigation test, a state diagram transition test, an external subtrack test and an open-air Hyperloop test. For further information on the detailed pod testing please refer to "Pod Testing" in the appendix A. The competition is rounded up by the final on Sunday of Competition week with the Hyperloop run in the closed, low-pressure tube. Only the top three pods from Competition week may participate in this final run. The team with the fastest pod wins the Hyperloop Pod Competition.

## 1.3 Swissloop

The Hyperloop team of ETH Zurich, Swissloop, was founded as an association in 2016 by a student of ETHZ and the team competed in the Hyperloop Pod Competition in July 2017 and in July 2018. In 2017, they placed third and in 2018 among the top ten. Each year, the team develops and builds a Hyperloop pod.

The association is composed of the board, the active team and alumni. Every year, the active team consists of roughly 20 students and after completing the competition year, they stay in the association as alumni and advisors for future active team members.

Most team members are from ETH Zurich with a background in mechanical engineering, electrical engineering or computer science. A few team members are from other Swiss universities from fields of business, law and design.

### 1.3.1 Active Team 2019

The active team of 2018/2019 consists of seven mechanical engineering students (Mechanical Team) and seven electrical engineering students (Electrical Team), as well as six students responsible for business, design and law affairs.

#### Work Distribution in the Swissloop Team

The different mechanical sections are distributed within the mechanical team. These include: structure, suspension, stability, brakes, battery box and aerodynamics. Each mechanical engineering student team member takes care of his or her own subsystem and is responsible for its complete design, manufacturing and testing as well as assuring that the interfaces between different subsystems fit perfectly to one another.

The electrical sections are distributed within the electrical team. They include: software, battery management system, circuit boards and propulsion. For the pod's propulsion, a linear induction motor (LIM) is used.

The aerodynamics part includes the shell design, planning and creation of computational fluid dynamics simulations, its iterations, analyses and improvement of the geometry. Thereafter, the shell is manufactured as a sandwich structure composite out of carbon fiber honeycomb. The manufacturing process is done by the team members.

#### Swissloop Hyperloop Pod 2019

The Hyperloop Pod of 2017 had a cold-gas propulsion system based on compressed air that exits the pod at low temperatures and expands at the nozzles and therefore providing a rocket-like acceleration. The pod was travelling on wheels

In 2018, the pod was equipped and powered by four electric motors. The pod was travelling on four wheels, each wheel was powered by one electric motor.

In 2019, a new and in technical terms very promising propulsion system is introduced. The pod is propelled by a double sided Linear Induction Motor (LIM). This is the first year in the Hyperloop Pod Competition that a Linear Induction Motor is used. Only two teams out of the 20 finalists compete with a LIM.

A Linear Induction Motor is designed to directly produce motion in a straight line. It works very similar to a typical induction motor, although it is arranged in a straight line and not, like the typical induction motor, in an endless loop. The finite length of the LIM generates end-effects. The pod is propelled by the force that is created by the LIM in the direction of motion. The pod's wheels are not propelled. The pod travels on small travelling wheels and it is guided on the I-beam by stability wheels. The LIM is not used for levitation.

The use of Linear Induction Motors is the basic idea for the Hyperloop concept. It provides several benefits compared to a permanent magnet motor.[8]

As the LIM can provide levitation, there would be no need for wheels for acceleration. By not relying on ground contact by wheels and therefore friction, the reachable speed is much higher than with using wheels to propel the pod.

## 1.4 Objectives of Aerodynamics

Aerodynamics plays a fundamental role in motor sports as well as in aviation to improve the performance. In motor sports, it is used to reduce the aerodynamic drag and, eventually, achieve higher speeds with the use of same or less fuel. The use of aerodynamics developed and improved over many years. Nowadays, it is one of the most fundamental concepts in the development of Formula racing cars.

The development of the Hyperloop is still in its initial phase. However, compared to the motor sport industry, in the case of the Hyperloop a profound aerodynamic investigation needs to be done at the very first stages and cannot be postponed to a later point. There are fundamental aerodynamic concepts that need to be addressed and investigated.

One fundamental aspect is the travel at high speeds in a closed tube. So-called choking occurs which means, depending on the ratio of tube cross section and pod cross section, a shock wave will be generated in front of the Hyperloop pod.

Another important aspect is the reduction of aerodynamic drag. Although the final Hyperloop idea is to travel at a pressure of 0.001 bar and drag would be almost negligible, it must be taken into account that first Hyperloop test infrastructures cannot permanently be operated at a pressure that low. At the Hyperloop Pod Competition, SpaceX offers the student teams to choose their desired operation pressure. Teams are free to choose in a range from 0.009 bar and 1.01 bar. The Swissloop team plans a performance at 0.15 bar. Therefore, a pod design with minimal aerodynamic drag is crucial.

The third important aspect is the generation of lift or down force. Especially lift force can be used to reduce the importance of suspension. By adjusting the vehicle's body, aerodynamic forces can be generated. This concept is very common in motor sports for the generation of down force.

# 2. Theoretical Background

## 2.1 Fluid Dynamics Basics

At the beginning of the theoretical background and explanations, an overview of fluid dynamics foundations will be given. Aerodynamics is a subfield of this area. General concepts and basic equations are considered as well as fundamental terms are explained.

### Streamline

Of importance in fluid dynamics is the so-called streamline. This curve is tangent to the instantaneous velocity field at each point. Streamlines can be understood as a "snapshot" of the stream.

[9]

When a fluid, such as air, encounters the surface of a solid, the air moves around it. The streamlines wrap around the outer shape of that body. If the streamlines and the flow itself follow exactly the outer shape of the surface, the flow is called attached. If the flow is unable to follow the surface, it is called separated. How well the flow is attached to a surface is very important for the field of aerodynamics. In figure 2.1 the difference between attached and separated flow is outlined. [9]

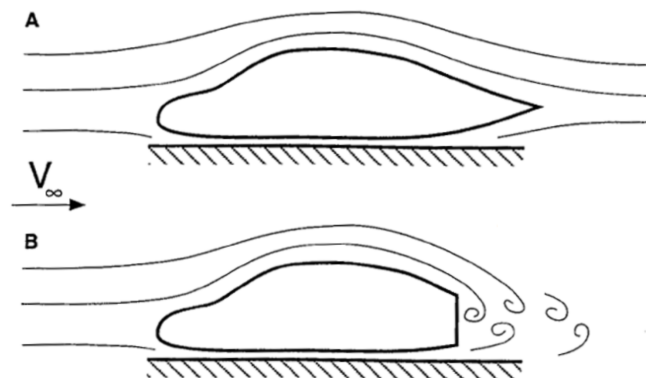


Figure 2.1: Streamlines for attached (A) and separated (B) flow [5]



### Reynolds Number

An important term in fluid dynamics is the Reynolds Number. The Reynolds Number  $Re$  is a dimensionless identifier. A large Reynolds number correlates with a very turbulent flow. Since the Reynolds number is dimensionless, it can be used to compare different flow situations. It is defined as

$$Re = \frac{\rho u L}{\mu} = \frac{u L}{\nu} \quad (2.1)$$

where  $\rho$  is the density of the fluid,  $u$  is the velocity of the fluid with respect to the object,  $L$  is a characteristic linear dimension,  $\mu$  is the dynamic viscosity of the fluid,  $\nu$  is the kinematic viscosity of the fluid.

### Speed of sound

The speed of sound is defined as

$$a = \sqrt{\gamma R T} \quad (2.2)$$

where  $\gamma$  is the heat capacity ratio,  $R$  is the ideal gas constant and  $T$  is the temperature of the fluid.

### Mach Number

The Mach number a dimensionless number indicating the ratio of flow velocity to the local speed of sound. It is defined as

$$Ma = \frac{u}{a} \quad (2.3)$$

Where  $u$  is the velocity of the fluid with respect to the object and  $a$  is the speed of sound.

### Laminar, Transitional and Turbulent Flows

All flows become unstable above a certain Reynolds number. At a low Reynolds Number, the flow is laminar, at an intermediate Reynolds number it is a transitional flow and at high Reynolds numbers the flow is turbulent. This is shown in the following Figure 2.2.

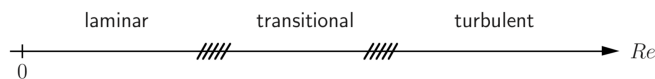


Figure 2.2: Reynolds number dependence of different flow states [4]

At values below the critical Reynolds number the flow is smooth. If the applied boundary conditions are constant in time the flow is steady. This is called laminar flow. If the value of the Reynolds number is higher, the flow character changes radically. In this state, a chaotic, random and unsteady state of motion develops. This flow is called turbulent flow. Velocity and pressure change continuously with time. [2]

Laminar flow is often found in free, statically formed flow conditions, while turbulent flow can occur, for example, in detachment areas behind a blunt body [4]. An illustration of laminar and turbulent flow can be seen in Figure 2.3.

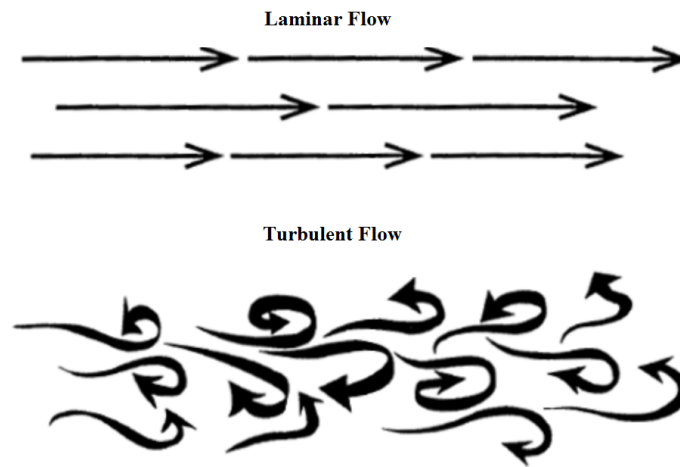


Figure 2.3: Streamlines for laminar and turbulent flow [5]

### Kinematic and Dynamic Viscosity

The kinematic viscosity  $\nu$  is a measure of the resistance of the fluid to disturbing movements. To study the aerodynamics of a vehicle, two interactions between vehicle and fluid on the surface are important: the friction and pressure exerted by the fluid on the vehicle surface.

This resistance induces a force tangent to the surface of the body in which the fluid is trying to move. This tangential force is the frictional force and is directly proportional to the flow velocity and the viscosity of the fluid.

Kinematic viscosity  $\nu$  is defined as the ratio of the dynamic viscosity  $\mu$  to the density of the fluid  $\rho$ . This holds

$$\nu = \frac{\mu}{\rho} \quad (2.4)$$

### Pressure Force

The pressure in the fluid results in a force perpendicular to the surface of the body. This is the pressure force. If a body separates two areas with different pressures, different pressure forces are created on the upper or lower side of the body. The result is a relative force on the side with the lower ambient pressure acting on the body.

### Friction Force

The friction force which the fluid exerts on the vehicle as it moves through the fluid at a relative speed results from the kinematic viscosity. The friction force is tangential to the surface of the vehicle and directly proportional to the flow velocity and the viscosity of the fluid.

### Total Force

The total force is the sum of pressure and friction force.

### Bernoulli's Equation

Along a continuous streamline pressure and velocity can be related with the Bernoulli equation. For incompressible flow, Bernoulli's equation holds

$$\frac{u^2}{2} + \frac{p}{\rho} = \text{const.} \quad (2.5)$$

The influence of the velocity on the resulting pressure is quadratic and a higher velocity results in a smaller pressure.

If the Mach number is higher than 0.3 the flow is compressible. For compressible flow, Bernoulli's equation holds

$$\frac{u^2}{2} + \left( \frac{\gamma}{\gamma - 1} \right) \frac{p}{\rho} = \text{const.} \quad (2.6)$$

The heat capacity ratio or also called Poisson constant  $\gamma$  is the ratio of the heat capacity at constant pressure ( $C_P$ ) to heat capacity at constant volume ( $C_V$ ). This equation holds

$$\gamma = \frac{C_P}{C_V} \quad (2.7)$$

For air, the value of  $\gamma$  is 1.4. Therefore, the Bernoulli equation for compressible flow with air holds

$$\frac{u^2}{2} + 3.5 \cdot \frac{p}{\rho} = \text{const.} \quad (2.8)$$

Compared to Bernoulli's equation for incompressible flow, for compressible flow the contribution of the fraction  $\frac{p}{\rho}$  becomes bigger. However, the relation of velocity and pressure stays the same. The influence of the velocity on the resulting pressure is quadratic and a higher velocity results in a smaller pressure.

Comparing incompressible to compressible flow, flow velocity, pressure and density vary. For compressible flow, the flow velocity is higher than for incompressible flow. Therefore, in the case of compressible flow, density decreases. Consequently, density of incompressible flow is higher than density of compressible flow.

### Conservation of Mass

This section addresses the principle of general conservation of mass. This applies in any case to the aerodynamic considerations of this work and is expressed by the continuity equation which states

$$\frac{\partial \rho}{\partial t} + \nabla(\rho \vec{u}) = 0 \quad (2.9)$$

In general, this equation shows that in steady state, all mass entering one system has to escape at another location. More practically, this law is formulated as follows:

$$\rho A_i u_i = \text{const.} \quad (2.10)$$

Hence, a reduction of the local flow cross-section  $A_i$  results in a higher local velocity  $u_i$ , assuming a constant density.

From these equations we can see why forces arise when flow streams around a body. Because the fluid is displaced by the body, the cross section of the flow changes. According to equation 2.10 this results in a higher (or lower) flow velocity. Therefore, a higher (or lower) speed results in a lower (or higher) pressure according to Bernoulli's equation.

Therefore, in front of a vehicle where the fluid is displaced, there is a lower pressure zone. The pressure decreases until the biggest cross section area is reached and the velocity increases until this point. When the surface retracts, the fluid is provided with a larger cross section area. Therefore, according to equation 2.10 the speed decreases and thus the pressure increases. Therefore, at the back of a vehicle the pressure recovers and increases.

## 2.2 Aerodynamics

The field of aerodynamics deals with reduction of a vehicle's resistance. As outlined before, there are two causes for resistance: First, frictional forces act on the surface of the vehicle, induced by the viscosity of the air. Second, the forces resulting from pressure differences always act perpendicular to the vehicle surface which contribute to the resistance. The main part of the resistance is due to pressure forces.

The aerodynamic influences that act on a vehicle can be summarized by three forces:

- Drag force
- Lift / Down force
- Side force

While aviation is interested in lift forces to keep a flying object in the air, motor sport works with down force. Aerodynamic developments focus mainly on drag and lift/down force, as the side force effects can be considered negligible. [5]

In order to be able to compare resistance and lift forces for different flow situations, dimensionless characteristic numbers are used. The most important key figures are the drag coefficient  $C_D$  and the lift coefficient  $C_L$ .

The drag coefficient  $C_D$  is defined as

$$C_D = \frac{F_D}{\frac{\rho}{2}u^2 A_{ref}} \quad (2.11)$$

Where  $F_D$  is the drag force which is the force component in the direction of the flow velocity,  $\rho$  is the density of the fluid,  $u$  is the flow speed of the object relative to the fluid and  $A_{ref}$  is the reference area.

The lift coefficient  $C_L$  is defined as

$$C_L = \frac{F_L}{\frac{\rho}{2}u^2 A_{ref}} \quad (2.12)$$

Where  $F_L$  is the lift force,  $\rho$  is the density of the fluid,  $u$  is the flow speed of the object relative to the fluid and  $A_{ref}$  is the reference area.

It can be seen that the forces change with the second power of the velocity. This corresponds to the relationship between pressure and velocity already discussed in Bernoulli's equation 2.6.

Some typical values of  $C_D$  and  $C_L$  are listed in Figure 2.4.

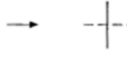

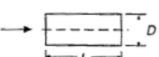




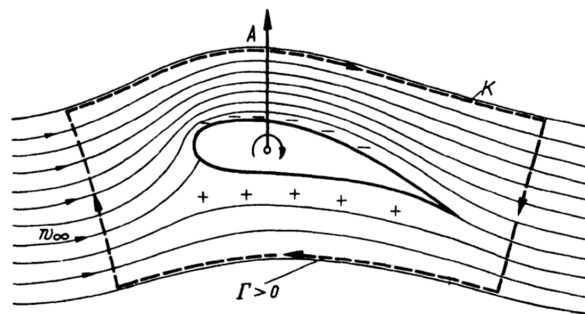
			$C_L$	$C_D$
1	Disk		0	1,17
2	Cylinder $L/D < 1$		0	1,15
3	Cylinder $L/D > 1$		0	0,82
4	Symmetric Airfoil		0	0,04
5	Vehicle with low air resistance near ground		0,18	0,15
6	Road Vehicle		0,32	0,43
7	Race Car		-3.00	0.75

Figure 2.4: Typical  $C_D$  and  $C_L$  values [5]

### Pressure distribution on a wing profile

As the theory of a wing profile is very fundamental in Aerodynamics and the sideways cross section of the pod's shell potentially looks like a wing profile, the background of force generation on wings is pointed out in this subsection.

Figure 2.5: Flow around an Airfoil with lift force  $A$ .  $\Gamma$ : circulation of the wing [1]

The basic principle of force generation on wings is based on a pressure difference between the top and bottom of the wing. By cleverly shaped wing profiles, e.g. by introducing a profile curvature, an acceleration of the flow above the wing and a deceleration below the wing can be achieved. By doing so, above the wing the speed increases which correlates with a pressure decrease according to Bernoulli's equation. Below the wing, it is the opposite that happens. The speed is lower than the flow velocity  $u$  why the pressure increases. Therefore, there is an overpressure on the underside and a negative pressure on the upper side of the wing. The resultant force is the buoyancy  $A$ , indicated in Figure 2.5. The buoyancy generation is very closely related to the circulation of the velocity field near the wing.

For the curve K, which encloses the profile according to Figure 2.5, it follows that the circulation is different from zero if lift is generated. One can think of the velocity field generated in the vicinity of the wing by a right-turning vortex, which is located inside the wing. The relationship between buoyancy  $A$ , the flow velocity  $u$  and the circulation  $\Gamma$  in the case of a plane flow is given by Kutta-Joukowski's formula which states

$$F = -\Gamma \rho u_{\infty} b \quad (2.13)$$

In addition to the curvature of the profile, a pressure difference can be caused with the angle of attack  $\alpha$ . In general, profiles with more angles of attack can achieve more pressure difference, because the flow is accelerated or decelerated by the more extreme geometric arrangement.

When stall occurs, the flow does not have the energy needed to follow the strongly bending profile, the current is no longer attached and the flow does not remain in contact with the wing surface. In that case, the desired pressure conditions no longer prevail on the wing surface and the force decreases significantly. Stalling should always be avoided. [1]

### Ground Effect

In case an airfoil approaches a ground, this produces the so-called ground effect. In aviation, this case is not very typical, however in motor sport, aerodynamic wings are often positioned close to the ground. As the Hyperloop pod's shell has more or less the shape of an airfoil and it travels very close to the ground, this effect is briefly addressed in this section.

The Ground effect describes a large increase in the forces on a wing as it continues to approach the ground. Again, this stronger acceleration and deceleration correlates with the Bernoulli equation 2.6 with stronger pressure gradients and therefore also with larger forces.

### Body Shape

In the case of Formula racing cars, down force is needed for a better general performance. To do so, inverted wings are used. For the Hyperloop pod, the general shape of the shell can be used as well to take advantages. By shaping the shell like an airfoil, a desired lift force can be induced. This can be used, for instance, to reduce the importance of the pod's levitation.

### Blockage Ratio

Aerodynamic phenomena are different when a vehicle travels in a closed tube than when it travels in the open air. Compression and expansion pressure waves are generated when the pod's velocity changes. This creates an aerodynamic load on the pod and tube.[7] . An important ratio in this context is the so-called blockage ratio. It is defined by the ratio of pod cross section area and tube cross section area.

$$\beta = \frac{\text{Pod cross section area}}{\text{Tube cross section area}} \quad (2.14)$$

Tunnels for high-speed Railways are designed for a blockage ratio of 0.1 to 0.17. For a partial vacuum tube like the Hyperloop however, larger blockage ratios can be considered. The blockage ratio in this case is between 0.4 and 0.5. [7]

## 2.3 Computational Fluid Dynamics (CFD)

Computational Fluid Dynamics (CFD) deals with methods for numerical solution of fluid mechanics problems and it is widely used in industry and research. These computer-aided methods are rapidly evolving due to computing capacity improvement. CFD is industrially interesting because it is faster and cheaper to work with fluid dynamics simulations than laboratory tests and physical models. Moreover, changes in models or boundary conditions are much easier to implement virtually than in experimental fluid dynamics. [6]

What makes CFD difficult is the uncertainty of the solution. Phenomena like turbulence for example are mathematically difficult to model. The chosen approach and quality of discretization affects the solution. [6]

### 2.3.1 Basic Equations

All numerical calculation models are based on three laws of conservation:

- Conservation of mass
- Conservation of momentum
- Conservation of energy

These conservation principles are summarized in the continuity equation for mass conservation, the Navier-Stokes equations for the three momentum components, and the energy equation (resulting from the 1st law of thermodynamics) for energy conservation.

As in the case for the Hyperloop, Mach 0.3 is exceeded and it is therefore dealt with compressible flow. Figure 2.6 shows the governing equations.

<b>Mass Conservation Equation</b>
$(m) \quad \frac{\partial \rho}{\partial t} + \frac{\partial(\rho u)}{\partial x} + \frac{\partial(\rho v)}{\partial y} + \frac{\partial(\rho w)}{\partial z} = 0$
<b>Momentum Equations</b>
$(M_x) \quad \frac{\partial(\rho u)}{\partial t} + \frac{\partial(\rho uu)}{\partial x} + \frac{\partial(\rho uv)}{\partial y} + \frac{\partial(\rho uw)}{\partial z} = \frac{\partial}{\partial x} \left[ (\mu + \mu_T) \frac{\partial u}{\partial x} \right] + \frac{\partial}{\partial y} \left[ (\mu + \mu_T) \frac{\partial u}{\partial y} \right] + \frac{\partial}{\partial z} \left[ (\mu + \mu_T) \frac{\partial u}{\partial z} \right] + \left( S_u = -\frac{\partial p}{\partial x} + S'_u \right)$
$(M_y) \quad \frac{\partial(\rho v)}{\partial t} + \frac{\partial(\rho uv)}{\partial x} + \frac{\partial(\rho vv)}{\partial y} + \frac{\partial(\rho vw)}{\partial z} = \frac{\partial}{\partial x} \left[ (\mu + \mu_T) \frac{\partial v}{\partial x} \right] + \frac{\partial}{\partial y} \left[ (\mu + \mu_T) \frac{\partial v}{\partial y} \right] + \frac{\partial}{\partial z} \left[ (\mu + \mu_T) \frac{\partial v}{\partial z} \right] + \left( S_v = -\frac{\partial p}{\partial y} + S'_v \right)$
$(M_z) \quad \frac{\partial(\rho w)}{\partial t} + \frac{\partial(\rho uw)}{\partial x} + \frac{\partial(\rho vw)}{\partial y} + \frac{\partial(\rho ww)}{\partial z} = \frac{\partial}{\partial x} \left[ (\mu + \mu_T) \frac{\partial w}{\partial x} \right] + \frac{\partial}{\partial y} \left[ (\mu + \mu_T) \frac{\partial w}{\partial y} \right] + \frac{\partial}{\partial z} \left[ (\mu + \mu_T) \frac{\partial w}{\partial z} \right] + \left( S_w = -\frac{\partial p}{\partial z} + S'_w \right)$
<b>Energy Equation</b>
$(E) \quad \frac{\partial(\rho h)}{\partial t} + \frac{\partial(\rho uh)}{\partial x} + \frac{\partial(\rho vh)}{\partial y} + \frac{\partial(\rho wh)}{\partial z} = \frac{\partial}{\partial x} \left[ \lambda \frac{\partial T}{\partial x} \right] + \frac{\partial}{\partial y} \left[ \lambda \frac{\partial T}{\partial y} \right] + \frac{\partial}{\partial z} \left[ \lambda \frac{\partial T}{\partial z} \right] + \frac{\partial}{\partial x} \left[ \mu_T \frac{\partial h}{\partial x} \right] + \frac{\partial}{\partial y} \left[ \mu_T \frac{\partial h}{\partial y} \right] + \frac{\partial}{\partial z} \left[ \mu_T \frac{\partial h}{\partial z} \right] + \frac{\partial p}{\partial t} + \Phi + S_T$

Figure 2.6: Governing equations for compressible flow



### 2.3.2 Discretization

In order to be able to numerically solve analytic equations of any kind, it is necessary to discretize the equations and the calculation domain. Various methods are available for this purpose. Some discretization methods that are commonly used are

- Finite difference method
- Finite volume method
- Spectral method
- Finite element method

Details of these procedures are not dealt with in detail within this framework.

### 2.3.3 Turbulence Modeling

Generally, there are three primary turbulence models used in CFD.

- DNS (Direct Numerical Simulation)
- LES (Large-Eddy Simulation)
- RANS (Reynolds Averaged Navier-Stokes)

DNS and LES require very high computational cost whereas RANS allows more simulations with the same computing time which results in a more efficient usage of development time. In this thesis, RANS is used as turbulence model.

#### Turbulence models for RANS

Many turbulence models are available for RANS, however only some are generally used in CFD. Some common models are:

- $k-\epsilon$  turbulence model
- $k-\omega$  turbulence model
- Spalart-Allmaras model
- Menter-SST- $k-\omega$  turbulence model

In this thesis, the Menter-SST- $k-\omega$  turbulence model is used.

### 2.3.4 Boundary Conditions

Like all mathematical problems involving differential equations, CFD problems are influenced by initial and boundary conditions. As the initial conditions are only important in transient problems, these are not discussed here.

The most important boundary conditions are discussed in this section. The application of correct boundary conditions is of crucial importance for the correctness of the solution of a CFD simulation, since all states calculated in the control volume are dependent on these. The most common cause of strongly faulty simulation results is the improper use of boundary conditions. [2]

#### Inlet

At the inlet, the distribution of all flow variables must be specified. For this purpose, the values which are stored in the outermost grid node level are transferred to the first physically real level. From the first physical level then the usual calculations are made. [2]

**Outlet**

If the outlet of the control volume is far downstream of all disturbances the flow eventually reaches a fully developed state where no change occurs in the flow direction. At this place we can put an outlet surface and define all variables (except pressure) to be zero in the flow direction. The outlet surface is placed perpendicular to the flow direction. If the outlet surface is defined too close to disturbances, the flow has not completely developed yet. Therefore, the outlet is often defined a few length scales behind the object. [2]

**Wall boundary condition**

In the scope of this thesis, no surface roughness is used. There is no slip-boundary condition on the pod.

**Pressure boundary condition**

If exact details of the flow distribution are unknown but the boundary values of pressure are known, the constant pressure condition is used. Typically it is used for free flow around objects like in aerodynamics. [2]

**Symmetry**

As objects often have a symmetrical outer geometry in the longitudinal direction, it is used to save computational resources. Therefore, only half the vehicle is modeled. In the symmetry division plane, the conditions are that no mass flow and no other scalar flows may pass over the separation plane. [2]



## 3. Goals

The goal of this Bachelor Thesis is (i) to develop a CFD simulation system for Hyperloop pods coupled with 3D CAD systems, and (ii) to design a pod shape with low drag force. This design-by-simulation system is created and used to analyze and improve the Hyperloop pod's geometry for the 2019 pod of ETHZ's Hyperloop team Swissloop. After performing the improvements the chosen final shape will be produced by the Swissloop team. This Hyperloop pod competes in the Hyperloop Pod Competition 2019 held by SpaceX in Los Angeles.

It will be outlined and explained, what meshing technique is used and which reference values, boundary conditions and physics conditions are set.

After the CFD environment has been set up, different pod versions will be simulated and analyzed. Before every new simulation, the results are analyzed and with the method of a screening optimization, the shape will be improved and adjusted manually until the best aerodynamic shape is found.

In this thesis, two shell versions are compared with each other and it is outlined which forces act on the pod surface. The version with the best performance, the final version, is simulated at different pressure conditions to investigate its behaviour in different pressure environments.



# 4. Concept

## 4.1 Target Setting

The procedure for the design process is outlined in this chapter. The design students who are part of the Swissloop team sketched the first drawings based on the important mechanical engineering inputs. From the mechanical point of view, fundamental points needed to be addressed and assured.

The exact inner pod geometry was analyzed and aerodynamic basics were considered for the first sketches. The shell is supposed to be as short and small as possible to be lightweight. Other important criteria were the manufacturability and transportability. There must be no sharp edges and no undercut. All inner pod subsystems need to fit within the shell geometry and it may not be too large as it needs to be shipped to Los Angeles.

Under these criteria, various conceivable combinations were investigated in a rough concept study.

## 4.2 Implementation

### 4.2.1 First Sketches

The following Figures show an extract from the many first sketches that were worked out.

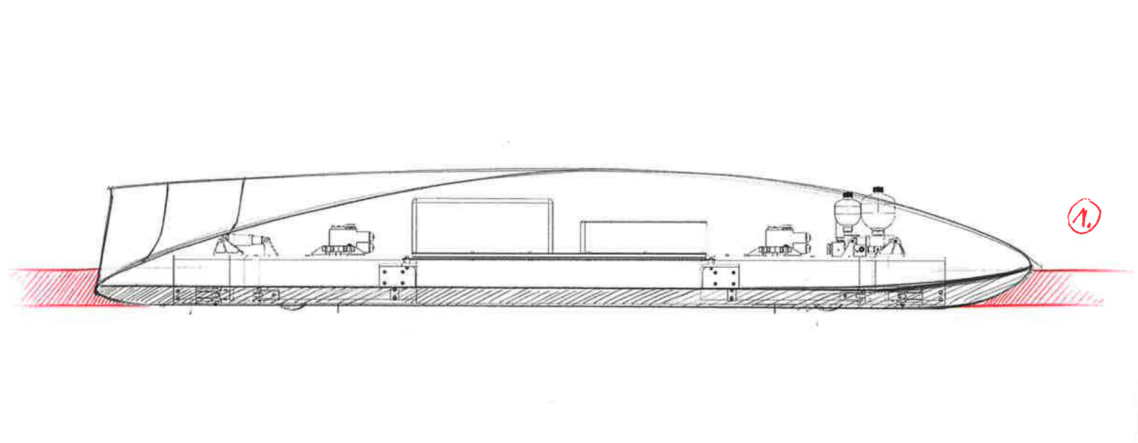


Figure 4.1: First Sketches

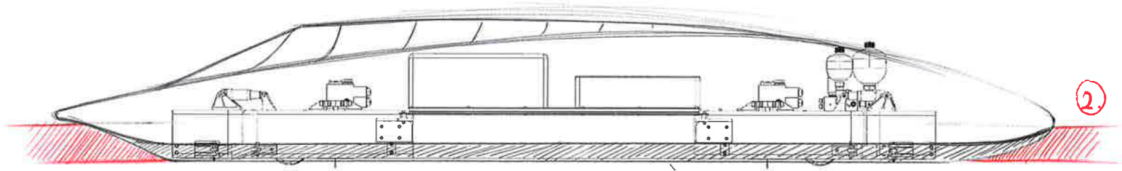


Figure 4.2: First Sketches

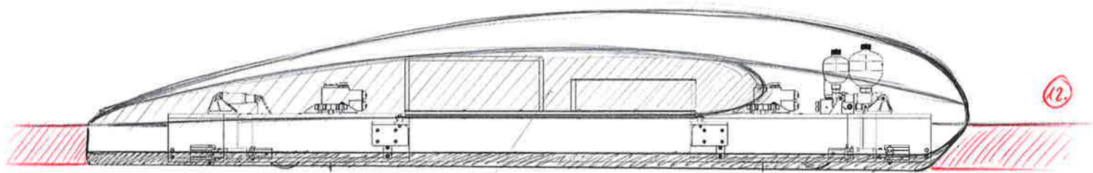


Figure 4.3: First Sketches

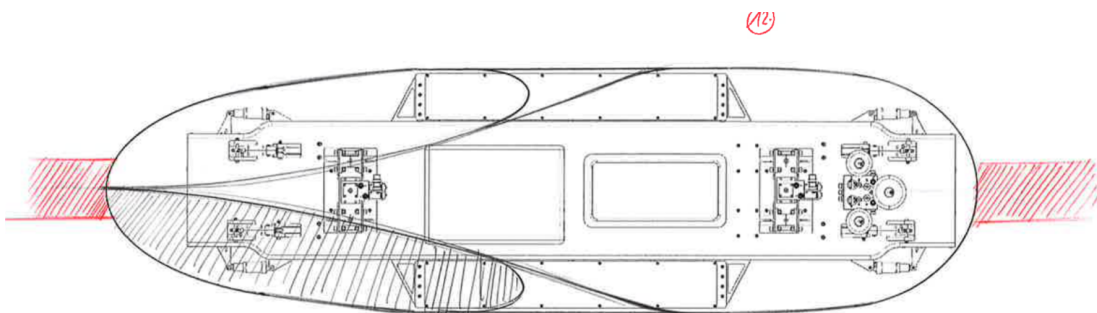


Figure 4.4: First Sketches

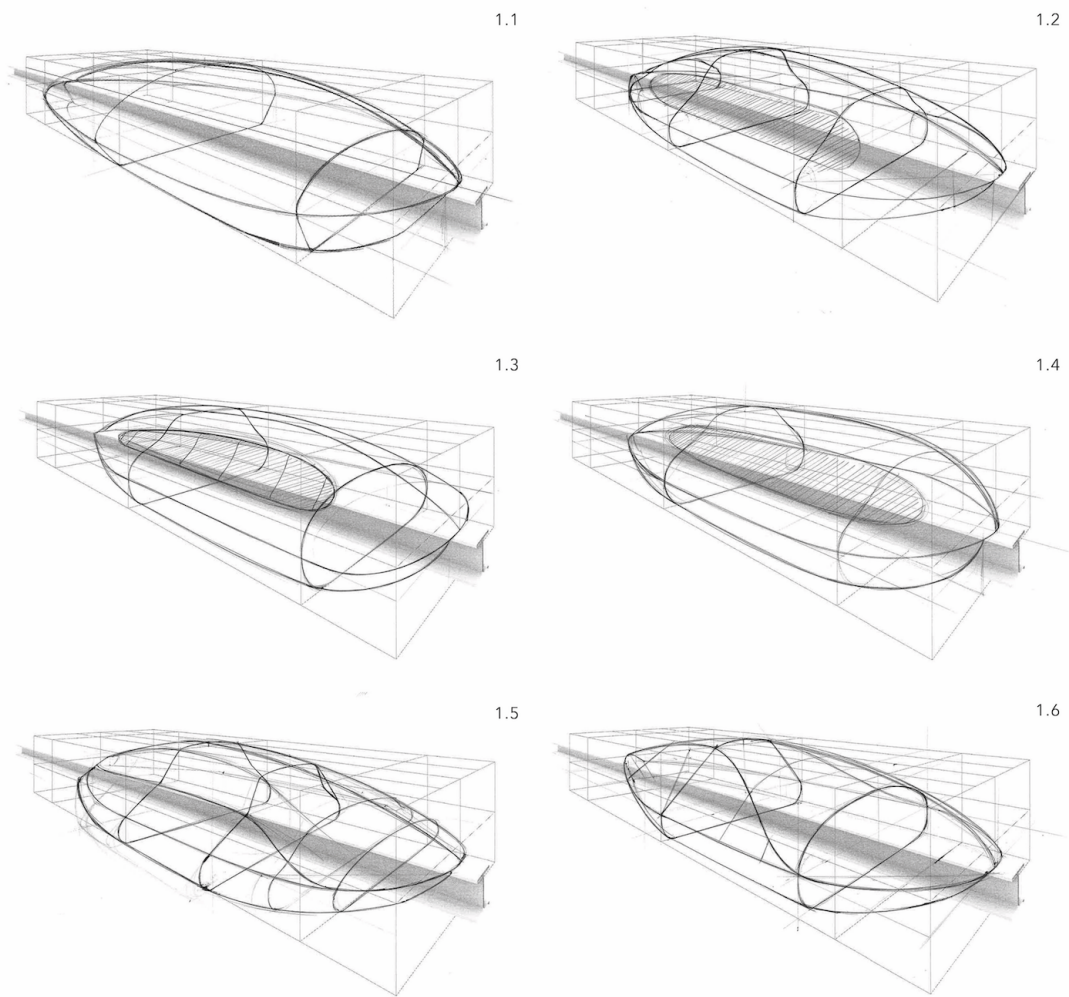


Figure 4.5: First Sketches



### 4.2.2 Concept Decision

The shell should wrap very closely around the inner pod structure and components and still maintain a clear streamline characteristic. Considering those aspects, various first sketches have been made by the designers.

In the second iteration, ideas that are manufacturable and seemed aerodynamic were filtered from ideas that cannot be realized. The many different ideas from the beginning were narrowed down. It was decided to shape the shell as good as possible like a symmetric airfoil (top view and half from side view). The overall concept developed in the previous part has now been iteratively adapted and improved. This led to the first CAD model (Version 1) which can be seen in Figure 4.6.



Figure 4.6: CAD Model Version 1

# 5. Simulation

## 5.1 Introduction

### 5.1.1 The CFD program STAR-CCM+

The program STAR-CCM+ from CD-adapco used in the scope of this thesis will be briefly presented in this section. CCM stands for computational continuum mechanics. With STAR-CCM+ the Navier-Stokes equations for the three-dimensional flow are solved with the Finite Volume Method. A huge advantage of the program is its close link to CAD programs. Therefore, geometries developed in a CAD program can easily and quickly be imported into STAR-CCM+ where they are further processed for the grid generation. The grid generation is automated, the only things the user specifies are grid fineness and areas of desired grid refinement in the given geometry. Various turbulence models can be chosen. Also for the solver there are various methods available. For objects with a symmetrical outer geometry, it is possible to only simulate the half-model. In this way, computing power is saved without loss of significant accuracy.

### 5.1.2 Calculation on Euler Cluster

To run the calculations, ETHZ's Euler Cluster is used. Every ETHZ student can run his or her simulations on this computer. Mesh generation is still done on the local computer while the run of solution is loaded to Euler Cluster. The advantage is the access to more cores and to save computational time. The computational cost for a simulation performed in this thesis and typical CPU time is six hours when using 24 cores.

### 5.1.3 Development Procedure

Like in aerodynamics for race cars, there are many parts that influence each other. For race cars, there is the front, underbody, rear wing etc. In the case of the Hyperloop pod, there is one component, the shell, that covers all the internal components (chassis, battery box, suspension, electronics box, inverter box with inverter, linear induction motor etc.). The advantage of one shell is that a change of an inner component does not have an influence on the outer aerodynamics. However, the inner components still influence the aerodynamics as they are in contact with the I-beam and the ground (suspension wheels and traveling wheels). As it is difficult to simulate all those factors and it would use too much computational effort, the complexity of the system is reduced. In this thesis, only the shell is simulated without any inner component.

#### 5.1.4 Sequence of a CFD-Simulation

Common CFD programs follow a typical structural step pattern. The approach is usually divided into three steps:

- Pre-processing
- Calculation
- Post-processing

In the first step, the problem to be solved is transformed from an abstract level to a numerically solvable problem. Hence, the geometry to be examined is passed to the CFD program where the grid will be generated. To save computational cost, not only the shell is imported as a half-model to the CFD software but also the tube, ground, I-beam, inlet, outlet and the symmetry plane. In STAR-CCM+, each component is represented in a different color and can be stored individually under assigned names. After the definition of the spatial model, the boundary conditions are set and the grid generated. The expected flow must already be known or at least estimated. Afterwards, the physical boundary conditions are defined.

In the second step, the program solves the problem which was posed in the pre-processing with numerical methods. The partial differential equations are solved for all volume elements for all grid cells. The calculation either stops after the stopping criteria is reached or it is terminated manually as soon as the result has converged. If the calculation diverges, no result is produced. The duration of calculation depends on the available computing power and the complexity of the model. In industrial applications this can take from a few hours to several days.

The last step is the post-processing. After the CFD calculation has terminated, all results are stored and included in the CFD file. From there they can be accessed and used. For instance, forces acting on the surface can be analyzed, pressure distribution and Mach numbers can be visualized. There is a huge variety of visualization options.

## 5.2 Preparation

Before the work in the CFD environment is explained, the settings and conditions are pointed out. STAR-CCM+ uses the Finite Volume Method to solve the Navier-Stokes equations. We deal with a compressible Newtonian fluid which is air and which may be considered as an ideal gas.

The expected temperature in Los Angeles in July is expected to be 30 degrees Celsius which corresponds to 303 Kelvin. The Swissloop team plans to perform in a pressure environment of 0.15 bar and with a maximal speed of 125 meters per second. Therefore, for the following calculations, pressure  $p$  is set to 0.15 bar and velocity  $u$  is set to  $125 \frac{m}{s}$ .

As pointed out in chapter 2, the speed of sound is calculated as follows

$$a = \sqrt{\gamma R T} = 348.95 \text{ m/s} \quad (5.1)$$

$\gamma$  is the heat capacity ratio and its value for air is 1.4,  $R$  is the ideal gas constant for air and has a value of  $287.05 \frac{J}{kgK}$  and  $T$  is the temperature of the fluid which is 303 Kelvin.

The density is calculated in the following way

$$\rho = \frac{p M}{R T} = 0.1724 \frac{kg}{m^3} \quad (5.2)$$

Here, the pressure  $p$  is 0.15 bar,  $M$  is the molar mass for air and its value is  $28.96 \frac{kg}{kmol}$ ,  $R$  is the ideal gas constant for air and has a value of  $287.05 \frac{J}{kgK}$  and  $T$  is the temperature of the fluid which is 303 Kelvin.

The viscosity  $\mu$  is assumed as constant and its value is  $1.855E-05 \frac{kg}{m s}$ .

For a pod height of 0.5 meters and with the values obtained above, the Reynolds number calculates to

$$Re = \frac{\rho u L}{\mu} = \frac{u L}{\nu} = 5.81E + 05 \quad (5.3)$$

The Mach number is

$$Ma = \frac{u}{a} = 0.358 \quad (5.4)$$

When the pod is traveling within the tube density, temperature and pressure are not constant.

### 5.3 Environment in STAR-CCM+

The concept described in the previous section is now applied to the Hyperloop pod's shell simulation. All implementation and settings are described in this section. The fundamental settings used are always the same for all simulations.

The geometry was prepared in a CAD software and imported into STAR-CCM+. This geometry includes not only the shell but also the tube, I-beam (rail), ground, inlet, outlet and the symmetry plane, everything as a half-model. Figure 5.1 shows the whole geometry after being imported in STAR-CCM+.

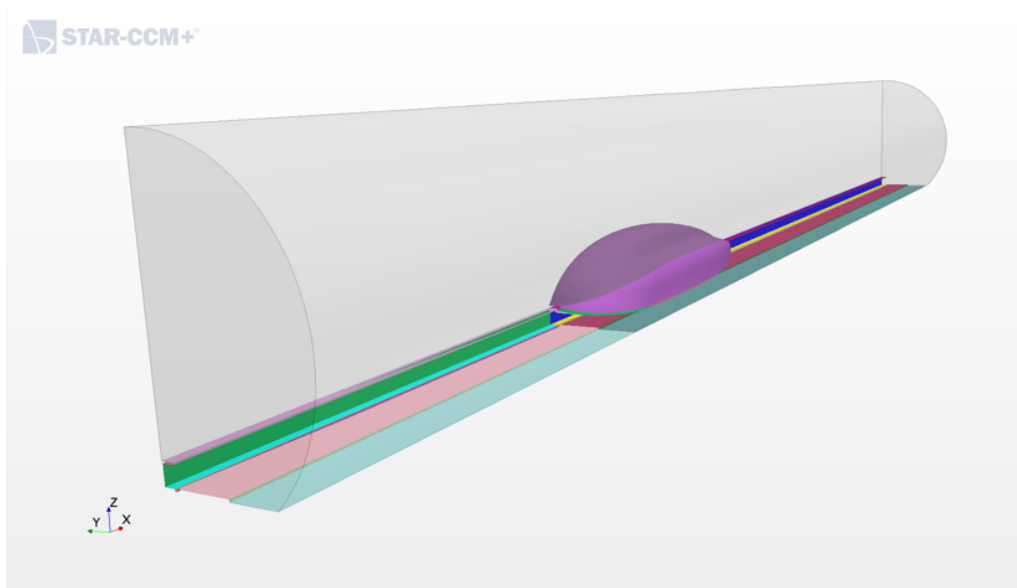


Figure 5.1: Imported geometry in STAR-CCM+

It is important to note that not the pod itself is analyzed, but the surrounding air volume from which the shell geometry is subtracted. The volume of air is designed as a channel, comparable to a wind tunnel in which the pod is located. The channel is the closed tube itself. An overview can be seen in Figure 5.2 and Figure 5.3.



Figure 5.2: Overview

The tube's length is extended to 3.5 meters (roughly one pod length) in front of the pod and 7 meters (roughly two pod lengths) behind the pod. This gives a total length for the simulated tube of 14 meters. All imported dimensions of the tube, I-beam and ground are shaped and dimensioned exactly as the test track setting at the Hyperloop Pod Competition. For information on the SpaceX Hyperloop test track please refer to Appendix A.

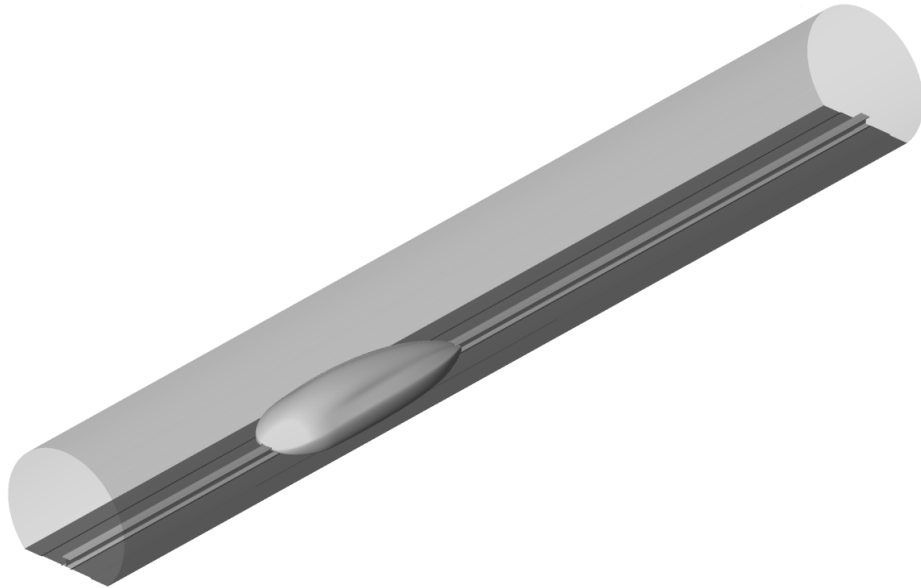


Figure 5.3: Three-dimensional Overview (mirrored at the symmetry plane)

## 5.4 Grid Generation

Important for the accuracy of CFD simulations is the mesh. The mesh size is the distance between two grid points. In order to achieve the most accurate results, a small mesh size is desirable. However, with a smaller mesh size, the total number of grid points increases and therefore the computation becomes more complex. What follows are higher computational costs. Thus, the smallest possible mesh is desirable. In general, there are two types of grids: structured and unstructured grids. [2]

### Structured grids

Structured grids consist of only one type of lattice cell and appear homogeneously (see Figure 5.4). The advantage is their low computational effort in the creation of the grid and in the solution of the differential equations. The disadvantage is they cannot properly describe complex geometries. [3]

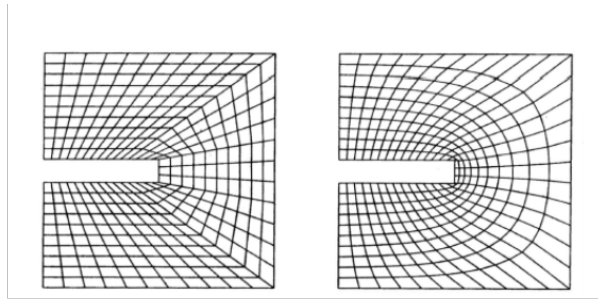


Figure 5.4: Structured Grid [10]

### Unstructured grids

Unstructured grids consist of several cell types. An example can be seen in Figure 5.5. Although they require more computational effort, they can describe complex geometries much better than structured grids. [3]

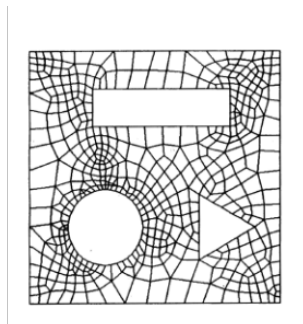


Figure 5.5: Unstructured Grid [10]

### 5.4.1 Chosen Grid structure

The following meshing models were chosen for the CFD-Simulation:

- Prism Layer Mesher
- Surface Remesher
- Trimmer

For an efficient grid generation the tube is divided into three sections. Between inlet and pod, the grid is coarser as well as in the back of the tube. With the shape of cylinders, two finer grids was created around the pod. The inner grid starts 0.5 meters before the pod and is 5 meters long. Its radius is 0.6 meters. A second cylinder with a radius of 0.8 meters provides a less coarser grid than the inner cylinder. It starts one meter in front of the pod and is 8 meters long.

A mix of structured and unstructured grid is used. The tube is discretized with structured grid and the shell body with unstructured grid and prism layers. In between as a connection of tube and pod, an unstructured grid is used.

When using prism layers, a stretching factor can be applied. By defining a stretching factor, the distribution of the prism layers for the boundary can be specified.

For instance, a prism layer stretching value of 1.5 means that each layer is 1.5 times the thickness of its neighbour layer. Values below 1.0 are not possible. For this thesis, two different stretching factors have been used, namely the factors 1.5 and 1.8. Two different factors have been chosen because not every geometry's result converged best for the first layup. Therefore, a second layup has been used for some simulations as the aim was to guarantee the best convergence in the result of the force for each geometry. Although the factor is different, the total prism layer thickness does not vary significantly.

The prism layers are composed in the following ways: The first simulations were done with 14 prism layers, a stretching factor of 1.5 and a total thickness of 0.0145 meters. The last simulations were set up with 10 prism layers, a stretching factor of 1.8 and a total thickness of 0.0142 meters. An overview of the two layups can be seen in Table 5.1.

		Layup 1	Layup 2
Stretching Factor		1.5	1.8
Layer No.	1	2.50E-05	3.20E-05
	2	0.0000375	0.0000576
	3	0.00005625	0.00010368
	4	0.000084375	0.000186624
	5	0.000126563	0.000335923
	6	0.000189844	0.000604662
	7	0.000284766	0.001088391
	8	0.000427148	0.001959104
	9	0.000640723	0.003526387
	10	0.000961084	0.006347497
	11	0.001441626	
	12	0.002162439	
	13	0.003243658	
	14	0.004865488	
Sum		0.0145	0.0142

Table 5.1: Prism Layer Layup Comparison



This means, for the first layup the prism layer number one has a thickness of 25 microns, the second one a thickness of 37.5 microns (first layer stretched by the stretching factor 1.5) and so on. The fourteenth and last prism layer is 4.87 millimeters thick. Together they have a thickness of 14.5 millimeters. In the second case, the first prism layer has a thickness of 32 microns, the second one is stretched by the stretching ratio of 1.8 and has therefore a thickness of 57.6 microns. The tenth and last prism layer has a thickness of 6.35 millimeters. Together they have a thickness of 14.2 millimeters.

The following Figures show what the mesh grid looks like. The example shown is the final shell version.

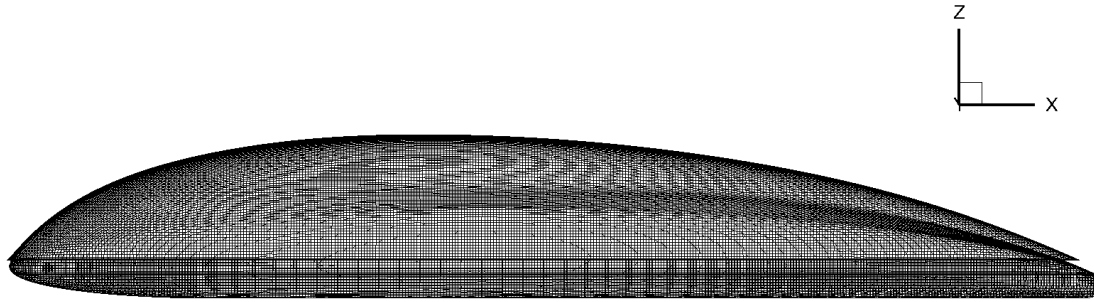


Figure 5.6: Mesh of pod surface

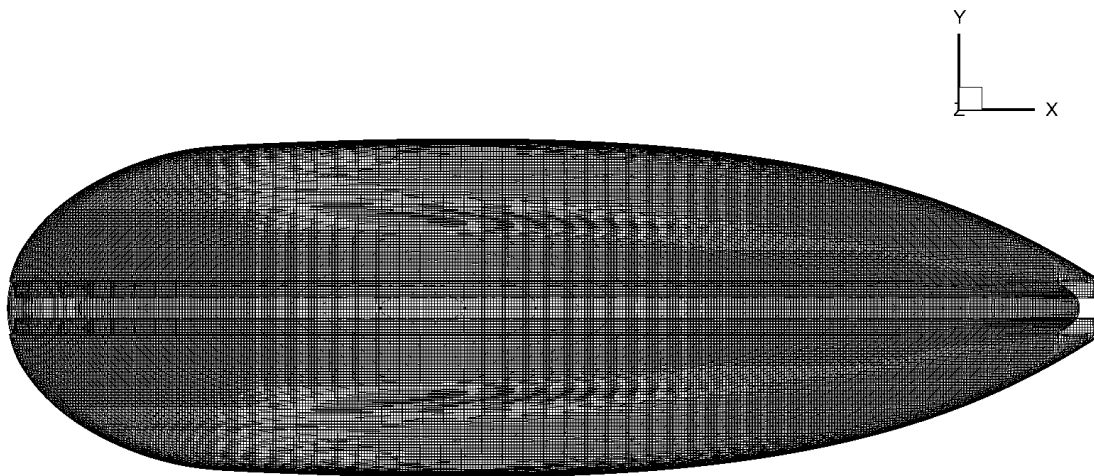


Figure 5.7: Mesh of pod surface

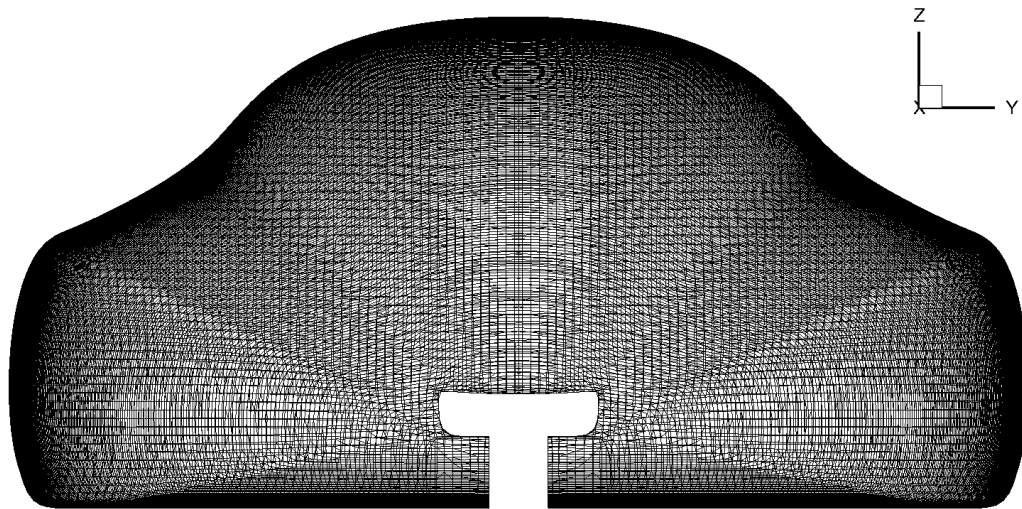


Figure 5.8: Mesh of pod surface

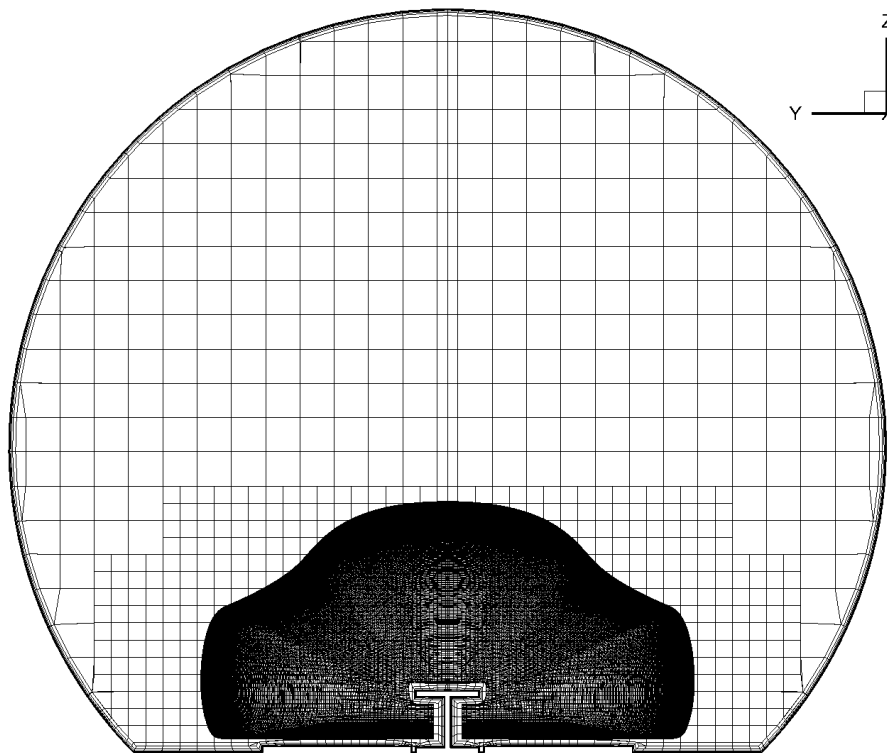


Figure 5.9: Mesh of pod surface and tube

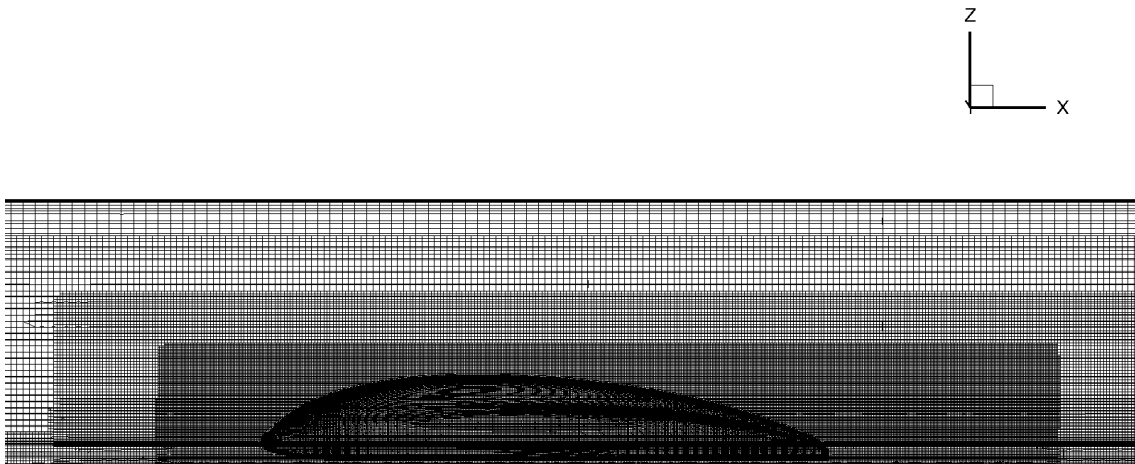


Figure 5.10: Mesh of pod surface and tube

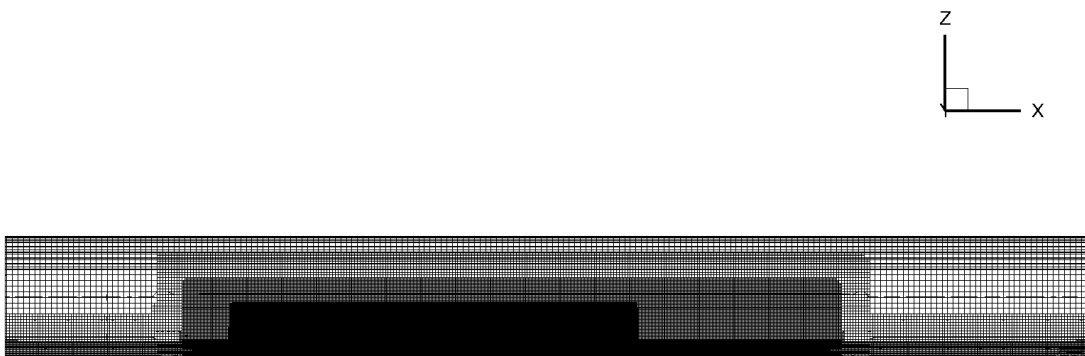


Figure 5.11: Mesh of tube

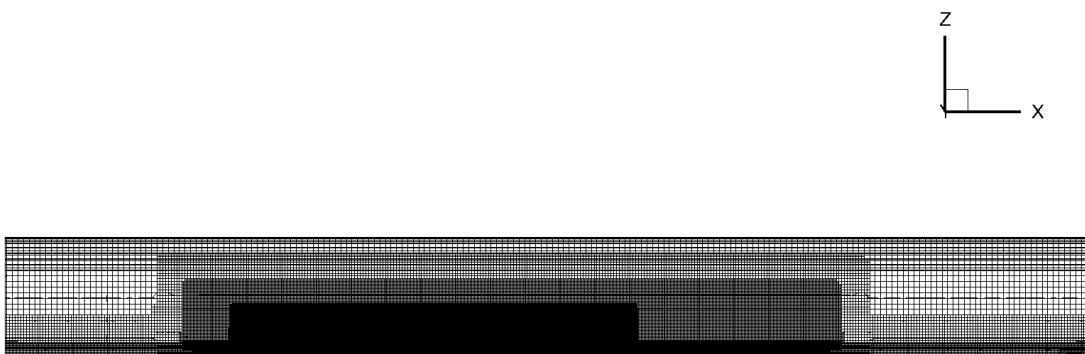


Figure 5.12: Mesh of tube

### Analysis of the chosen Grid Structure

The following Figures show in detail how the layup 2 with ten prism layers is composed. It is interesting to note that the prism layers evolve from all surfaces, the pod, ground, I-beam and tube. For a better illustration, the pictures are zoomed as required.

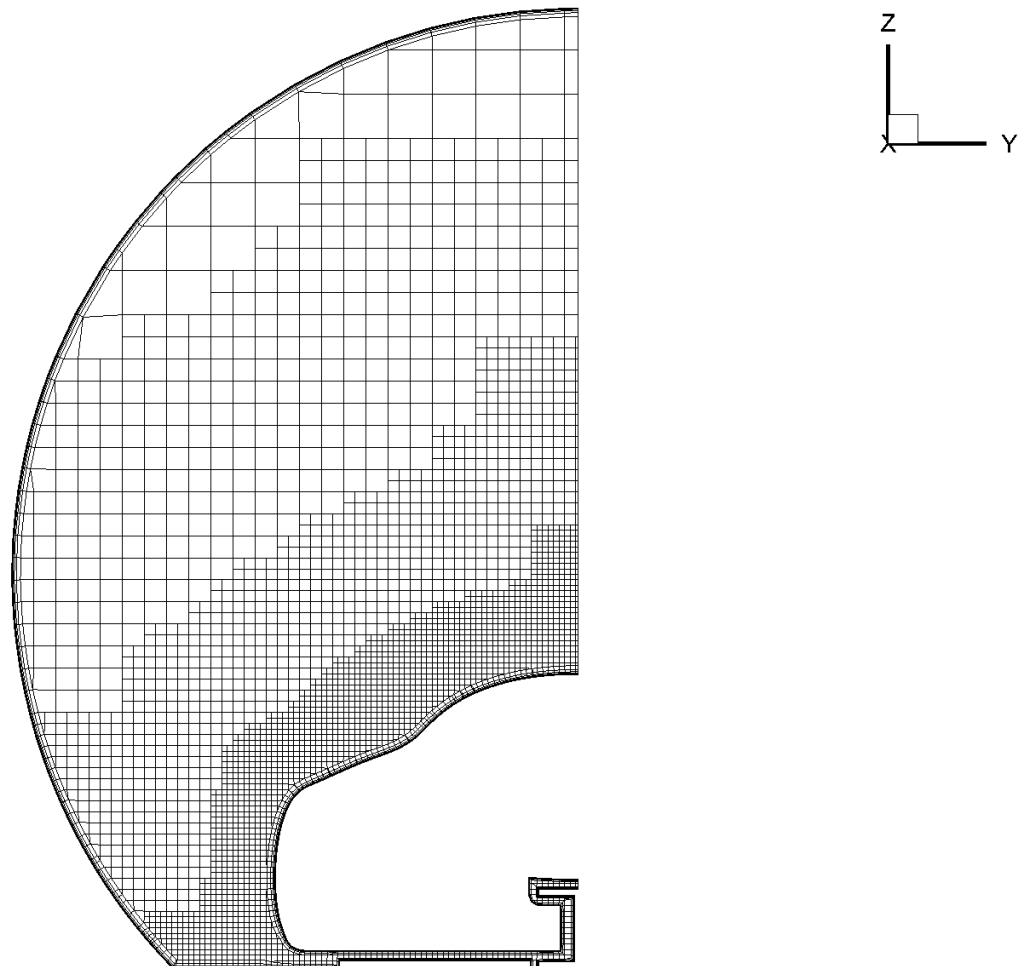


Figure 5.13: Mesh of pod

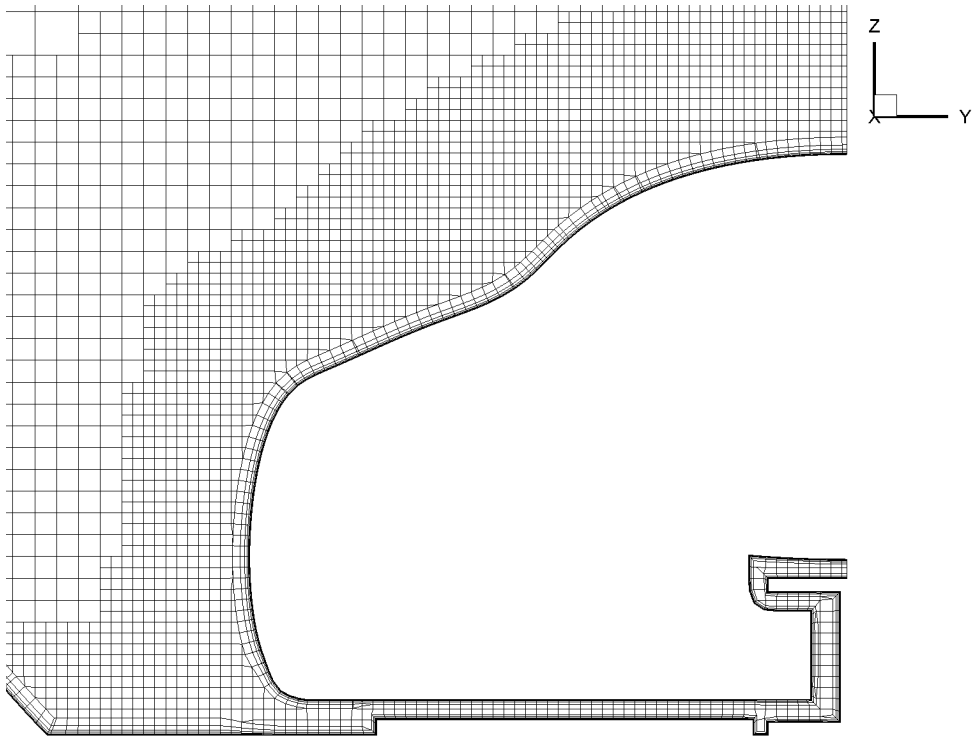


Figure 5.14: Mesh of pod

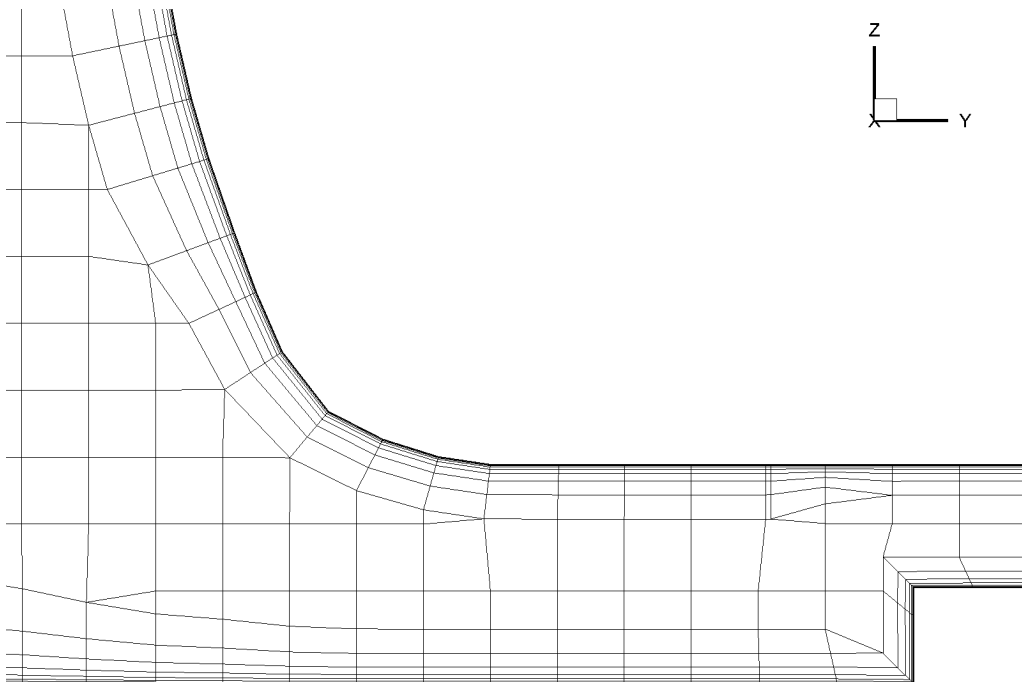


Figure 5.15: Mesh of pod

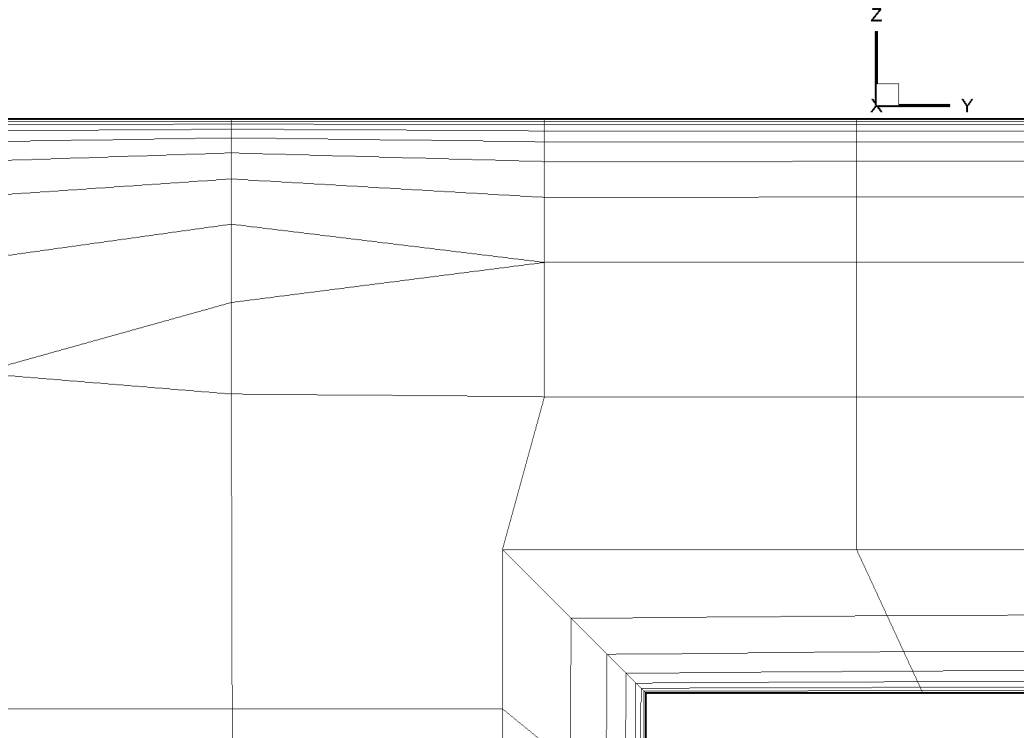


Figure 5.16: Mesh of pod. Which stretching Factor 1.8

In this Figure it can be seen how the prism layers develop and stretch from the ground and the pod surface towards each other.

## 5.5 Physics Conditions

The physics conditions in STAR-CCM+ are set as follows:

- Low  $y^+$  Wall treatment
- Gamma Transition
- Exact Wall distance
- SST-Menter  $k-\omega$  turbulence
- RANS
- turbulent
- coupled energy
- coupled flow
- ideal gas; air
- steady
- three-dimensional

It is important to note that RANS was chosen together with the SST-Menter  $k-\omega$  turbulence model.

### 5.5.1 Reference Values

The reference pressure is set to 0.15 bar as this is the operating pressure Swissloop aims for at the Pod Competition. The velocity is set to 125 meters per second (450 kilometers per hour). This is the planned maximum speed for the Swissloop pod.

### 5.5.2 Boundary Conditions

In terms of the frame of reference, the pod is fixed and stands still. The tube, I-beam and ground travel with the set velocity. The air is stagnant. Therefore, the boundary condition for ground, I-beam and tube is set to 125 meters per second, the inlet is defined as a velocity inlet with 125 meters per second and the outlet is defined as a pressure outlet.

After the general design of the aerodynamics package was defined, the iteration work began. The aim was to achieve the minimal result for the drag force. The pod shape was modified in terms of length, height, width and curvature of the outer geometry. The iteration process, comments about the first results and the final results are outlined in the next chapter.

# 6. Results

## 6.1 First Results

After obtaining the first results, some settings needed to be adjusted, more prism layers needed to be added until the exact setting and layup described in the previous chapter was reached.

After eleven versions and iterations the inner dimensions of the pod did not change anymore. Up until then, there were still some modifications done in the mechanical team which had an influence on the possible shell's shape. The inner pod geometry was now frozen and everything that was adjusted and iterated from now on was the outside shape and dimensions (length, height, width, curvature).

## 6.2 Design Iteration

After every simulation, the results were thoroughly analyzed. The pod shape was modified in terms of length, height, width and curvature of the outer geometry. In Figure 6.1 an overview of different versions is given.

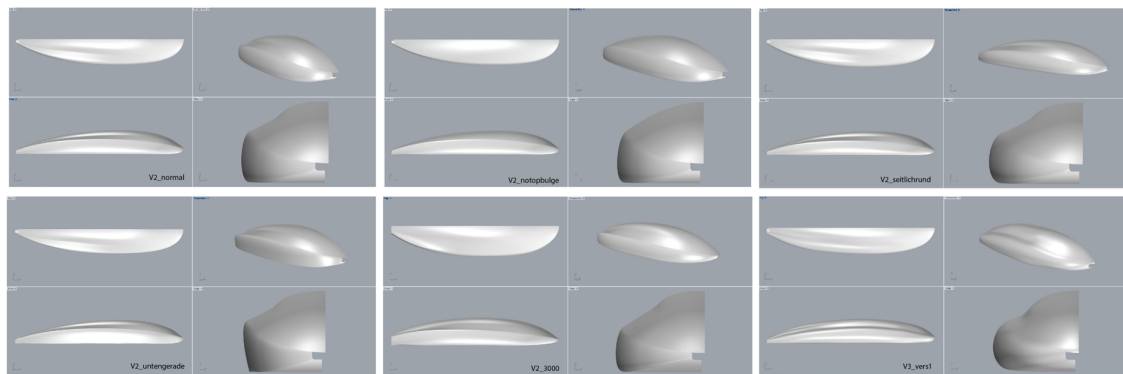


Figure 6.1: Different Versions

Finally, the geometry was optimized more and more and the drag force reduced step by step. In the following section, two of those versions are compared with each other.



## 6.3 Comparison of two Versions

In total, 23 different versions with different geometries have been simulated, evaluated and analyzed. In this chapter, two of these versions are compared based on different aspects. Their geometries, calculated forces and various plots are compared.

One of the goals was to design the shell as short as possible. Not only in terms of manufacturing and transportation this is of great benefit, but also from a weight point of view. Since there is a massive amount of single components included in the pod, every part is kept as light as possible. This is the reason why a short shell version was created. However, this was only possible with a chopped back. Otherwise, there was no space for the inner components of the pod.

The second version to be compared is 27 *cm* longer. In this way, all technical components fit within the pod's shell without having a chopped back. This geometry is the shortest possible to fulfill this criteria.

In the following subchapters, these two versions will be named version A and version B and are compared to each other. At the end, it is concluded why to proceed with the corresponding version and why to select it as the final shell geometry.

### 6.3.1 Dimensions

#### Version A

Table 6.1 presents the dimensions of Version A.

length [m]	3.004
width [m]	1.104
height [m]	0.504

---

$S_{\text{frontal}} [\text{m}^2]$	0.4413
$S_{\text{Tube}} [\text{m}^2]$	2.320
Blockage Ratio $\beta$	0.190

Table 6.1: Dimensions Version A

#### Version B

Table 6.2 presents the dimensions of Version B.

length [m]	3.27
width [m]	1.018
height [m]	0.489

---

$S_{\text{frontal}} [\text{m}^2]$	0.386
$S_{\text{Tube}} [\text{m}^2]$	2.320
Blockage Ratio $\beta$	0.166

Table 6.2: Dimensions Version B

#### Comparison

The absolute dimension differences can be seen in Table 6.3.

length [m]	0.27
width [m]	0.09
height [m]	0.02

---

$S_{\text{frontal}} [\text{m}^2]$	0.055
Blockage Ratio $\beta$	0.024

Table 6.3: Absolute differences from dimensions Version A and Version B

Version A is significantly shorter than Version B, namely 27 centimeters. Version A is 9 centimeters wider, 2 centimeters higher and its frontal surface area is 0.055 square meters bigger. The blockage ratio of Version A is therefore higher as well. The blockage ratio of Version A is 0.190 and the blockage ratio of Version B is 0.166. This is a difference of 0.024 and 14.5 percent.

Note that in both cases the blockage ratio is below 0.4. Therefore choking will not occur in neither of the two cases. The Mach number will not increase significantly and therefore no sonic conditions occur.

### 6.3.2 Geometries

The following Figures show the geometries of Version A and Version B in different perspectives. The scale is in meters.

#### Geometry Version A

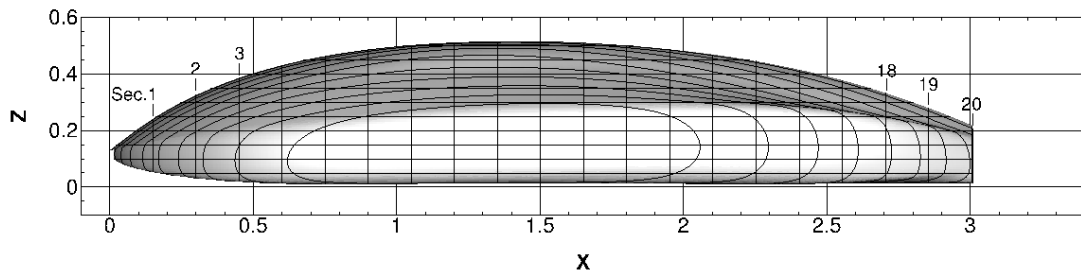


Figure 6.2: Sheer Plan Version A

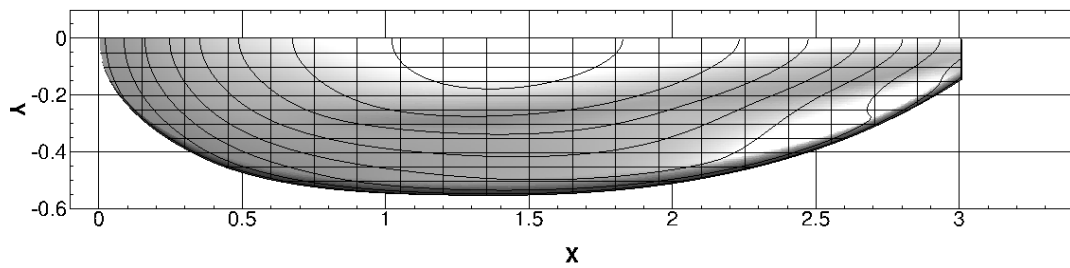


Figure 6.3: Half-breadth Plan Version A

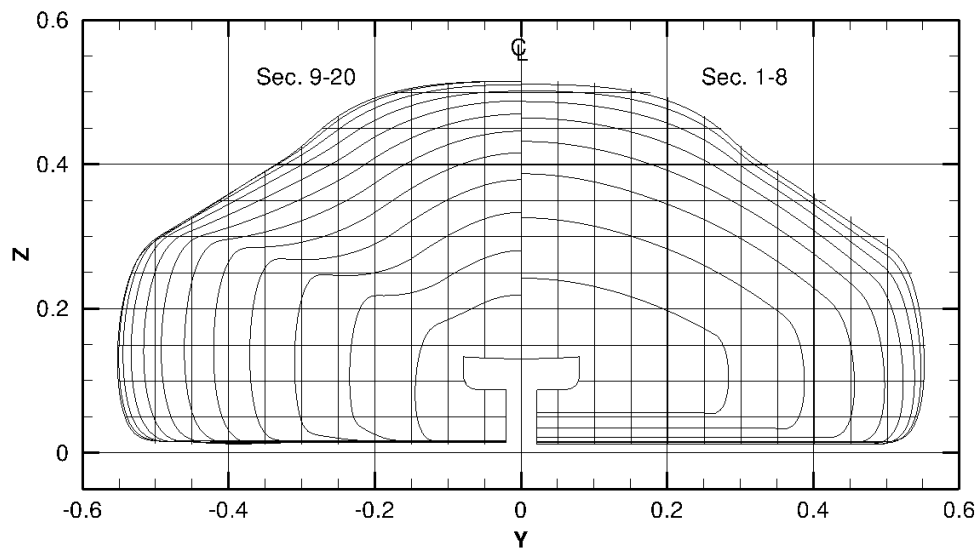


Figure 6.4: Body Plan Version A

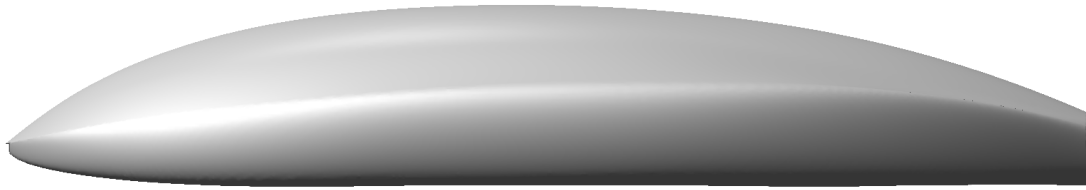


Figure 6.5: Side View Version A

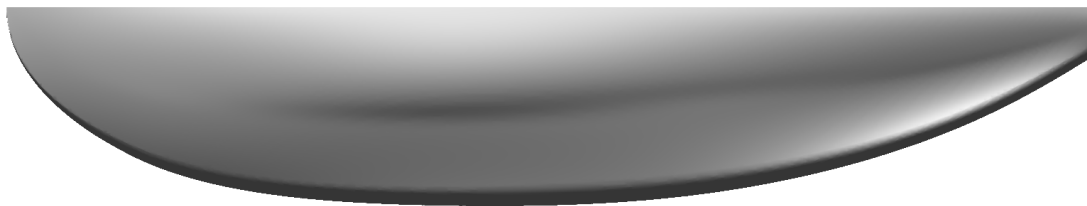


Figure 6.6: Top View Version A

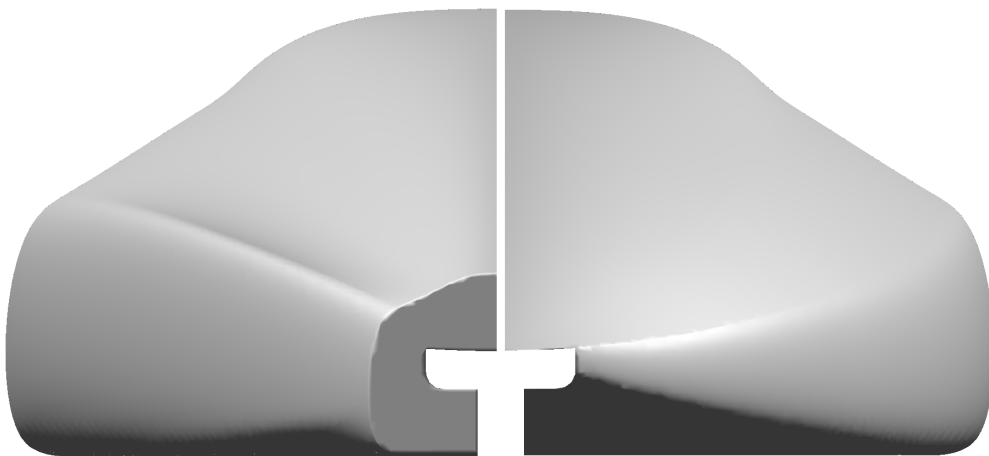


Figure 6.7: Front View (right half) and Rear View (left half) of Version A

### Geometry Version B

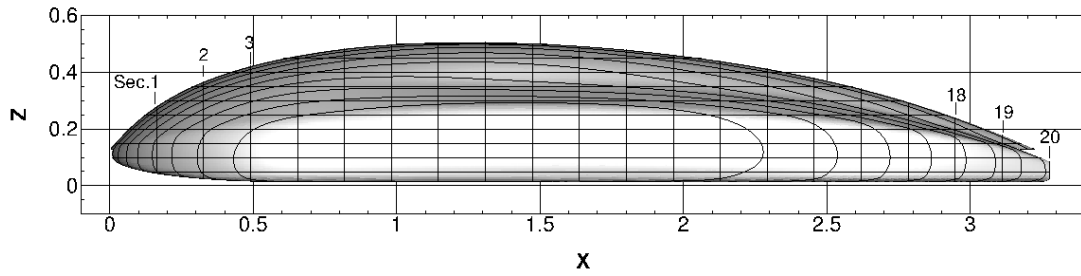


Figure 6.8: Sheer Plan Version B

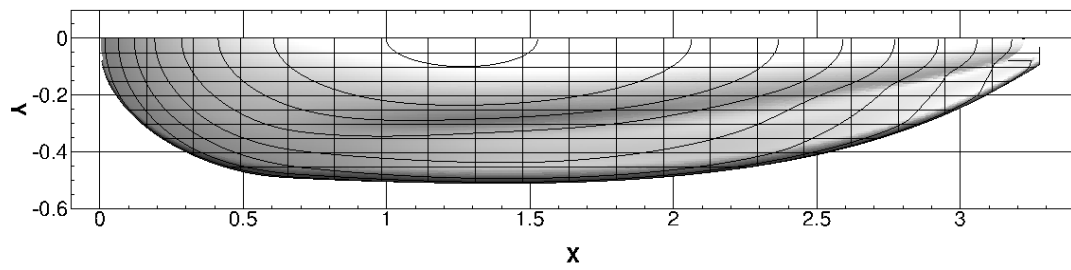


Figure 6.9: Half-breadth Plan Version B

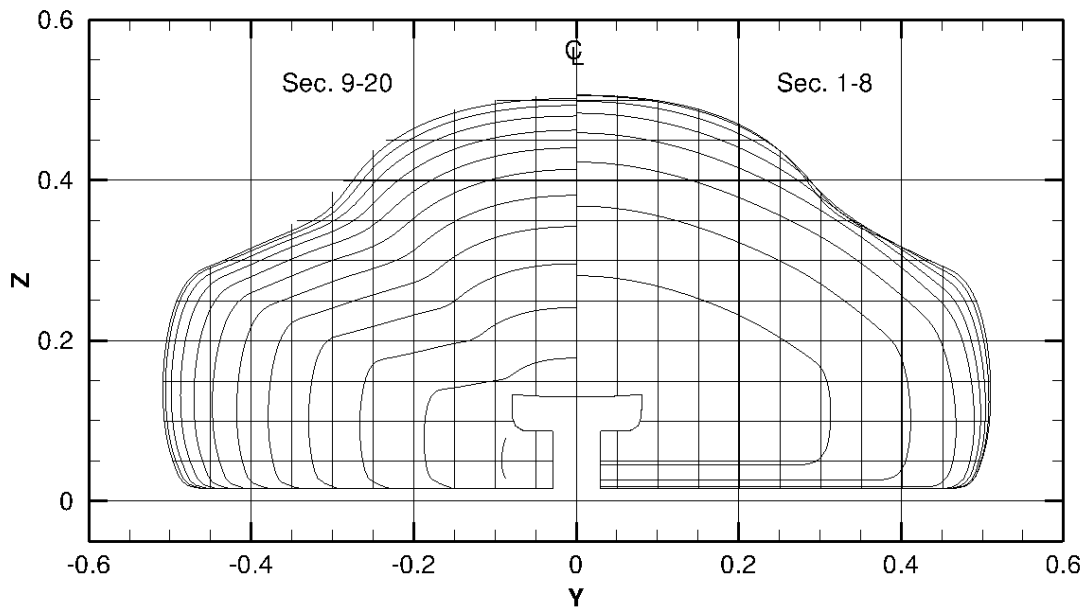


Figure 6.10: Body Plan Version B



Figure 6.11: Side View Version B



Figure 6.12: Top View Version B

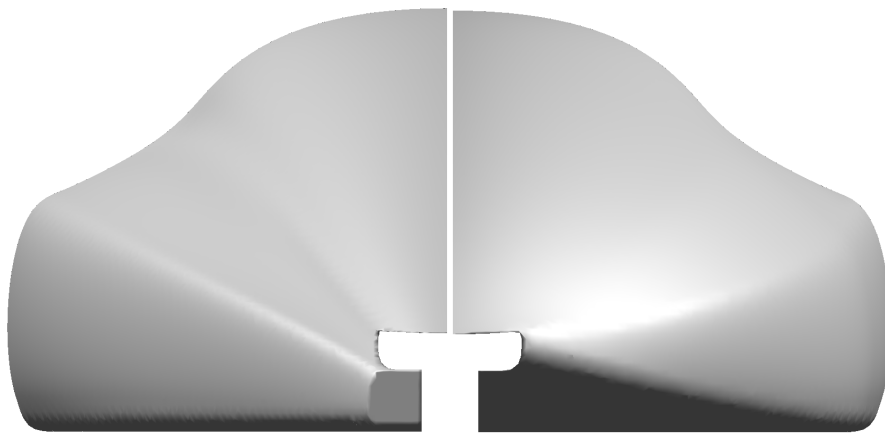


Figure 6.13: Front View (right half) and Rear View (left half) of Version B

### 6.3.3 Forces

This subchapter looks at the calculated forces that act on the shell's surface for both Version A and Version B. All results are obtained for a speed of 450 m/s and a pressure of 0.15 bar set as boundary conditions.

#### Results of Version A at 0.15 bar

For Version A at a pressure of 0.15 bar, the total drag force in the x-direction is 74.58 newton and the total lift force in the z-direction is -6.22 newton.  $C_{total}$ ,  $C_f$  and  $C_p$  values are calculated from  $F_{total}$ ,  $F_{friction}$  and  $F_{pressure}$  as it was outlined in chapter 2.  $C_{total}$  for drag is 0.13 and  $C_{total}$  for lift is -0.01. The values are shown in Table 6.4. Note that the y-direction can be ignored as the pod is simulated as a half-model with the xz-plane as the symmetry plane. The unit of all forces is Newton whereas the values  $C_{total}$ ,  $C_f$  and  $C_p$  are dimensionless. It holds:  $F_{total} = F_{friction} + F_{pressure}$  and  $C_{total} = C_f + C_p$ .

	Drag (x-direction)	Lift (z-direction)
$F_{total}$ [N]	74.58	-6.22
$F_{friction}$ [N]	34.77	-0.68
$F_{pressure}$ [N]	39.81	-5.54
$C_{total}$	0.13	-0.01
$C_f$	0.06	0.00
$C_p$	0.07	-0.01

Table 6.4: Computed Results of Version A at 0.15 bar

It may be deduced from these results that the total drag force is higher than the total lift force. Friction force and pressure force for drag do not differ much. Out of the total drag force, the friction force is 47 percent and the pressure force is 53 percent. This is a difference of 6 percent.

It is noted that the lift force is negative which means it is a down force. Its total value of -6.22 newton is very small however and can be neglected.

It needs to be investigated if there is a momentum acting on the pod as the lift force does not act at the center of mass. The center of mass is expected to lie in the middle of the pod ( $x = 1.5$  meters). As it can be seen in Figure 6.16 the low pressure area lies in the front half of the pod and therefore the lift force does not act at the center of mass.

The pod's total mass is 200 kilograms which corresponds to 1962 newton weight force. The down force has an absolute value of 6.22 newton. Compared to the weight force this is 0.3 percent. This influence can be neglected. Therefore, there is no momentum acting on the pod due to down force.

Table 6.5 shows an overview of the grid parameters, prism layers, and flow parameters for the present calculation.

Grid parameters:	
Cells	4735864
Faces	14083407
Prism Layers:	
Number	14
Stretching	1.5
Thickness [m]	0.014
Flow parameters:	
Re	5.86E+05
Ma	0.358

Table 6.5: Grid Parameters, Prism Layers, and Flow Parameters of Version A at 0.15 bar

In the present calculation the number of cells is 4735864 and the number of faces amounts to 14083407. There are 14 prism layers with a stretching factor of 1.5 and total thickness of 0.014 meters. The Reynolds number for the set condition is 5.86E+05 and the Mach number for this condition is 0.358.

The following Figure 6.14 shows the converged Force Monitor Plot of Version A at a pressure of 0.15 bar. The number of time steps for the computation is 21400.

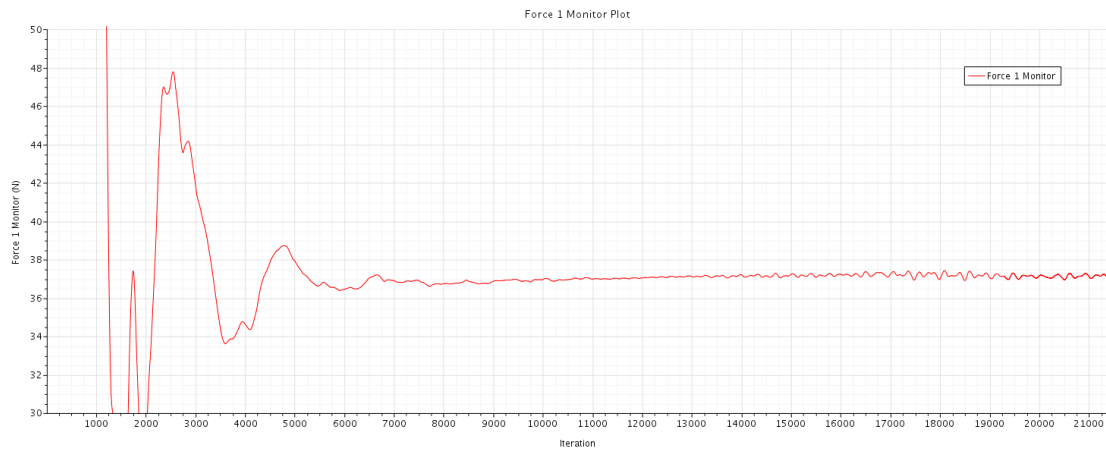


Figure 6.14: Force Monitor Plot of Version A at 0.15 bar

After 21400 time steps, the result was still oscillating with an amplitude of  $\pm 0.25$  newton. This can be neglected and the result has converged.



### Results of Version B at 0.15 bar

For Version B at a pressure of 0.15 bar, the total drag force in the x-direction is 60.59 newton and the total lift force in the z-direction is 76.86 newton.  $C_{total}$ ,  $C_f$  and  $C_p$  values are calculated from  $F_{total}$ ,  $F_{friction}$  and  $F_{pressure}$  as it was outlined in chapter 2.  $C_{total}$  for drag is 0.12 and  $C_{total}$  for lift is 0.15. The values are shown in Table 6.6. Note that the y-direction can be ignored as the pod is simulated as a half-model with the xz-plane as the symmetry plane. The unit of all forces is Newton whereas the values  $C_{total}$ ,  $C_f$  and  $C_p$  are dimensionless. It holds:  $F_{total} = F_{friction} + F_{pressure}$  and  $C_{total} = C_f + C_p$ .

	Drag (x-direction)	Lift (z-direction)
$F_{total}$ [N]	60.59	76.86
$F_{friction}$ [N]	30.75	-0.66
$F_{pressure}$ [N]	29.83	77.52
$C_{total}$	0.12	0.15
$C_f$	0.06	0.00
$C_p$	0.06	0.15

Table 6.6: Computed Results at 0.15 bar

It may be deduced from these results that the total drag force is smaller than the total lift force. There is not a huge difference between friction force and pressure force for drag. Out of the total drag force, the friction force is 51 percent and the pressure force is 49 percent. This is a difference of 2 percent.

It is noted that the lift force is positive. It needs to be investigated if there is a momentum acting on the pod as the lift force does not act at the center of mass. The center of mass is expected to lie in the middle of the pod ( $x = 1.64$  meters). As it can be seen in Figure 6.23 the low pressure area lies in the front half of the pod and therefore the lift force does not act at the center of mass. The pod's total mass is 200 kilograms which corresponds to 1962 newton weight force. As a lift force value of 76.86 newton can be neglected compared to 1962 newton weight force, there is no momentum acting on the pod due to lift force.

Table 6.7 shows an overview of the grid parameters, prism layers, and flow parameters for the present calculation.

Grid parameters:	
Cells	4040105
Faces	12018556
Prism Layers:	
Number	10
Stretching	1.8
Thickness [m]	0.014
Flow parameters:	
Re	5.68E+05
Ma	0.358

Table 6.7: Grid parameters, Prism Layers, and Flow parameters of Version B at 0.15 bar

In the present calculation the number of cells is 4040105 and the number of faces amounts to 12018556. There are 10 prism layers with a stretching factor of 1.8 and a total thickness of 0.014 meters. The Reynolds number for the set condition is 5.68E+05 and the Mach number for this condition is 0.358. The Reynolds number of Version B differs from the Reynolds number of Version A because the characteristic linear dimension (the height) is different. The Mach number remains unchanged as the speed of the pod and the speed of sound stay the same.

The following Figure 6.15 shows the converged Force Monitor Plot at a pressure of 0.15 bar. The number of time steps for the computation is 35000.

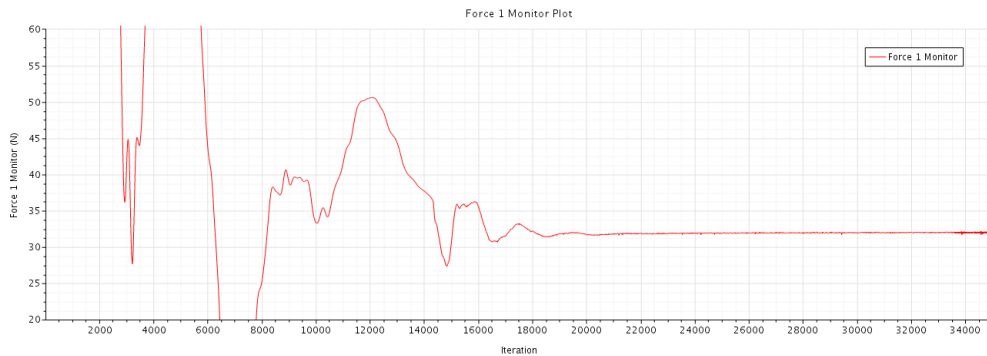


Figure 6.15: Force Monitor Plot of Version B at 0.15 bar

After 35000 time steps, the simulation was terminated. The small oscillation with an amplitude of  $\pm 0.25$  newton can be neglected.

### 6.3.4 Visualization of Flow Field

The following visualizations show the relative pressure of Version A and Version B. All visualizations are obtained for a speed of 450 m/s and a pressure of 0.15 bar set as reference values.

#### Relative Pressure Version A

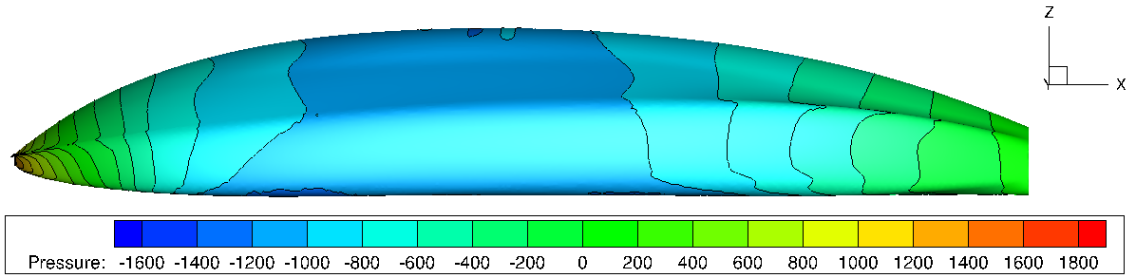


Figure 6.16: Relative Pressure Side View Version A

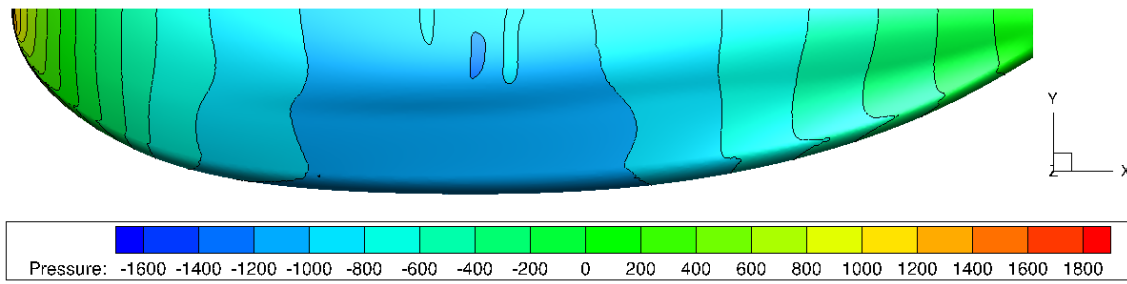


Figure 6.17: Relative Pressure Top View Version A

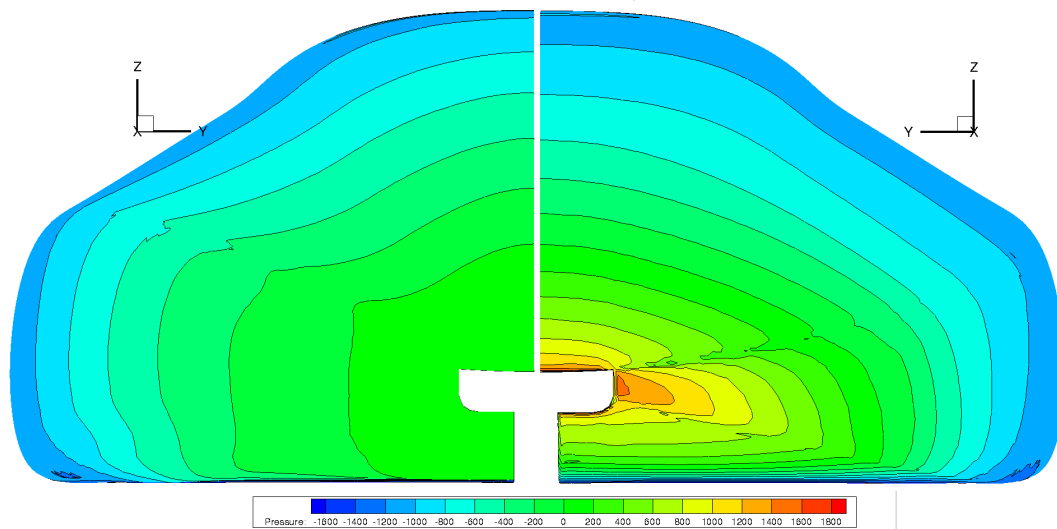


Figure 6.18: Relative Pressure Front View (right) and Rear View (left) of Version A

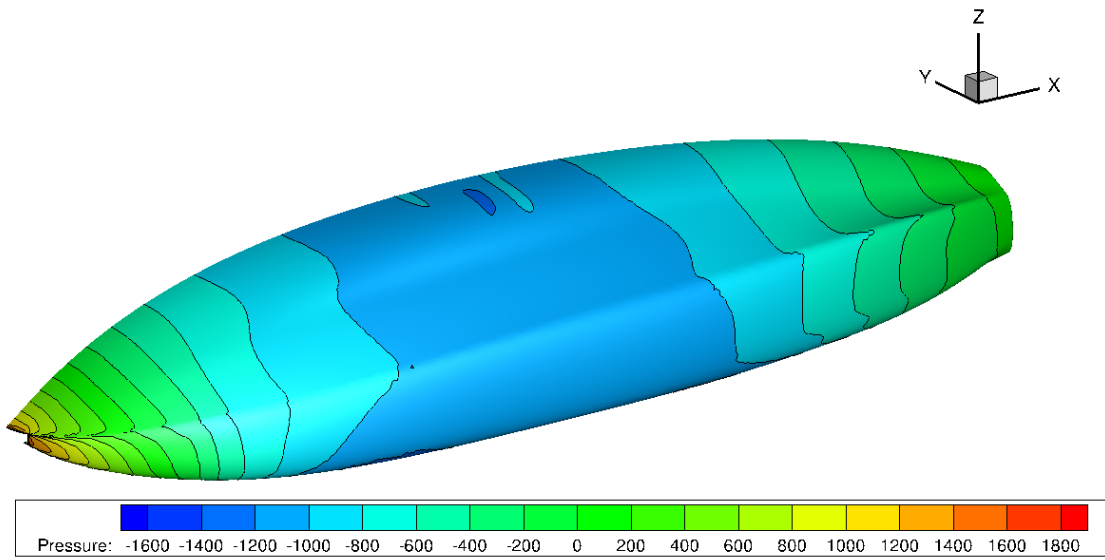


Figure 6.19: Relative Pressure 3D View Version A

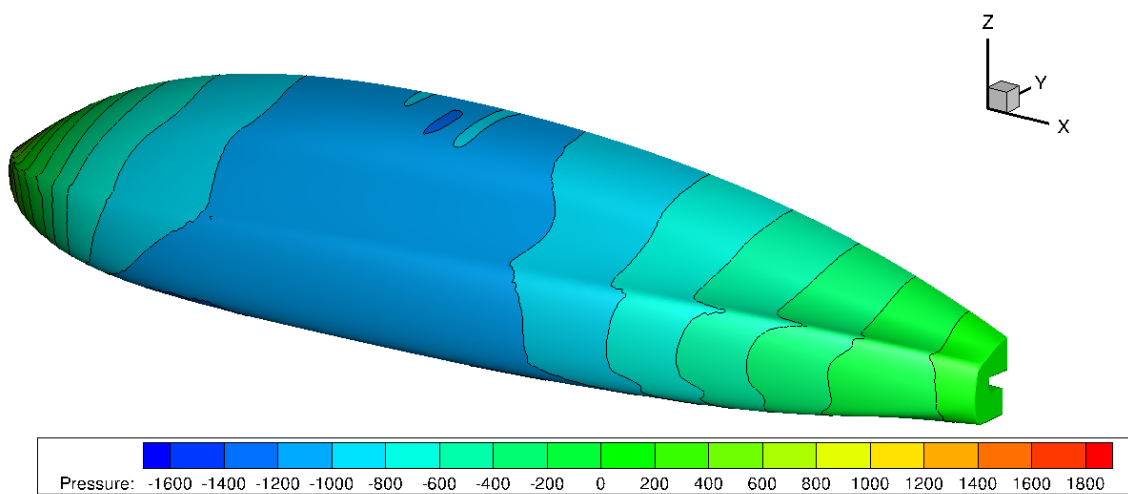


Figure 6.20: Relative Pressure 3D View Version A

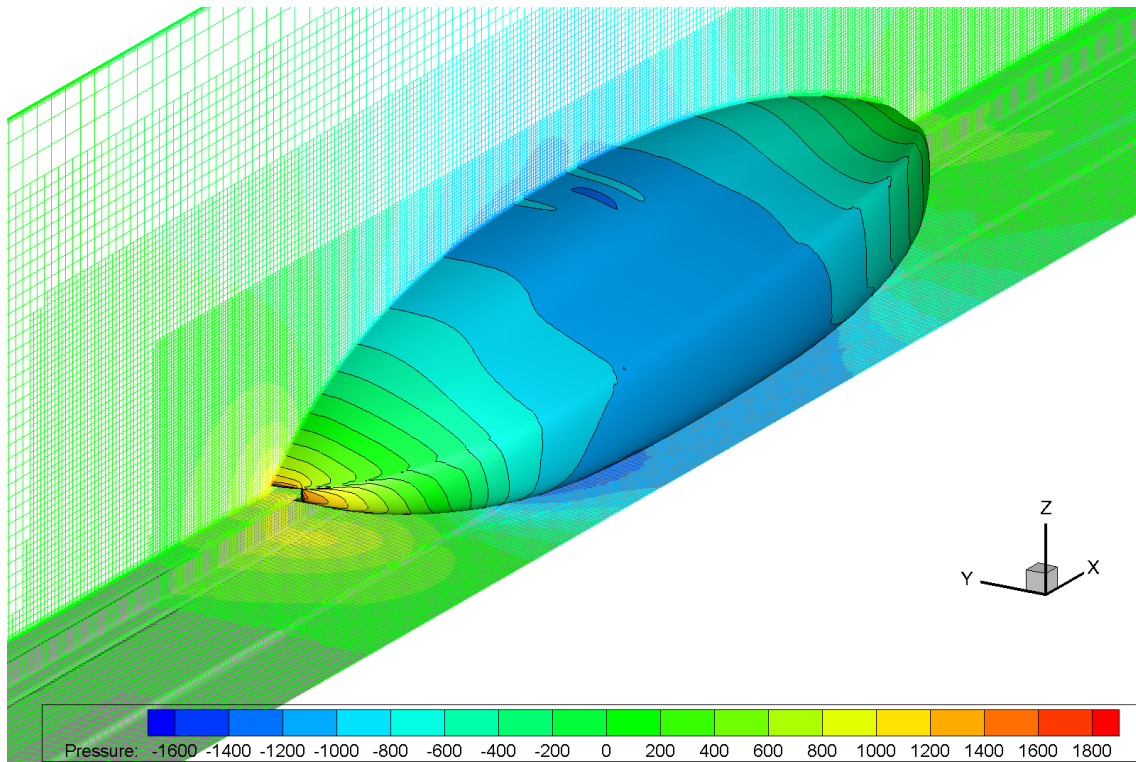


Figure 6.21: Relative Pressure 3D View Version A

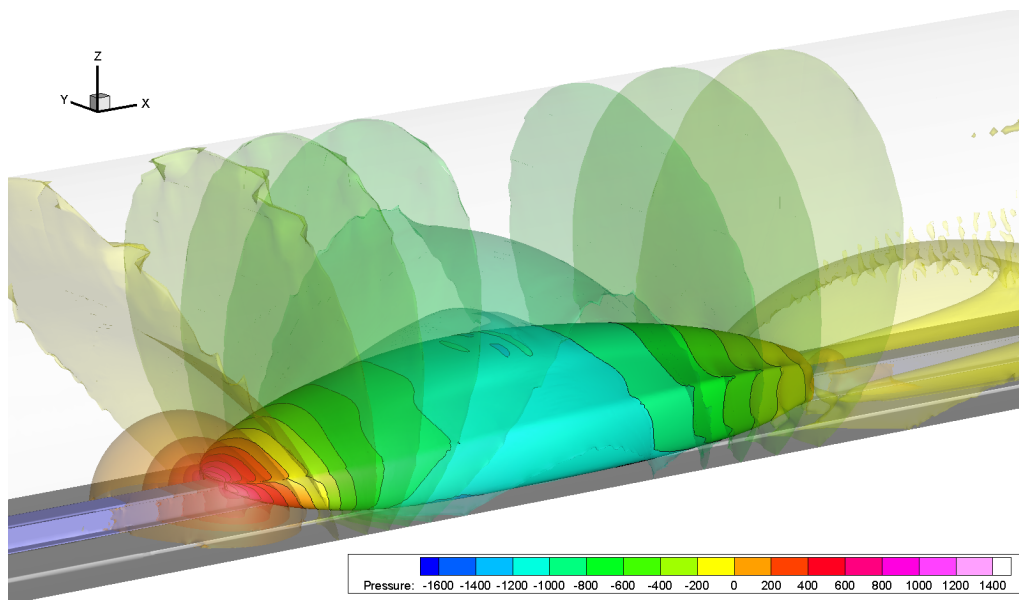


Figure 6.22: Relative Pressure 3D View Version A

The plots show that there is a huge pressure gradient on the surface as long as the cross section area increases in the x-direction. When the cross section area decreases the pressure increases. This phenomenon has been discussed with the Bernoulli equation. At the stagnation point the highest pressure occurs.

Relative Pressure Version B

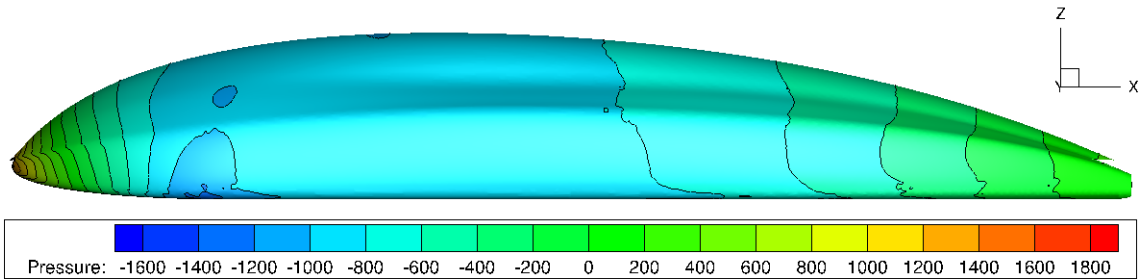


Figure 6.23: Relative Pressure Side View Version B

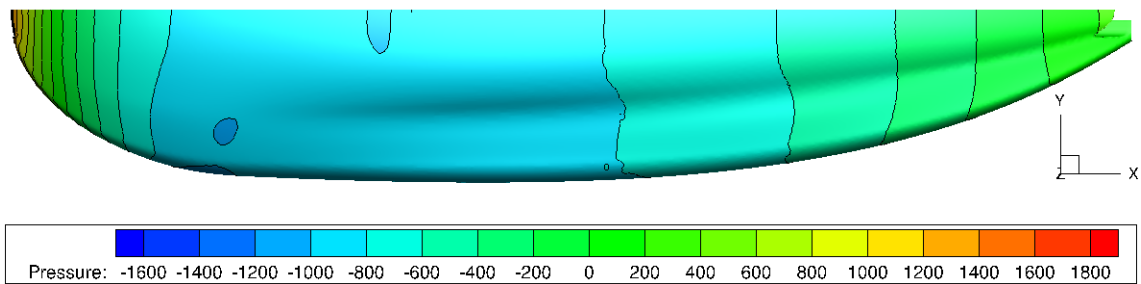


Figure 6.24: Relative Pressure Top View Version B

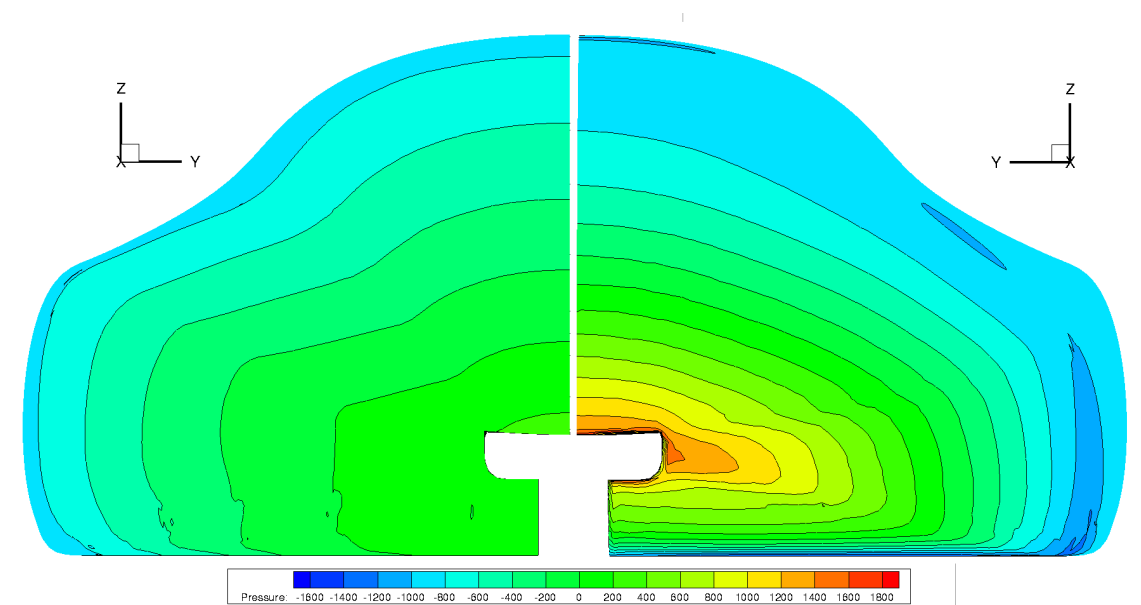


Figure 6.25: Relative Pressure Front View (right) and Rear View (left) of Version B

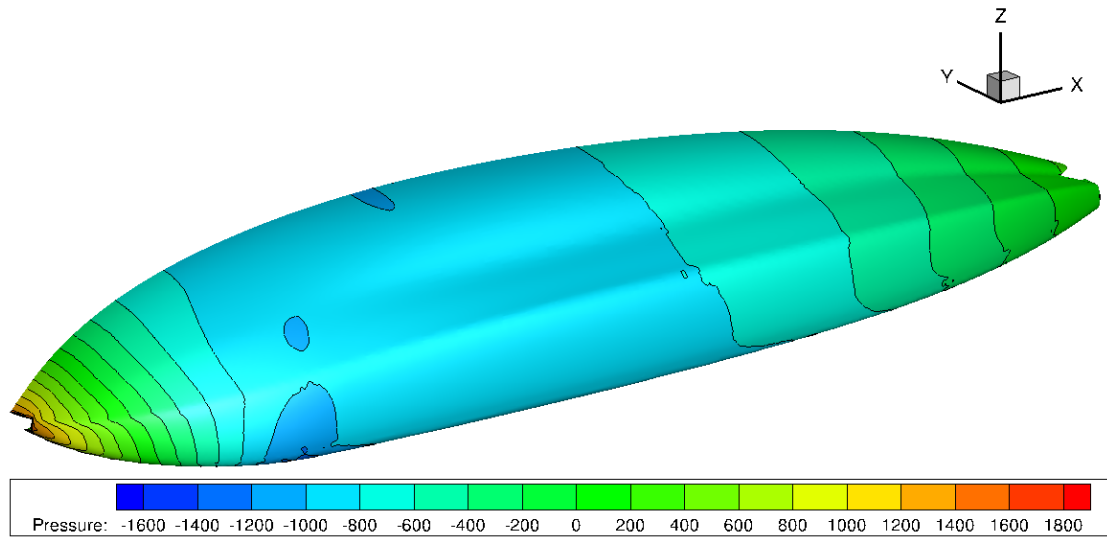


Figure 6.26: Relative Pressure 3D View Version B

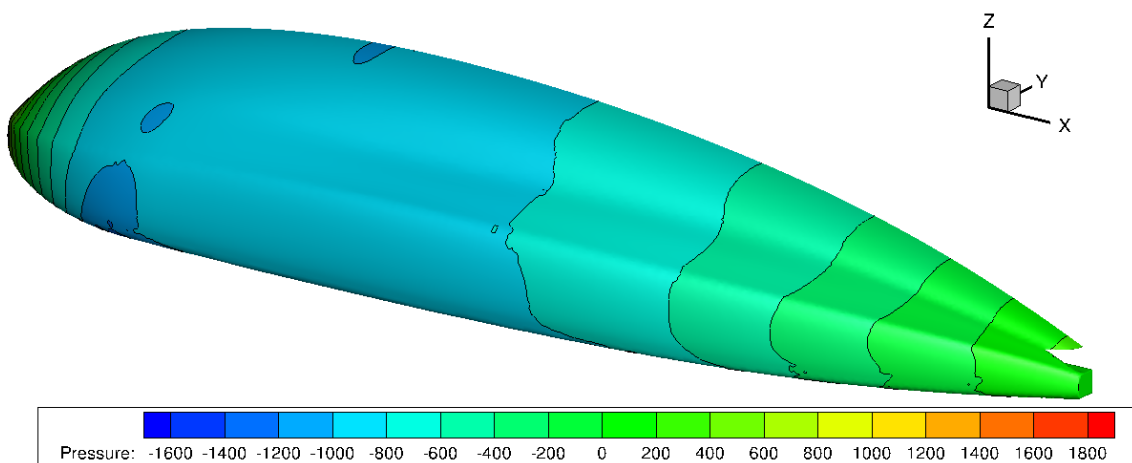


Figure 6.27: Relative Pressure 3D View Version B



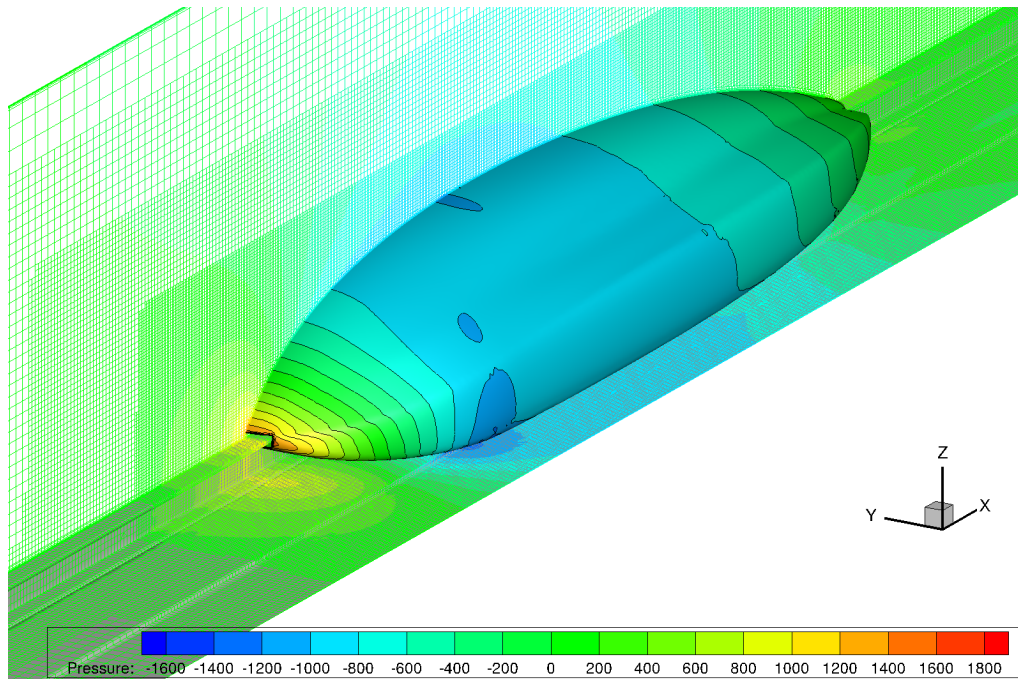


Figure 6.28: Relative Pressure 3D View Version B

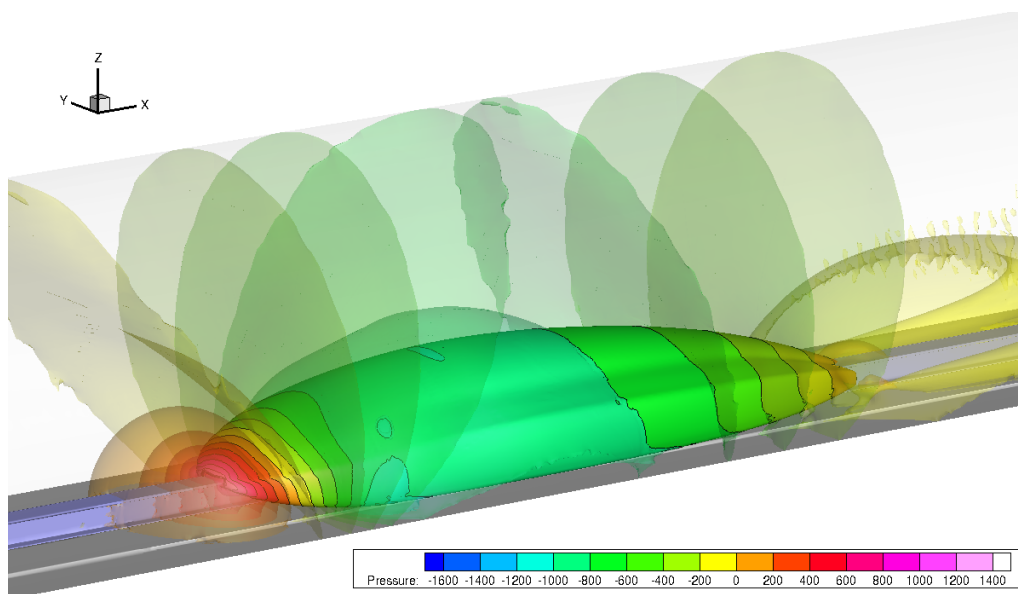


Figure 6.29: Relative Pressure 3D View Version B

The plots show that there is a huge pressure gradient on the surface as long as the cross section area increases in the x-direction. When the cross section area decreases the pressure increases. This phenomenon has been discussed with the Bernoulli equation. At the stagnation point the highest pressure occurs.

Compared to Version A, Version B has a smaller pressure gradient and shows therefore the better performance.



The following visualizations show the skin friction coefficient of Version A and Version B. All visualizations are obtained for a speed of 450 m/s and a pressure of 0.15 bar set as reference values.

### Skin Friction Coefficient Version A

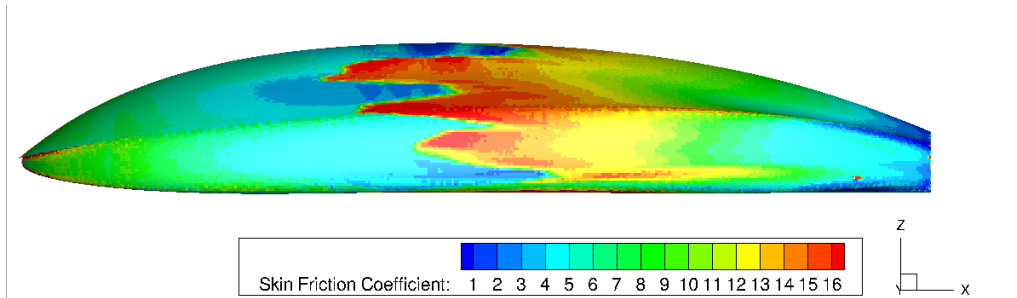


Figure 6.30: Skin Friction Coefficient Side View Version A

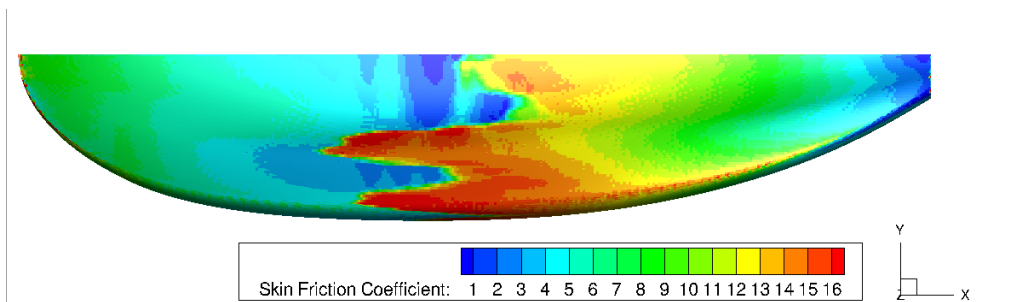


Figure 6.31: Skin Friction Coefficient Top View Version A

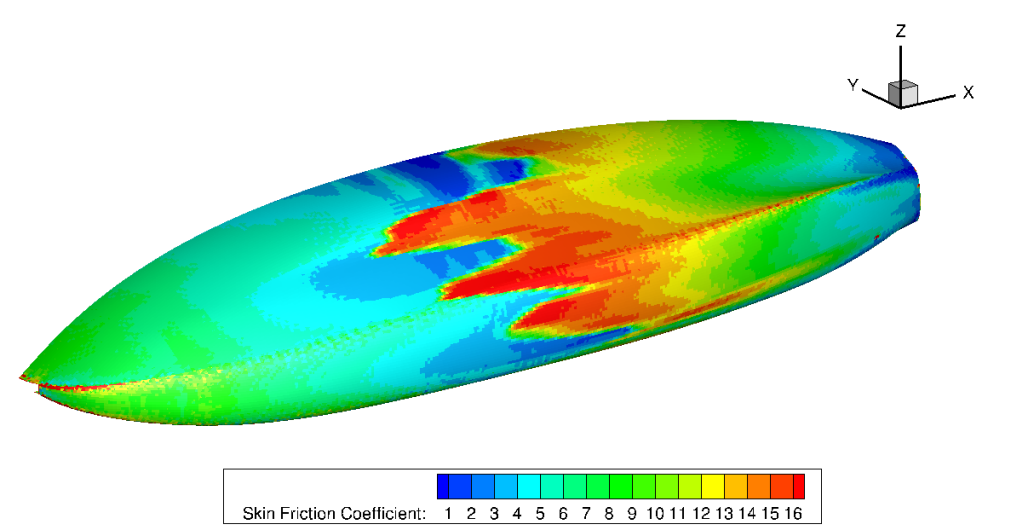


Figure 6.32: Skin Friction Coefficient 3D View Version A

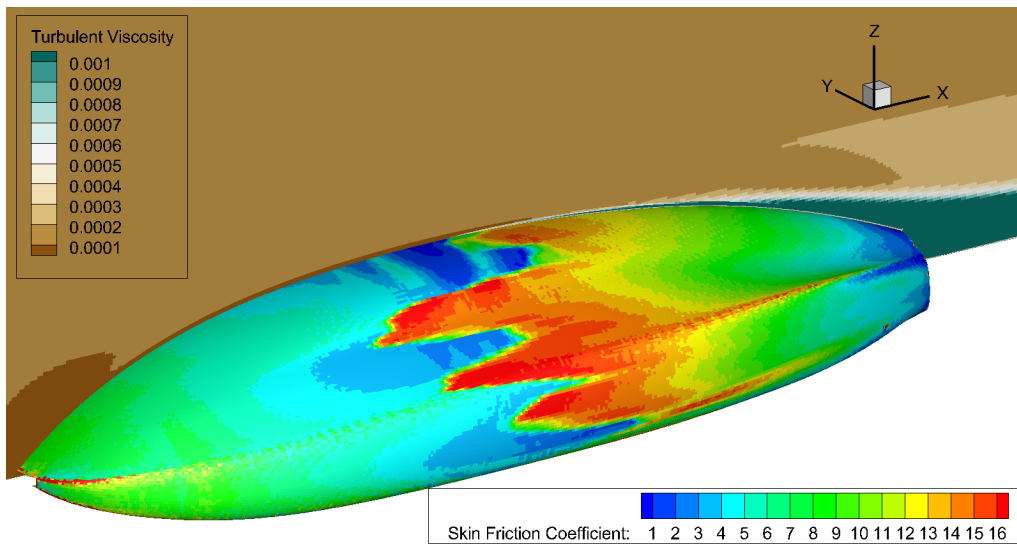


Figure 6.33: Skin Friction Coefficient 3D View Version A

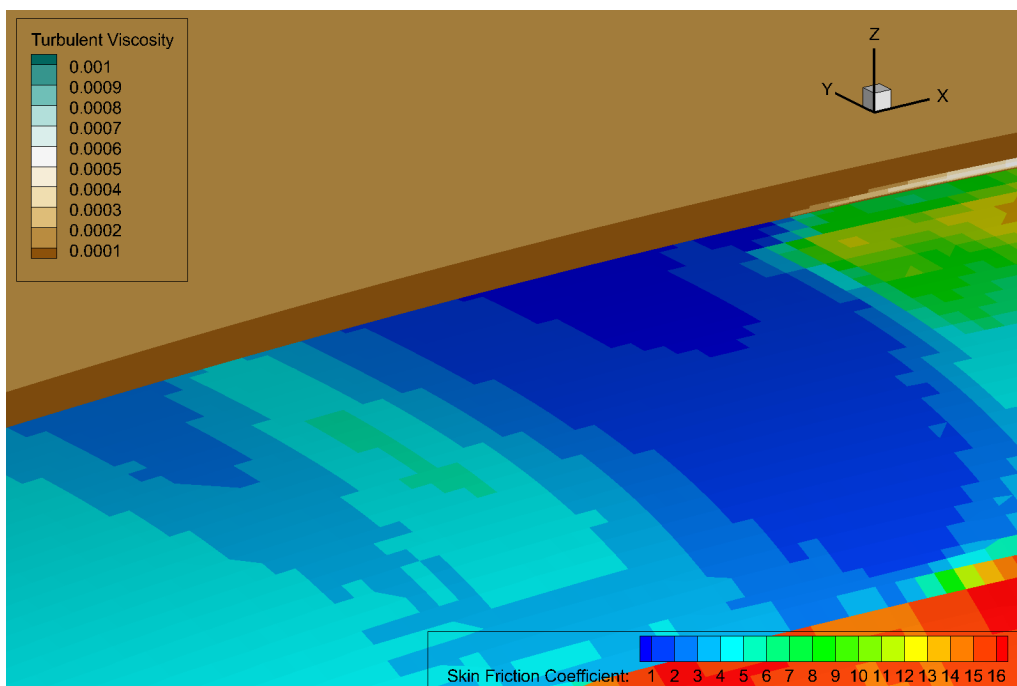


Figure 6.34: Skin Friction Coefficient 3D View Version A - zoomed in

As it can be seen in the plots, the skin friction coefficient is huge on the side and top surface of the pod. This is not a desirable result. There should be a smooth transition.

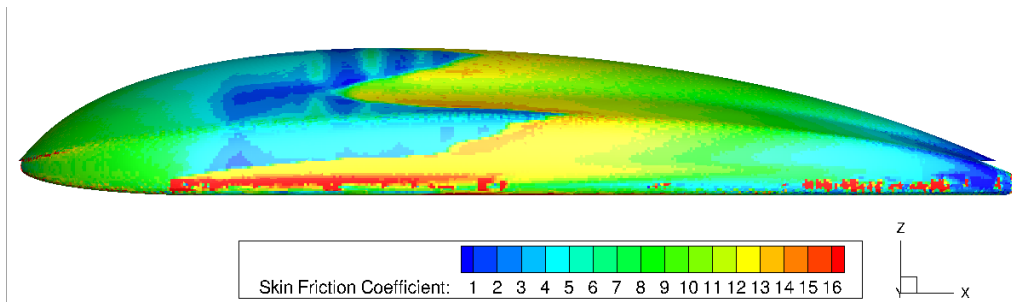
**Skin Friction Coefficient Version B**

Figure 6.35: Skin Friction Coefficient Side View Version B

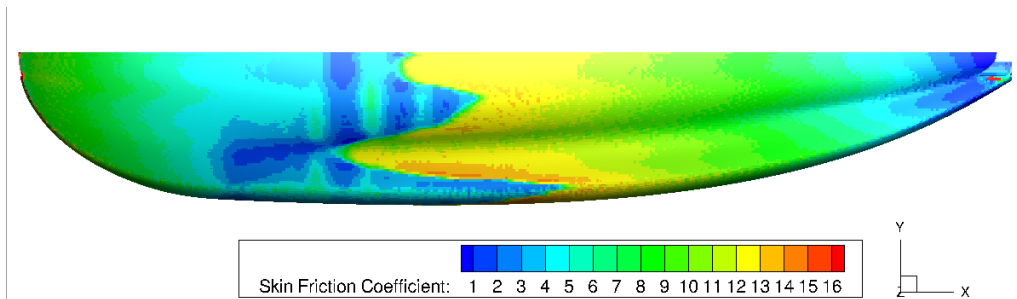


Figure 6.36: Skin Friction Coefficient Top View Version B

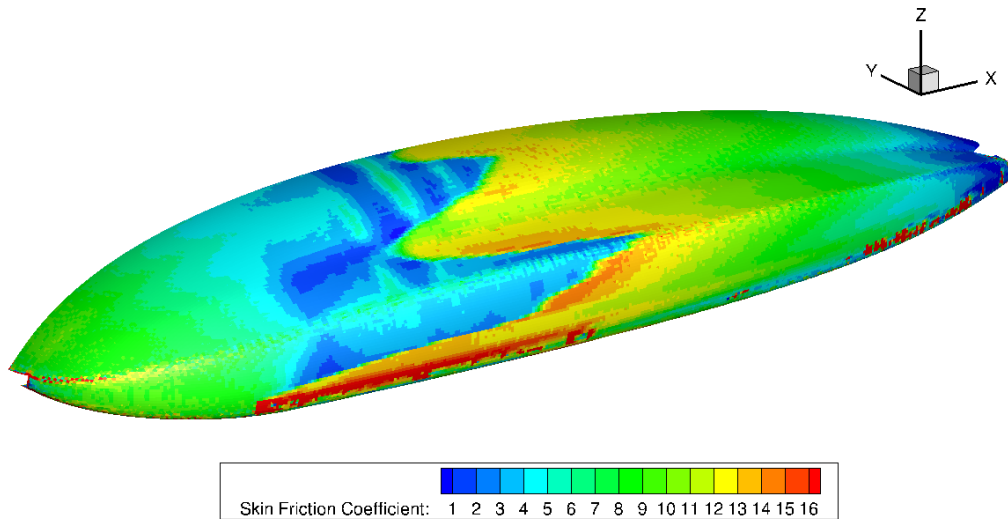


Figure 6.37: Skin Friction Coefficient 3D View Version B

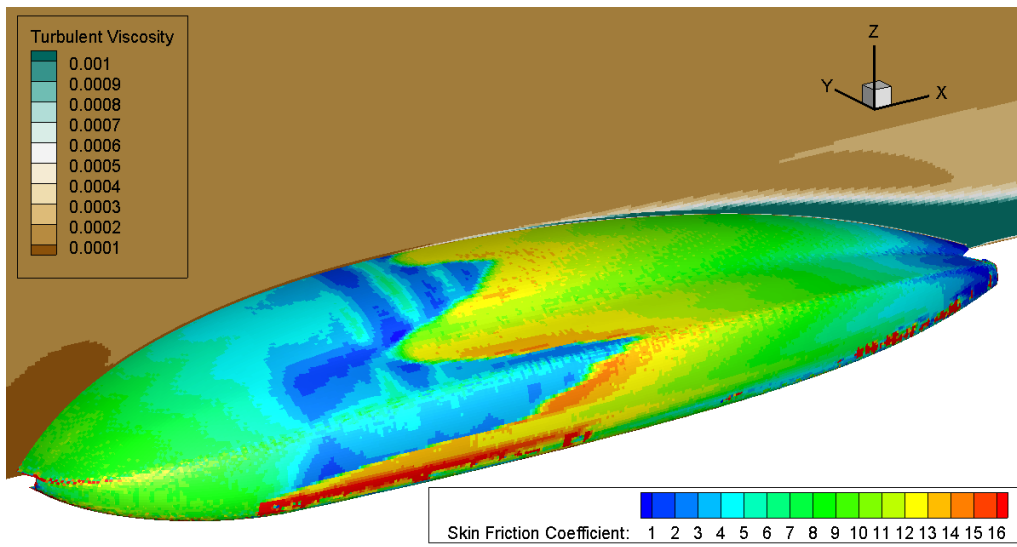


Figure 6.38: Skin Friction Coefficient 3D View Version B

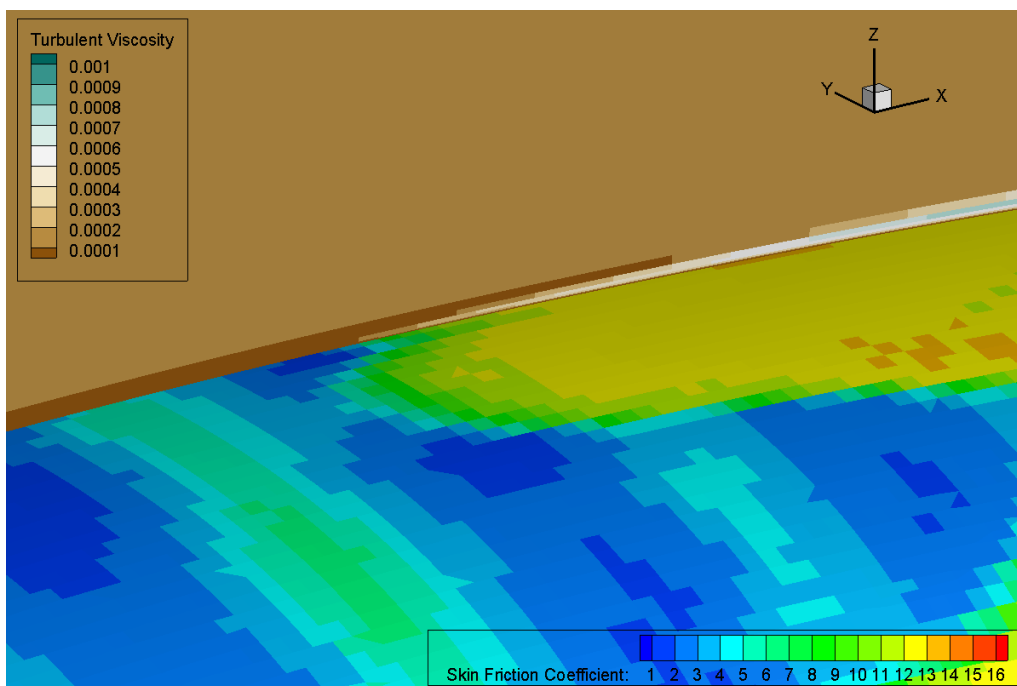


Figure 6.39: Skin Friction Coefficient 3D View Version B - zoomed in

As it can be seen in the plots, the skin friction coefficient is only huge on the lower side surface of the pod. The top side shows now a smooth transition. Compared to Version A this result is much better.

The following visualizations show the streamlines with the velocity magnitude of Version A and Version B. All visualizations are obtained for a speed of 450 m/s and a pressure of 0.15 bar set as reference values.

### Streamlines Version A

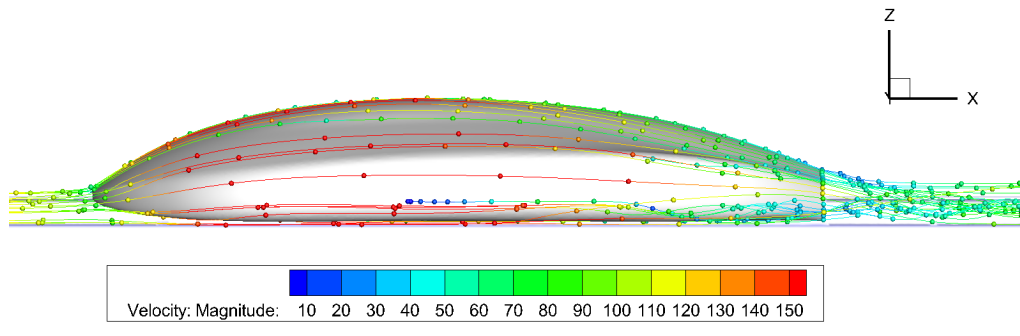


Figure 6.40: Streamlines Version A

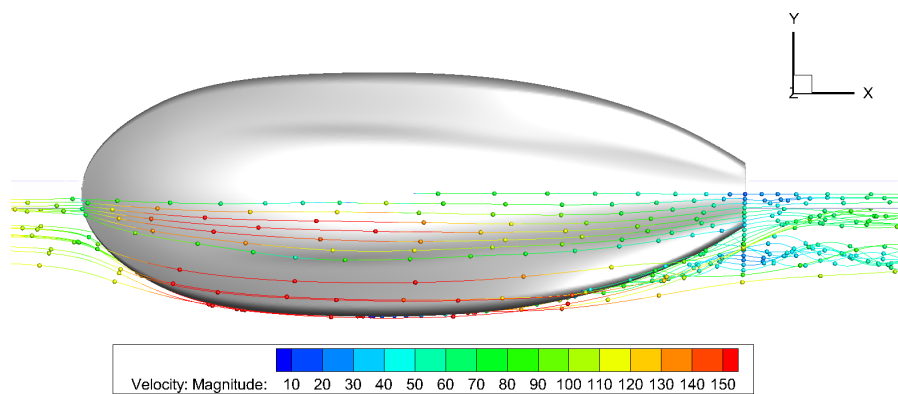


Figure 6.41: Streamlines Version A

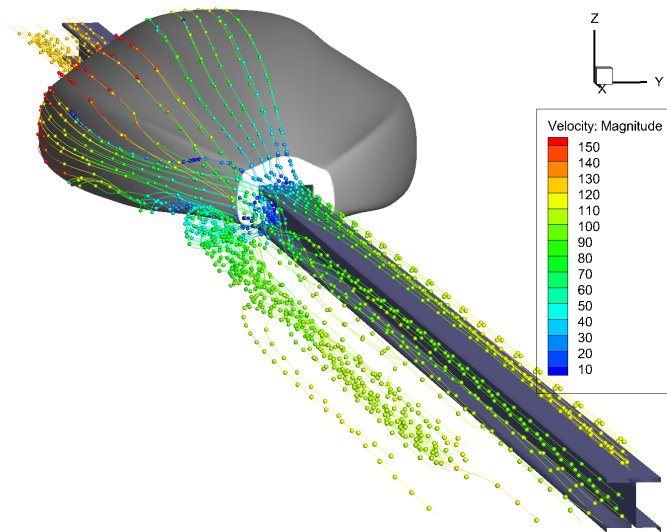


Figure 6.42: Streamlines Version A

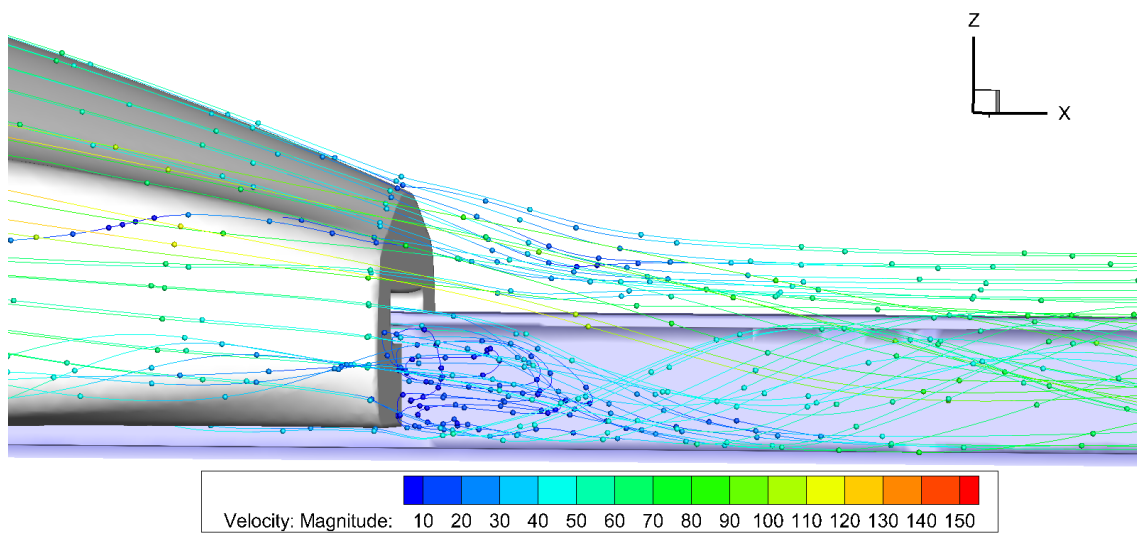


Figure 6.43: Streamlines Version A

The flow is attached in the front, side and top part of the shell. However, it separates at the rear side of Version A.

### Streamlines Version B

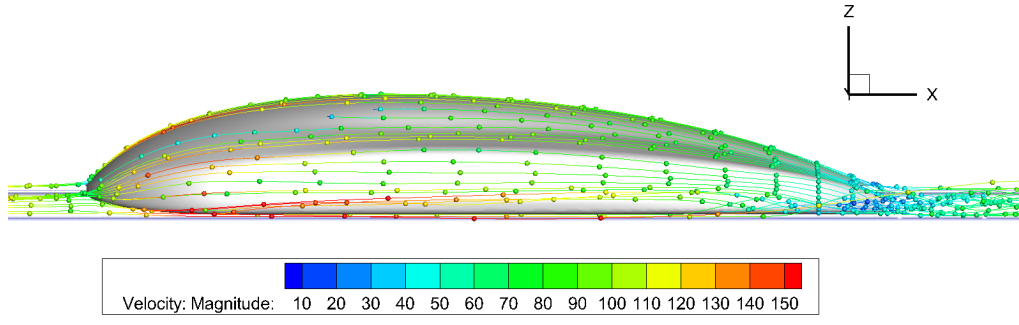


Figure 6.44: Streamlines Version B

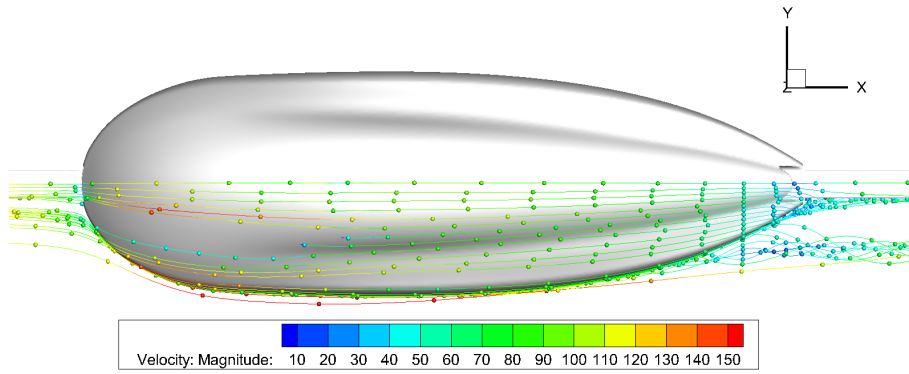


Figure 6.45: Streamlines Version B

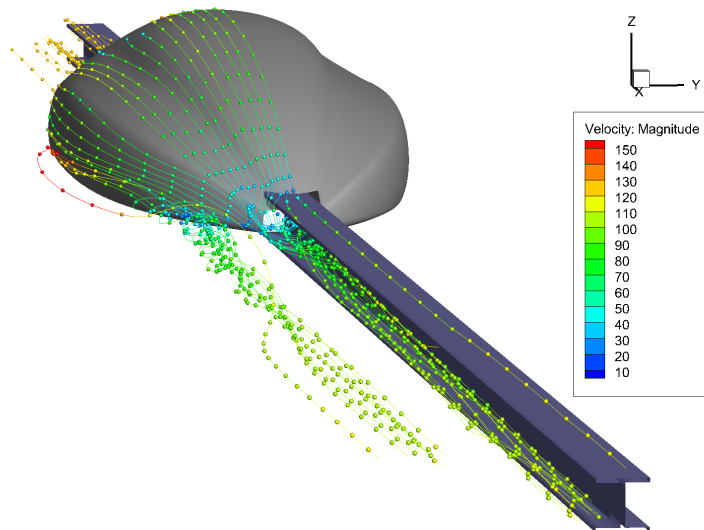


Figure 6.46: Streamlines Version B

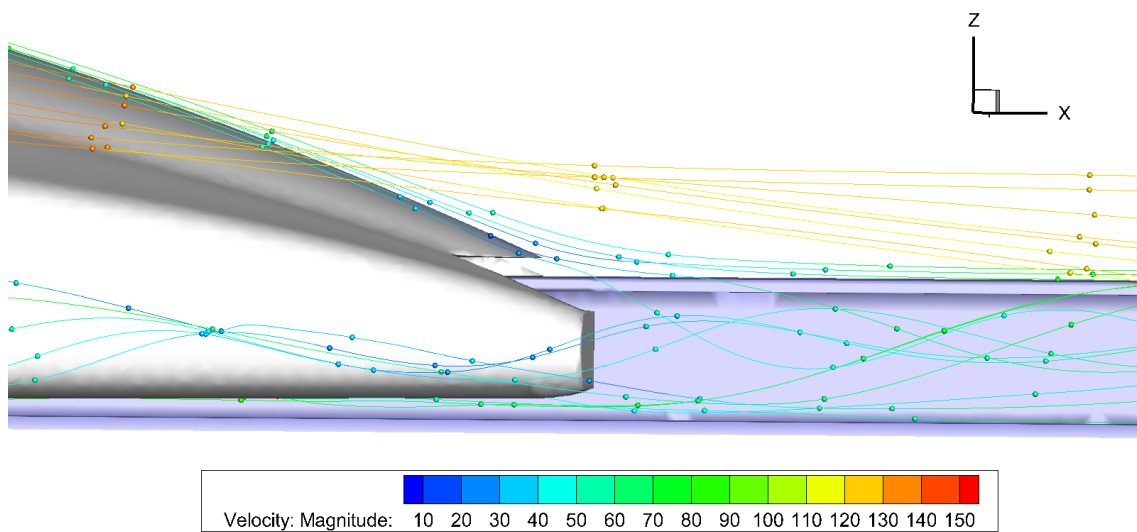


Figure 6.47: Streamlines Version B

The flow is attached in the front, side and top part of the shell. Compared to Version A, there is less flow separation at the rear side. Therefore, Version B shows a better result.



The following visualizations are velocity plots of Version A and Version B. All visualizations are obtained for a speed of 450 m/s and a pressure of 0.15 bar set as reference values.

### Velocity Version A

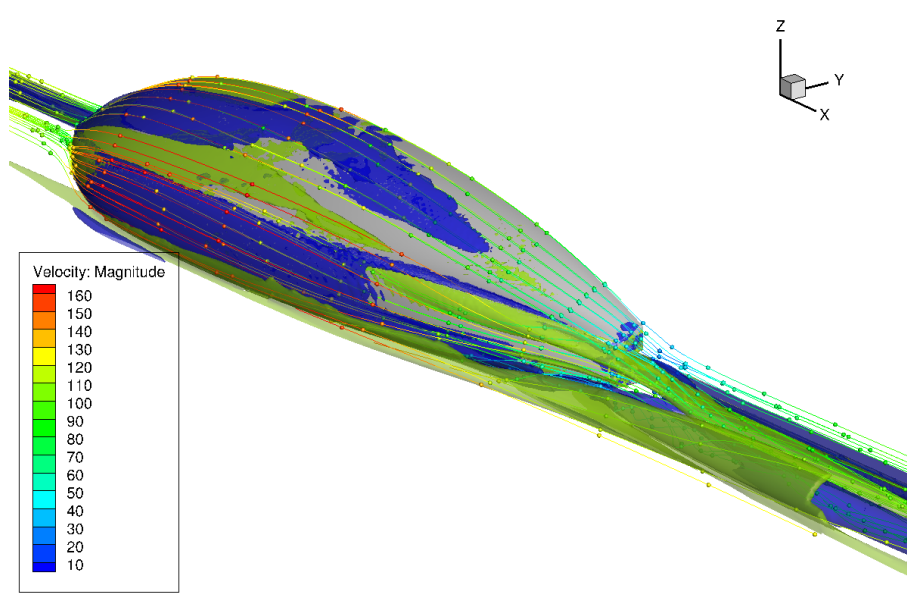


Figure 6.48: Velocity Field Version A

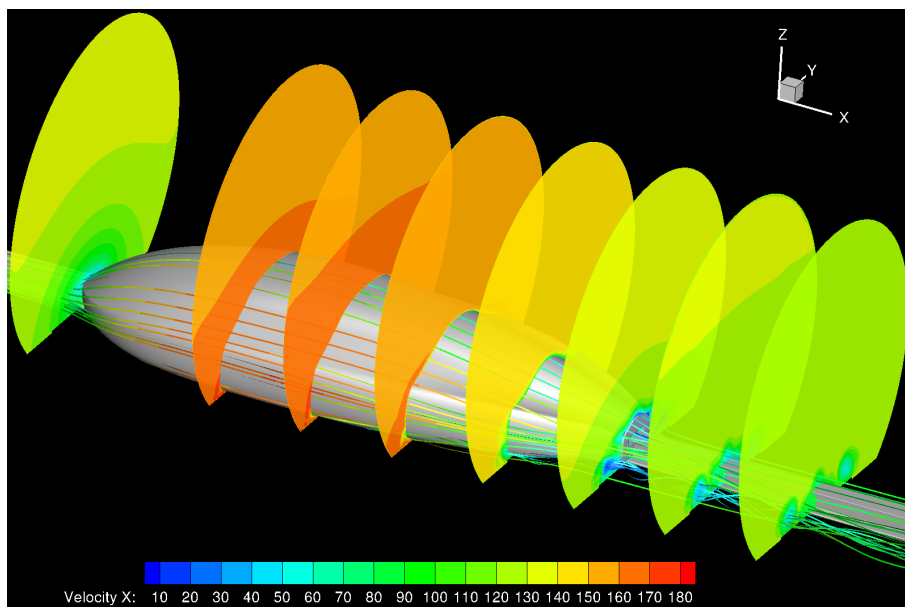


Figure 6.49: Velocity Field Version A

### Velocity Version B

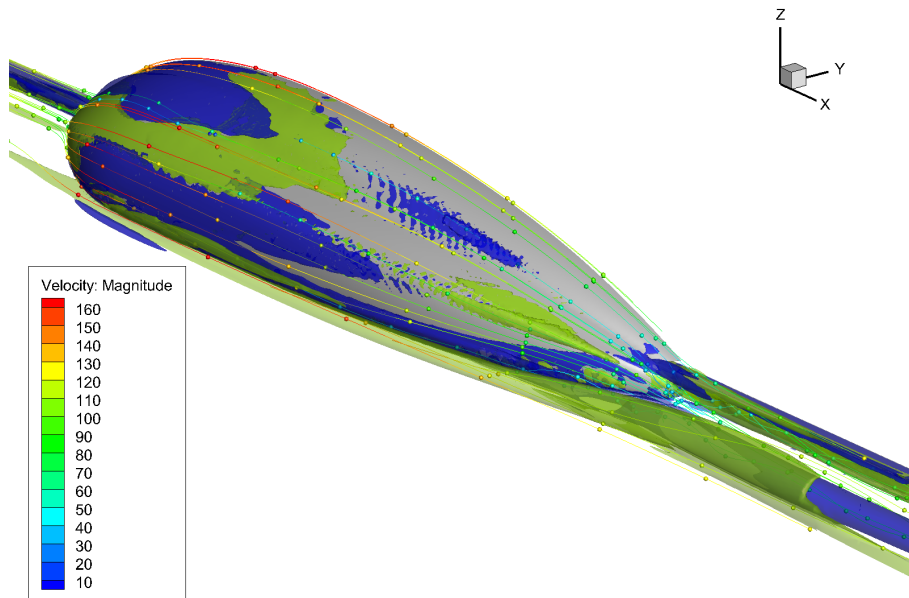


Figure 6.50: Velocity Field Version B

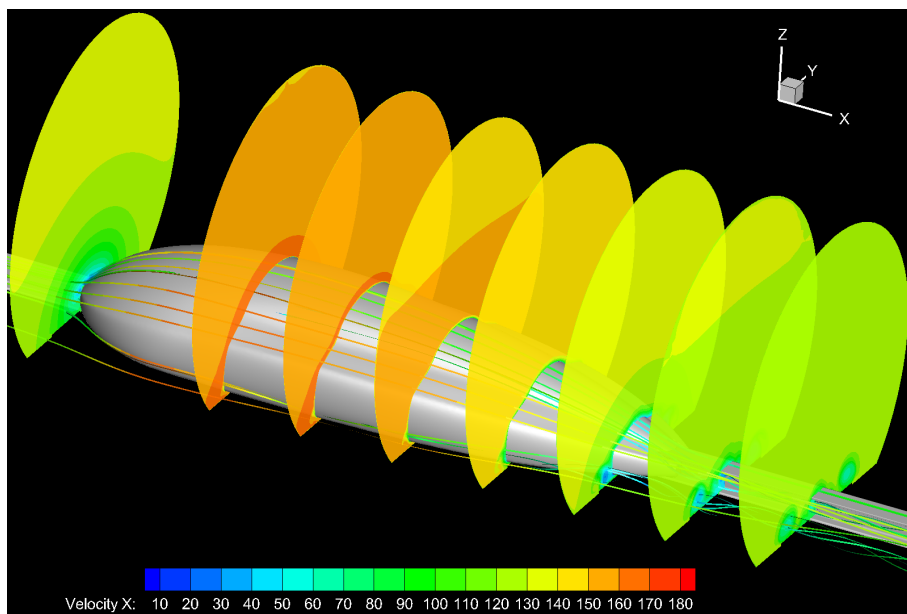


Figure 6.51: Velocity Field Version B

### 6.3.5 Conclusion

Two different geometric versions have been simulated and analyzed. One version is chosen as the final version for the Swissloop team. In this section, it is outlined which geometry was chosen and what reasons led to this decision.

#### Geometry

Version A is shorter than Version B, namely 27 centimeters. Version A is 9 centimeters wider, 2 centimeters higher and its frontal surface area is 0.055 square meters bigger. The blockage ratio of Version A is therefore higher as well. The blockage ratio of Version A is 0.190 and the blockage ratio of Version B is 0.166. This is a difference of 0.024 and 14.5 percent.

As a smaller cross section area corresponds to a smaller drag force and a smaller blockage ratio, a small cross section area is desirable. Version B has a smaller cross section area than version A and is therefore preferred in terms of geometry.

#### Forces

As the goal of the thesis is to reduce the drag force of the pod, the smallest possible drag force is aimed at. Version A has a total drag force of 74.58 newton. Version B has total drag force of 60.59 newton. The drag force of Version B is 19 percent lower.

It was shown that no lift force had an influence on the pod's performance as it could always be neglected. Therefore, only the drag force is taken into account.

Hence, Version B is preferred.

#### Plots

The plots show what can already be deduced by the force results. Version B shows a smaller pressure gradient and therefore better pressure distribution than Version A. Also the plots of skin friction coefficient show much better results and a smoother distribution for Version B than for Version A.

Hence, Version B is preferred.

Besides Version A and Version B there were 23 other versions that were simulated. Version B showed the best results. Therefore, Version B was chosen as the final geometry for the Swissloop team.

### 6.3.6 General Analysis of the Final Version

The following Figures with a translucent shell show the pod interior with all technical components. It can be seen how tight the shell's shape wraps around the inner geometric constraints.



Figure 6.52: Final Version

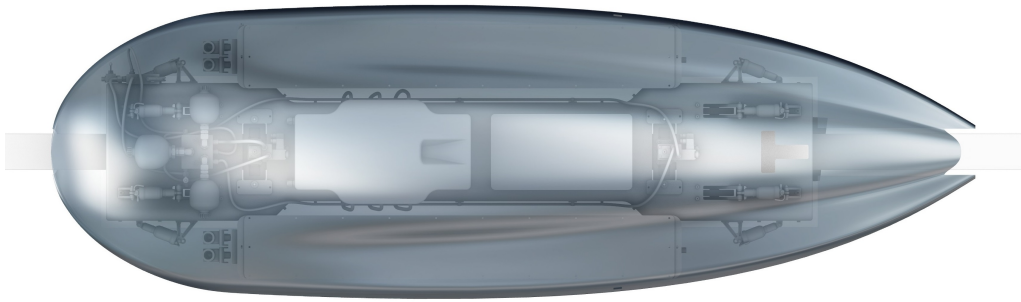


Figure 6.53: Final Version

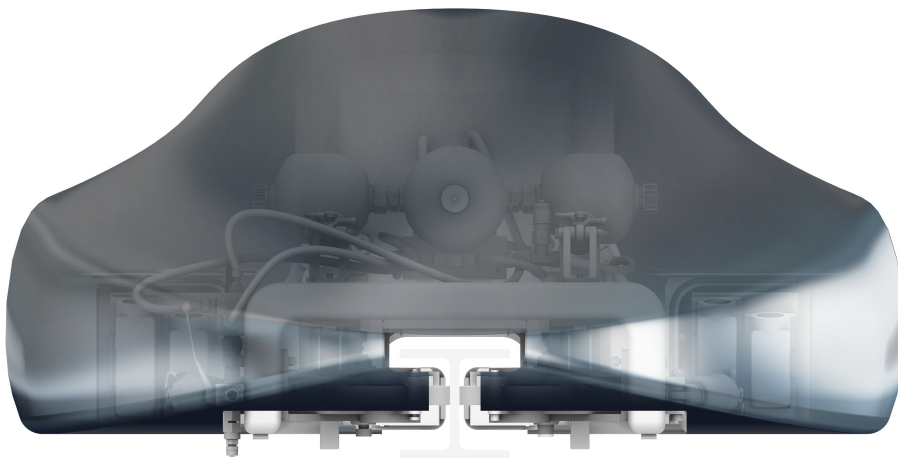


Figure 6.54: Final Version

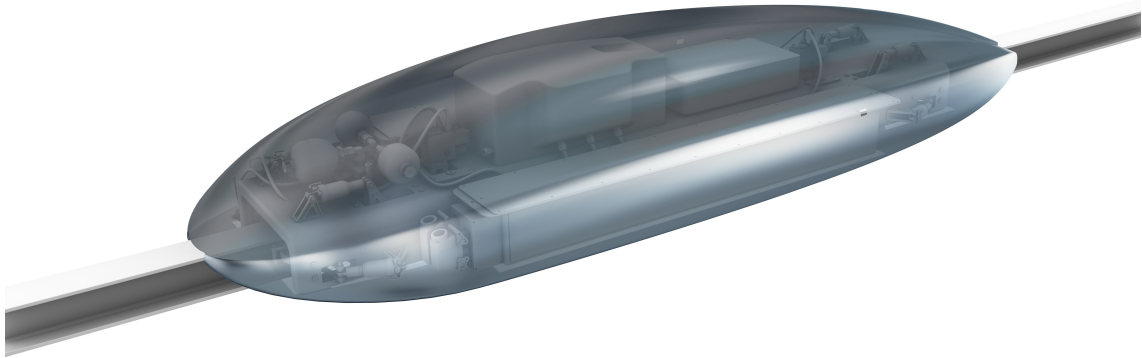


Figure 6.55: Final Version

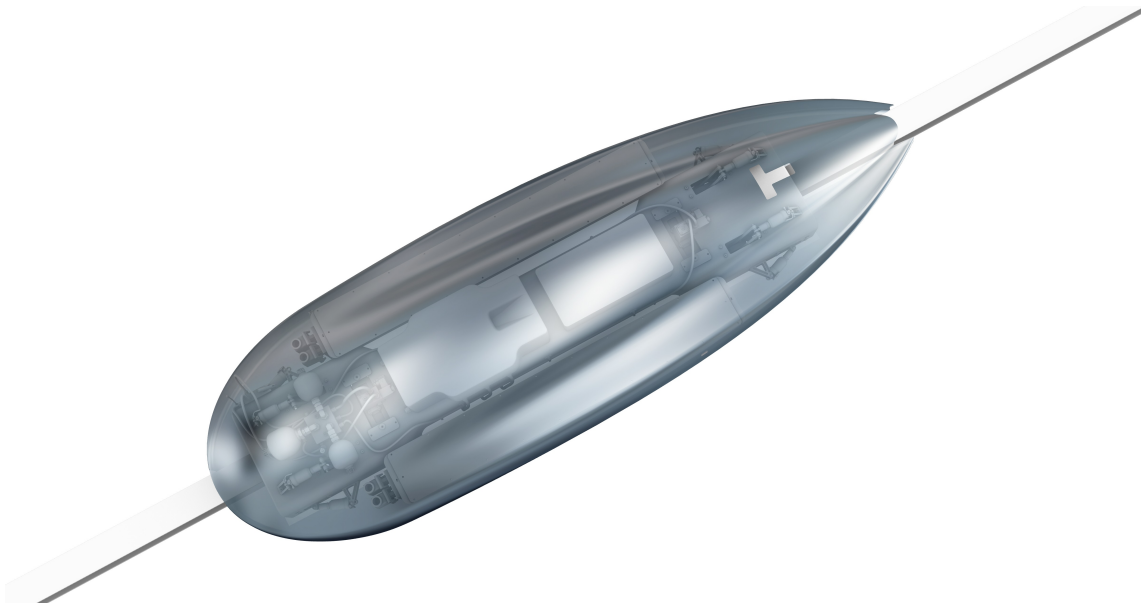


Figure 6.56: Final Version

## 6.4 Final Version

Version B was chosen as the final shell geometry. This version is chosen and manufactured by the Swissloop team and will perform in the Hyperloop Pod Competition 2019.

The final version was further simulated at different pressure conditions to investigate how this shape behaves at different pressures. The results are presented in this chapter.

In the following sections, the final version is analyzed at three different pressure conditions. All other conditions stay the same. First, a run in open air (atmospheric pressure) is carried out, second at 0.01 bar and third at 0.001 bar. The last condition at 1 millibar is the main idea of the Hyperloop concept.

### 6.4.1 Results in Open-Air (Atmospheric Pressure)

To assure a proper comparison with the following simulations at 0.01 bar and 0.001 bar, a logarithmic scale is maintained. Therefore, for simulating at open-air conditions, not the atmospheric pressure of 1.013 bar but a simple number of 1 bar was chosen. The difference to atmospheric condition is therefore 1 percent.

At a pressure of 1 bar, the total drag force in the x-direction is 412.1 newton and the total lift force in the z-direction is 301.4 newton.  $C_{total}$ ,  $C_f$  and  $C_p$  values are calculated from  $F_{total}$ ,  $F_{friction}$  and  $F_{pressure}$  as it was outlined in chapter 2.  $C_{total}$  for drag is 0.12 and  $C_{total}$  for lift is 0.09. The values are shown in Table 6.8. Note that the y-direction can be ignored as the pod is simulated as a half-model with the xz-plane as the symmetry plane. The unit of all forces is Newton whereas the values  $C_{total}$ ,  $C_f$  and  $C_p$  are dimensionless. It holds:  $F_{total} = F_{friction} + F_{pressure}$  and  $C_{total} = C_f + C_p$ .

	Drag (x-direction)	Lift (z-direction)
$F_{total}$ [N]	412.1	301.4
$F_{friction}$ [N]	231.0	1.0
$F_{pressure}$ [N]	181.1	300.4
$C_{total}$	0.12	0.09
$C_f$	0.07	0.00
$C_p$	0.05	0.09

Table 6.8: Computed Forces and C-values at 1 bar

It may be deduced from these results that the total drag force is higher than the total lift force. Out of the total drag force, the friction force is 56 percent and the pressure force is 44 percent. This amounts to a difference of 12 percent.

It is noted that the lift force is positive. It needs to be investigated if there is a momentum acting on the pod as the lift force does not act at the center of mass. The center of mass is expected to lie in the middle of the pod ( $x = 1.64$  meters). As it was shown in the previous chapter the low pressure area lies in the front half of the pod and therefore the lift force does not act at the center of mass.

The pod's total mass is 200 kilograms which corresponds to 1962 newton weight force. The lift force has a value of 301.4 newton. Compared to the weight force this is 13.3 percent. This value cannot be neglected. It shows that in open-air lift force could be used to improve suspension.

Table 6.9 shows an overview of the grid parameters, prism layers, and flow parameters for the present calculation.

Grid parameters:	
Cells	4040105
Faces	12018556
Prism Layers:	
Number	10
Stretching	1.8
Thickness [m]	0.014
Flow parameters:	
Re	3.79E+06
Ma	0.358

Table 6.9: Grid parameters, Prism Layers, and Flow parameters at 1 bar

In the present calculation the number of cells is 4040105 and the number of faces amounts to 12018556. There are 10 prism layers with a stretching factor of 1.8 and a total thickness of 0.014 meters. The Reynolds number for the set condition is  $3.79 \times 10^6$  and the Mach number for this condition is 0.358.

The geometry of Version B was already simulated and presented in the previous chapter. As the same meshing was used, the grid parameters and the prism layer layup stay the same. Also the Mach number remains unchanged as the speed of the pod and the speed of sound do not change. The Reynolds number has a different value as it depends on density. Density is proportional to pressure. If the pressure increases also the density increases and therefore the Reynolds number increases.

The following Figure 6.57 shows the converged Force Monitor Plot at a pressure of 1 bar. The number of time steps for the computation is 24000.

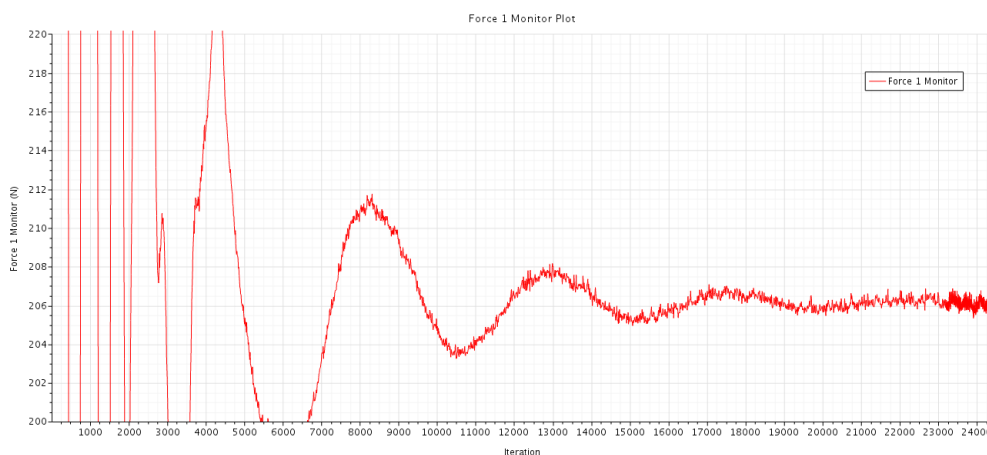


Figure 6.57: Force Monitor Plot of Version B at 1 bar

The simulation was manually terminated at a time step of 24000. The result was still oscillating with an amplitude of  $\pm 0.75$  newton. However this small oscillation can be neglected. The result has converged.



### 6.4.2 Results at 0.01 bar

At a pressure of 0.01 bar, the total drag force in the x-direction is 8.17 newton and the total lift force in the z-direction is 13.2 newton.  $C_{total}$ ,  $C_f$  and  $C_p$  values are calculated from  $F_{total}$ ,  $F_{friction}$  and  $F_{pressure}$  as it was outlined in chapter 2.  $C_{total}$  for drag is 0.24 and  $C_{total}$  for lift is 0.38. The values are shown in Table 6.10. Note that the y-direction can be ignored as the pod is simulated as a half-model with the xz-plane as the symmetry plane. The unit of all forces is Newton whereas the values  $C_{total}$ ,  $C_f$  and  $C_p$  are dimensionless. It holds:  $F_{total} = F_{friction} + F_{pressure}$  and  $C_{total} = C_f + C_p$ .

	Drag (x-direction)	Lift (z-direction)
$F_{total}$ [N]	8.17	13.20
$F_{friction}$ [N]	2.83	0.17
$F_{pressure}$ [N]	5.33	13.03
$C_{total}$	0.24	0.38
$C_f$	0.08	0.00
$C_p$	0.15	0.38

Table 6.10: Computed Results at 0.01 bar

It may be deduced from these results that the total drag force is smaller than the total lift force. Out of the total drag force, the friction force is 35 percent and the pressure force is 65 percent. This amounts to a difference of 30 percent.

It is noted that the lift force is positive. It needs to be investigated if there is a momentum acting on the pod as the lift force does not act at the center of mass. The center of mass is expected to lie in the middle of the pod ( $x = 1.64$  meters). As it was shown in the previous chapter the low pressure area lies in the front half of the pod and therefore the lift force does not act at the center of mass.

The pod's total mass is 200 kilograms which corresponds to 1962 newton weight force. The lift force has a value of 13.2 newton. Compared to the weight force this is 0.7 percent and this influence can be neglected. Therefore, there is no momentum due to lift force.

Table 6.11 shows an overview of the grid parameters, prism layers, and flow parameters for the present calculation.

Grid parameters:	
Cells	4040105
Faces	12018556
Prism Layers:	
Number	10
Stretching	1.8
Thickness [m]	0.014
Flow parameters:	
Re	3.79E+04
Ma	0.358

Table 6.11: Grid parameters, Prism Layers, and Flow parameters at 0.01 bar

In the present calculation the number of cells is 4040105 and the number of faces amounts to 12018556. There are 10 prism layers with a stretching factor of 1.8 and a total thickness of 0.014 meters. The Reynolds number for the set condition is  $3.79 \times 10^4$  and the Mach number for this condition is 0.358.

The geometry of Version B was already simulated and presented in the previous chapter. As the same meshing was used, the grid parameters and the prism layer layup stay the same. Also the Mach number remains unchanged as the speed of the pod and the speed of sound do not change. The Reynolds number has a different value as it depends on density. Density is proportional to pressure. If the pressure decreases also the density decreases and therefore the Reynolds number decreases.

The following Figure 6.58 shows the converged Force Monitor Plot at a pressure of 0.01 bar. The number of time steps for the computation is 75000.



Figure 6.58: Force Monitor Plot of Version B at 0.01 bar

It took much longer for the result to converge than for the other simulated pressures. The simulation was manually terminated at a time step of 75000. The result was still oscillating with an amplitude of  $\pm 0.125$  newton. However, this small oscillation can be neglected. The result has converged.

### 6.4.3 Results at 0.001 bar (Hyperloop concept Condition)

At a pressure of 0.001 bar, the total drag force in the x-direction is 2.28 newton and the total lift force in the z-direction is 4.32 newton.  $C_{total}$ ,  $C_f$  and  $C_p$  values are calculated from  $F_{total}$ ,  $F_{friction}$  and  $F_{pressure}$  as it was outlined in chapter 2.  $C_{total}$  for drag is 0.66 and  $C_{total}$  for lift is 1.25. The values are shown in Table 6.12. Note that the y-direction can be ignored as the pod is simulated as a half-model with the xz-plane as the symmetry plane. The unit of all forces is Newton whereas the values  $C_{total}$ ,  $C_f$  and  $C_p$  are dimensionless. It holds:  $F_{total} = F_{friction} + F_{pressure}$  and  $C_{total} = C_f + C_p$ .

	Drag (x-direction)	Lift (z-direction)
$F_{total}$ [N]	2.28	4.32
$F_{friction}$ [N]	1.03	0.07
$F_{pressure}$ [N]	1.25	4.25
$C_{total}$	0.66	1.25
$C_f$	0.30	0.02
$C_p$	0.36	1.23

Table 6.12: Computed Results at 0.001 bar

It may be deduced from these results that the total drag force is smaller than the total lift force. Out of the total drag force, the friction force is 45 percent and the pressure force is 55 percent. This amounts to a difference of 20 percent.

It is noted that the lift force is positive. It needs to be investigated if there is a momentum acting on the pod as the lift force does not act at the center of mass. The center of mass is expected to lie in the middle of the pod ( $x = 1.64$  meters). As it was shown in the previous chapter the low pressure area lies in the front half of the pod and therefore the lift force does not act at the center of mass.

The pod's total mass is 200 kilograms which corresponds to 1962 newton weight force. The lift force has a value of 4.32 newton. Compared to the weight force this is 0.2 percent and this influence can be neglected. Therefore, there is no momentum due to lift force.

Table 6.13 shows an overview of the grid parameters, prism layers, and flow parameters for the present calculation.

Grid parameters:	
Cells	4040105
Faces	12018556
Prism Layers:	
Number	10
Stretching	1.8
Thickness [m]	0.014
Flow parameters:	
Re	3.79E+03
Ma	0.358

Table 6.13: Grid parameters, Prism Layers, and Flow parameters at 0.001 bar

In the present calculation the number of cells is 4040105 and the number of faces amounts to 12018556. There are 10 prism layers with a stretching factor of 1.8 and a total thickness of 0.014 meters. The Reynolds number for the set condition is  $3.79 \times 10^3$  and the Mach number for this condition is 0.358.

The geometry of Version B was already simulated and presented in the previous chapter. As the same meshing was used, the grid parameters and the prism layer layup stay the same. Also the Mach number remains unchanged as the speed of the pod and the speed of sound do not change. The Reynolds number has a different value as it depends on density. Density is proportional to pressure. If the pressure decreases also the density decreases and therefore the Reynolds number decreases.

The following Figure 6.59 shows the converged Force Monitor Plot at a pressure of 0.15 bar. The number of time steps for the computation is 31000.

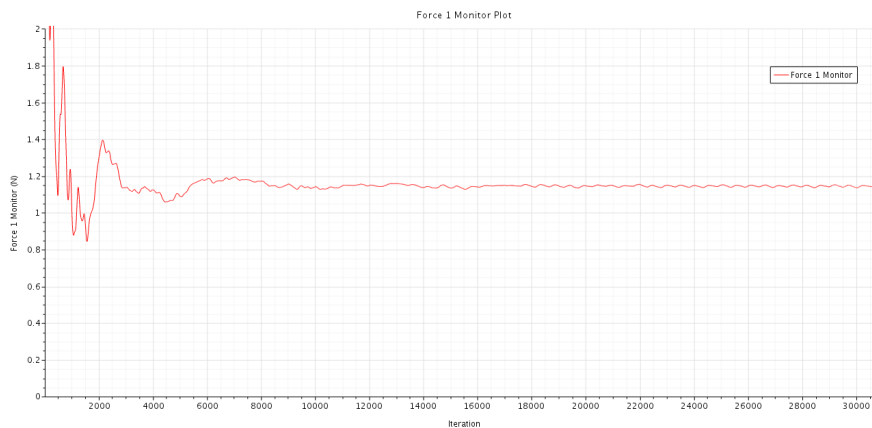


Figure 6.59: Force Monitor Plot of Version B at 0.001 bar

The simulation was manually terminated at a time step of 31000. The result was still oscillating with an amplitude of  $\pm 0.025$  newton. However, this small oscillation can be neglected. The result has converged.

#### 6.4.4 Influence of System Pressure on the total Drag Coefficient $C_{tot}$ for Version B

In the following plot, the influence of system pressure to the total drag coefficient  $C_{tot}$  is shown for the final Version B.

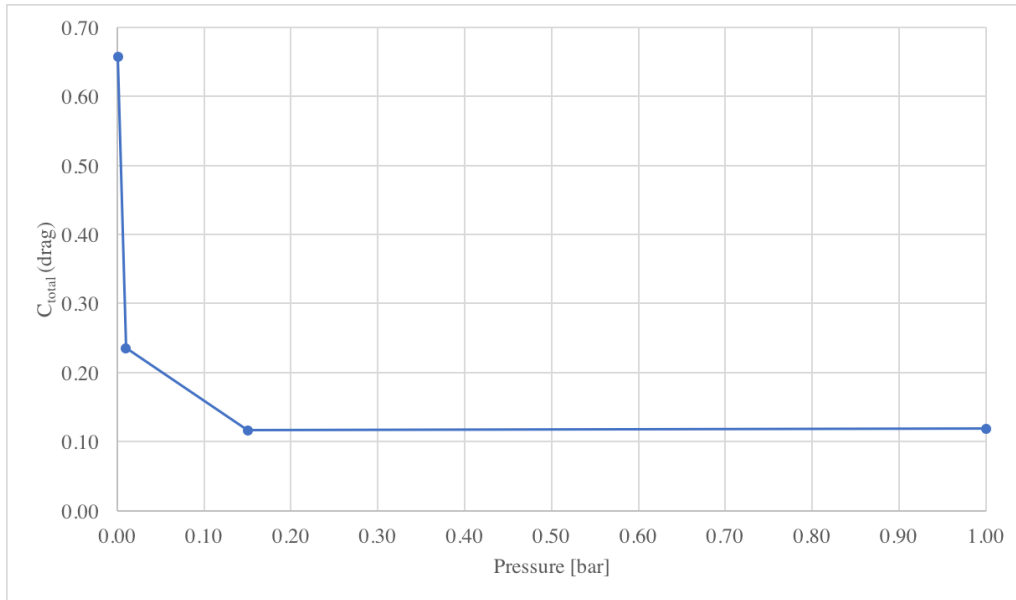


Figure 6.60: Influence of System Pressure on the total Drag Coefficient  $C_{tot}$  for final Version

The graph illustrates that  $C_{tot}$  for the drag force is constant above a pressure of 0.15 bar. However, at a pressure range between 1 millibar and 0.15 bar there is a sharp increase. Therefore, simulations in low-pressure environments are necessary as the occurring values cannot be predicted.

# 7. Conclusions

## 7.1 Conclusions

The goal of this Bachelor Thesis was (i) to develop a CFD simulation system for Hyperloop pods coupled with 3D CAD systems, and (ii) to design a pod shape with low drag force. This design-by-simulation system has been created and used to analyze and improve the Hyperloop pod's geometry for the 2019 pod of ETHZ's Hyperloop team Swissloop. The shape could significantly be improved and the drag force was reduced by 19 percent compared to the initial design. This Hyperloop pod geometry is manufactured and competes in the Hyperloop Pod Competition 2019 held by SpaceX in Los Angeles.

Further, it was outlined and explained, what meshing technique was used and which reference values, boundary conditions and physics conditions were set.

After the CFD environment has been set up, different pod versions were simulated and analyzed. Before every new simulation, the results were analyzed and with the method of a screening optimization, the shape was improved and adjusted manually until the best aerodynamic shape was found.

In the end, two shell versions were compared with each other and it was outlined which forces act on the pod surface. The version with the best performance, the final version, was simulated for conditions with different system pressure to investigate its behaviour in different pressure environments.

## 7.2 Outlook

As a next step in the development it is suggested to validate the results obtained by Computational Fluid Dynamics. By simulating the pod in a wind tunnel, the forces can be measured and compared to the numerically calculated forces. This procedure is used in motor sports and is very conclusive.

In addition, it is necessary to do on-track tests which assure the environment with low pressure. It is very likely that Hyperloop test infrastructures are going to be built in the next years where such tests can be executed.



# A. Pod Competition Rules

On the following pages an extract of the 2019 SpaceX Hyperloop Pod Competition Rules and Requirements can be found.



## 5 POD REQUIREMENTS

### *General Pod Requirements*

The Pod requirements for the competition are intentionally broad in order to encourage diversity of design.

1. Mass: Less than 3,300 lbm (1,500 kg).
2. Dimensions: Pods shall fit within the cross-section provided in this document. Pod minimum length is 5 feet. Pod maximum length is 24 feet.
3. Service Propulsion System: The Pod shall be moveable at low speeds when not in operation, which may be accomplished by physically pushing it (wheels), physically lifting it (even with a dolly), or remotely controlling it.
4. Propulsion System: All Pods must be self-propelled.

### *Pod Transport and Lifting Requirements*

1. Each Pod needs a method to move around either on a cart or on its own wheels, by hand push with 2-4 persons.
2. Each Pod needs to be able to be lifted from above using a standard warehouse forklift with a 5,000 lbm capacity. SpaceX will provide a forklift swivel hook adaptor, but teams must provide all lifting equipment needed below the hook of the forklift adaptors such as spreader bars, shackles and straps.
3. All straps, chains, shackles or slings must have at least a safety factor of 2 and show the rating on them.
4. If the student team has designed a lifting fixture, it must be designed to at least a safety factor of 2 and be proof tested to 1.5 times the maximum expected load prior to arrival at SpaceX.
5. If you believe your Pod cannot meet the above requirements, special approval will need to be given by a Volunteer Adviser.
6. If the Pod is hand-lifted, the maximum allowable weight per person shall be limited to 50lbs. In addition, clearly marked lifting points for each person are required.
7. If more than 6 people are required to lift your Pod, special approval will need to be given by a Volunteer Adviser.
8. Time limits at testing facilities:
  - a. 10 minutes to prepare for lift by forklift once Pod is by the Staging Area
  - b. 10 minutes to mate to the track once on the Staging Area
  - c. 10 minutes to prepare for launch once Pod is mated



## 10 HYPERLOOP TEST TRACK OVERVIEW

The test track will be a steel tube, fitted with an aluminum subtrack and rail mounted to a concrete fill bed. At the tube's egress door, there is a "foam pit" to help mitigate the {hopefully non-occurring} case of a Pod braking system failure. The tube sections will rest on concrete cradles, reinforced with steel and fitted with PTFE slip bearings.

The parameters of the Hyperloop test track are:

- Material: ASTM A1018 Grade 36
- Outer diameter: 72.0 inches
- Inner diameter: 70.6 inches
- Wall thickness: 0.70 inches
- Length: 4150 feet (1.25 km)
- Radius of curvature: Greater than 15 miles (24 km) at all points
- Instantaneous bends: Less than 0.16° in pitch and 0.07° in yaw
- Subtrack material: Aluminum 6101-T61
- Subtrack roughness: 125 RMS with potential for occasional surface scratches up to 0.008"
- Subtrack thickness: 0.5 inches
- Concrete height: 10.4 inches
- Rail material: Aluminum 6061-T6
- Internal pressure: 0.125 – 14.7 PSI (see note at end of section)

All critical dimensions and tolerances are outlined on the drawing in Figure 5. Please note that the latest drawing revision will always supersede the following reference notes:

- The flatness profile per unit square is 0.04". This means that local undulations of the plate as installed will be 0.04" or less over a 15" x 15" square.
- The maximum variation of the top plane of the track relative to the theoretical center point of the tube is +/-0.4". Important to note is that this variation does not mean you could have an abrupt step, as the maximum slope of the track in the longitudinal direction is limited to 0.04" per foot.
- Maximum slope of the track in the lateral direction is covered by the parallelism callout and will be 0.06" per subtrack plate.
- See drawing for smoothness values for pipe section joint and helical pipe weld.
- SpaceX will potentially coat the aluminum in order to increase its smoothness.
- SpaceX is working on optimizing the overall plate lengths and installation gaps. The current baseline is a gap pitch of every 12.5 feet with a maximum gap size of 0.1" to 0.125". We will strive to reduce the gap size to 0.05" for the first several hundred feet of the track. Gaps may or may not be filled with a non-conductive flexible filler. Maximum steps in height between plates on the track will be limited to 0.04" or less.



The test track is designed to be flexible and to allow competitors to implement, at a minimum, the following three types of levitation/suspension:

1. **Wheels:** The concrete flat section along the outside allow for a good wheel surface and aluminum rail(s) allow for horizontally oriented wheels, as implemented on certain roller coasters.
2. **Air Bearings:** The aluminum plate allows for a much smoother and flatter surface than the steel tube itself. The rail(s) can be used for lateral control, either through side-mounted bearings or wheels.
3. **Magnetic levitation:** Several forms of magnetic levitation require a conductive non-magnetic surface (e.g. copper or aluminum). The subtrack allows for magnetic levitation and the rail(s) allow for lateral control.

#### *Notes on Tube Pressure and Temperature*

Per parameters above, the internal pressure of the tube shall be between 0.125 – 14.7 psi. In order to support various types of propulsion systems, compressors (if applicable), and outer mold lines, the Pod team may select the tube's operating pressure from within that range (pending SpaceX approval).

The test track will not include a thermal control system, so tube temperatures will vary based on the time of day and weather. Teams request their specific operating pressure in the tube, but should be aware that at lower pressures, cooling by convection will become very inefficient. Designs without careful consideration or mitigation of thermal hotspots may not be able to survive the vacuum pump down time. The pump down period to reach the minimum pressure rating of 0.125 psi will likely be 25-35 minutes. The repressurization period will likely be 15-20 minutes.

#### *Staging Area (Loading) and Exit Area (Unloading)*

The Staging Area (see pictures below and on next page) is a platform exterior to the tube that is approximately level with the concrete inside the tube. The deck material is wood. On top of the deck are aluminum plates and rail that mimic the interior subtrack. Pods can be placed on the loading deck using a forklift provided by SpaceX. To load Pods, there are two options:

- Pods can be placed, from above, directly onto the Staging Area rail
- A 20 feet section of the Staging Area rail can be removed for Pods to be placed directly on the wooden deck or on the aluminum side plates. The Pod can then be rolled into the Hyperloop, approaching the Hyperloop rail from behind.

The egress area is similar but does not have a rail installed. There will be an additional forklift available for unload at the egress area. Pods will be transported from the egress area on a flatbed truck.

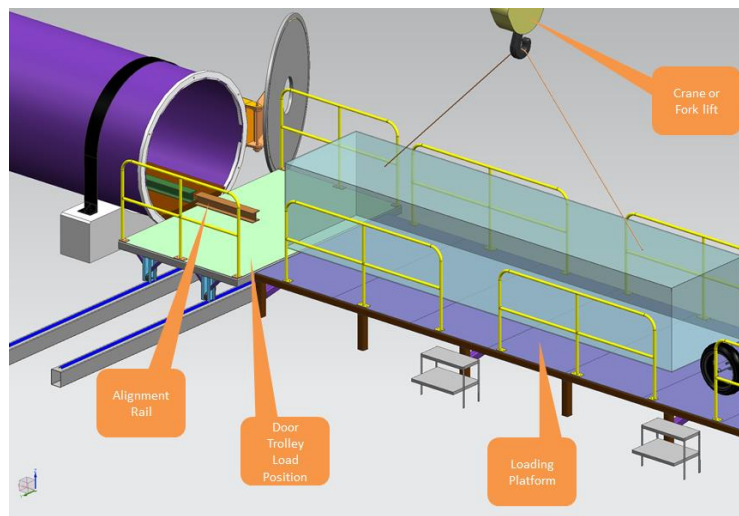


Figure 3 – Staging Area (for Pod loading)

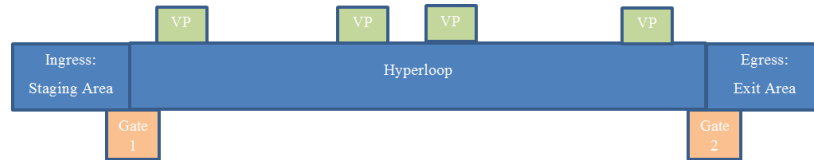


Figure 4 – Functional Diagram of the Hyperloop Test Track (VP refers to Vacuum Pumps)

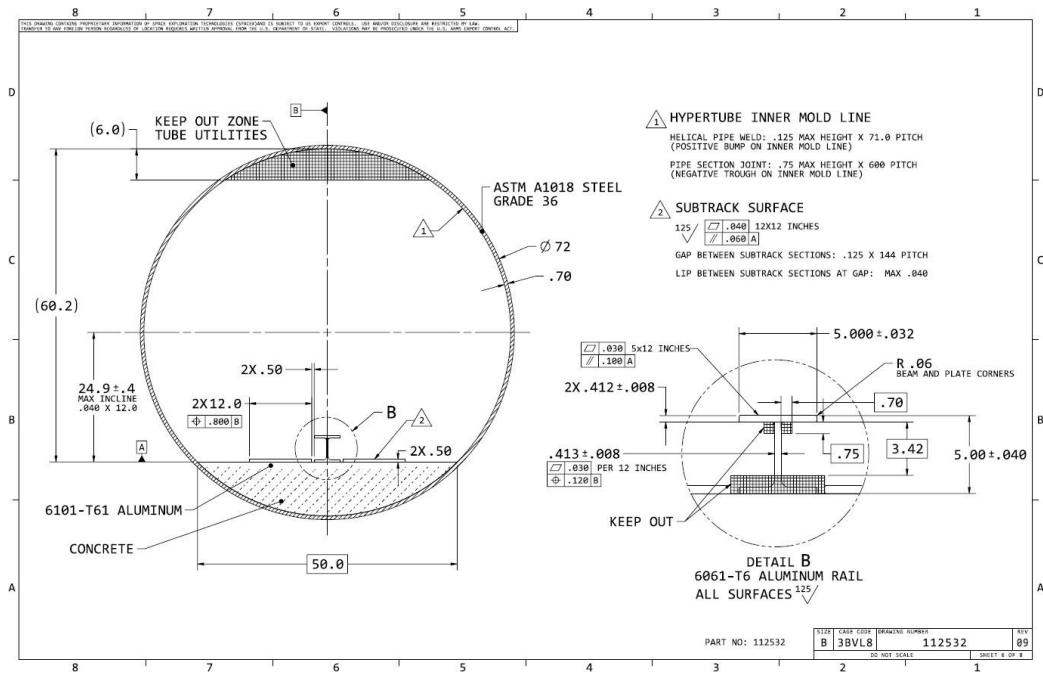


Figure 5— Dimensioned drawings of Hyperloop Test Track (including aluminum central rail (all dimensions in inches)

## 12 OTHER TESTING FACILITIES

### *Pod Vacuum Chamber*

Before being placed in the Hyperloop, Pods will have to demonstrate vacuum compatibility. To do so, SpaceX will provide a full-scale vacuum chamber. The chamber is the same diameter as the Hyperloop and has a length of 25 feet. The chamber has the same subtrack as the Hyperloop with the exception that the I-beam rail is only 12.5 feet long and does not span the entire length of the chamber. A wooden loading platform will be available to use for Pod ingress and egress into the chamber. The vacuum chamber will have a subset of the optical markings described in Section 6 for sensor tests, which will include reflectors.



*Figure 7—Vacuum Chamber used for testing*

### *Pod External Subtrack*

Before being placed in the Hyperloop, Pods will have to demonstrate basic low-speed motion, including braking and potentially levitating. To do so, SpaceX shall provide an external 150-foot long full-scale aluminum subtrack (the aluminum plate and rail).



## 18 POD TESTING

*Below is a list of tests and inspections that must be completed onsite at SpaceX during Competition Week by teams selected to compete. Any testing that requires a SpaceX Facility (Vacuum Chamber, External Subtrack, and Hyperloop Test Track) must be scheduled with the SpaceX Master Scheduler while onsite. All other tests can be scheduled directly with Volunteer Advisers.*

### 1. Pressure Systems Inspection

- a. Entry Criteria
  - i. Approval from Volunteer Advisers of all items provided in the safety briefing.
- b. What will be inspected?
  - i. Schematic printout for each pressure system
  - ii. Printout of the parts list for each pressure system
  - iii. Evidence that each pressure system has been proof-tested – this could be a video or photos to show the test and pressure gauges
  - iv. Evidence that all components have been torqued to the appropriate value and are marked with torque stripes to show any evidence of loose fittings
  - v. Full procedures for the following:
    - a. Filling/pressurizing
    - b. Venting under nominal conditions
    - c. Venting if there is loss of power
    - d. Venting if there is loss of communication
  - e. For Pods that use air pressure for levitation: If power is lost, what state does the levitation system enter? (Example response: "Air supply is isolated, and the Pod descends.")
- c. Exit criteria: Approval by Volunteer Advisers

### 2. Mechanical Fit Check

- a. This can be done either:
  - i. Coarsely in Team Headquarters with SpaceX-provided pieces of aluminum rail and plate (does not have to be scheduled).
  - ii. More accurately on the External Subtrack (must be scheduled)
- b. Entry Criteria
  - i. Approval from Volunteer Advisers.
  - ii. *If the External Subtrack is used:* Approval by Volunteer Advisers of Pod Transport Procedure
  - iii. Vehicle has all structural and mechanical systems fully assembled as it would run on track.
  - iv. *If Pod is in any state beyond inert (i.e. powered or pressurized):* Successfully passing Functional Test
  - v. *For Pods who wish to levitate in place:* Successfully passing Functional Test
- c. What is tested?
  - i. The operation of loading Pod onto the plate and rail
  - ii. Proper fit of everything that comes in contact with or in near contact of the track, rail, or tube. (This includes but is not limited to: vertical support wheels, levitation components, alignment wheels/magnets, underslung wheels if applicable, brakes, traction systems, etc.)

1. Proper fit will be interpreted as having acceptable clearances with an understanding of expected motions of the chassis during the run. This includes the pod response to rail imperfections considering pod vertical, lateral, yaw, pitch, and roll motions
2. The first point of contact with the rail or track in foreseeable motion must be a component that is designed for that contact and will withstand the contact while not damaging the track or rail
- iii. Proper fit when all brakes are disengaged and engaged
- iv. The operation of unloading the Pod onto the aluminum plate and rail
- d. Exit criteria: The six criteria above all test nominally, as agreed to by the Team and by the Volunteer Advisers

### 3. Structural Inspection

- a. Entry criteria
  - i. Approval from Volunteer Advisers to unpack and assemble Pod
  - ii. Approval from Volunteer Advisers to integrate magnets and batteries (if applicable)
  - iii. Vehicle power is off (i.e. battery is offline)
  - iv. Vehicle has all structural and mechanical systems fully assembled as it would run on track.
- b. What will be inspected?
  - i. Basic visual inspection of Pod
  - ii. Primary structural components
    1. Fasteners are torqued to appropriate values
    2. Critical fasteners have positive retention to prevent their unintended loosening
      - a. Critical fasteners are all fasteners associated with the chassis structure, suspension, alignment, brakes, wheels, motors, magnets, etc.
      - b. Acceptable methods for positive retention include: safety wire, cotter pins, nylon (up to 80C) or distorted thread nuts, prevailing torque nuts, and patch bolts (in blind holes)
      - c. Lock washers, and thread locking compound (Loctite®, etc.), are not considered acceptable methods of positive retention
  - iii. Pressurized systems
    1. Fittings are torqued to appropriate values
    2. No damage to critical components during transport
  - iv. All connectors and harnesses are properly secured
  - v. Rotating Components
    1. All rotating components (wheels, shafts, bearings, etc.) used for support, alignment, propulsion etc. will need to be demonstrated (by specification or proof testing) as being structurally suitable for their expected speeds and loads
    2. Any rotating components that will need to be run at any time outside of the vacuum chamber or the Hyperloop Test Track (e.g. in the team tent or on the external subtrack) must have been previously proof tested at a minimum of 1.22 times the speed to be run. Volunteer Advisers shall be present for any running, E-stop shall be present and accessible, and



speed shall be monitored during running. Non-critical personnel shall be outside the clear zone for the expected speed.

*Note:* Structural calculations will be required for one or several systems on the Pod at the choosing of the inspector, based on the visual inspection. Teams should be prepared to discuss the structural worthiness (static and dynamic loads, safety factor and margin) of any and all parts/systems of the vehicle.

- c. Exit criteria: Approval by Volunteer Advisers

#### 4. Battery Inspection

- a. Entry Criteria:
  - i. Approval from Volunteer Advisers to unpack and assemble Pod
- b. What will be inspected?
  - i. Battery Procedures
  - ii. Low Voltage Systems Power On
    - 1. Team is able to identify nominal and maximum values for current draw
  - iii. Mechanical Reliability
    - 1. Build quality is acceptable
    - 2. Enclosure layout is acceptable and feedthroughs/connectors are properly placed
    - 3. Critical arcing clearances have been achieved
    - 4. Proper cooling has been implemented
    - 5. No loose cables or parts are present
  - iv. High Voltage Pack Install and Power On
    - 1. Assembly Procedure is safe and comprehensive
    - 2. No high voltage conductors are exposed, and all parts are properly secured
    - 3. Manual Service Disconnect is accessible and is properly placed in the circuit
  - v. BMS Functionality
    - 1. Pod is telemetering the following values:
      - a. State of Charge
      - b. Pack Voltage
      - c. Pack Current
      - d. Minimum cell voltage (measured value, not calculated)
      - e. Maximum cell voltage (measured value, not calculated)
      - f. Temperature on at least 25% of cells in the pack
    - 2. Verify contactor and pre-charge circuit
    - 3. Verify Emergency Stop
    - 4. Team demonstrates an understanding of how the BMS responds to over-charging and overcurrent scenarios
  - vi. Charging Procedures



1. Team demonstrates an understanding of the assembly and disassembly process
  2. Team is able to identify maximum voltage and SOC during charging
  3. Overcharge protection is present and sufficient
- c. Exit Criteria
- i. All systems described above are safe and nominal
  - ii. Approval by Volunteer Advisers

## 5. Functional Test

- a. Entry criteria
- i. Approval from Volunteer Advisers of Pod Health Check List
  - ii. Successfully passing Structural Inspection
  - iii. Approval from Volunteer Advisers to power on Pod
  - iv. Approval from Volunteer Advisers to install high voltage batteries and power on high voltage systems
  - v. Approval from Volunteer Advisers of pressurized systems (proof testing and leak checking complete)
- b. What will be inspected?
- i. Pod is powered on and nominal current draw is observed
  - ii. Proper flight computer state is achieved
  - iii. Sensors are properly telemetering data, including but not limited to:
    1. Battery temperature sensors
    2. Battery state of charge
    3. Battery voltage
    4. Navigation sensors
  - iv. Any actuations that are safe to test on the bench:
    1. Actuations of primary and secondary brakes
    2. Valve state changes
    3. Relay state changes
    4. Rotation of magnetic arrays, if applicable
  - v. Pod Health Check, where Volunteer Advisers can see that all variables on the Pod Health Check list are updating and within range.
  - vi. If possible, battery discharge at maximum load
  - vii. Relevant pressurization and pressure relief testing, as determined by the Volunteer Advisers
  - viii. If NAP is not available, verification of manual commanding through Wi-Fi or Ethernet, including safety-critical commands such as "Emergency Stop" or "Battery off Bus"
  - ix. NAP Network Testing (can be done at a separate time if NAP is not available)
    1. Confirm that all IP addresses are within the specified range of 192.168.0.5-254.
    2. Disable all network interfaces on the laptop which will not be used for communicating with the Hyperloop Network.
    3. Confirm that the power interface to the NAP provides 9-36VDC and is able to source 20W. Confirm the polarity of the power interface matches the NAP specification.
    4. Confirm that the team's laptop can communicate over the specified IP address region to the Pod.



5. Verify remote commanding through NAP, including safety-critical commands such as “Emergency Stop” or “Battery Off Bus”
  6. Verify Pod telemetry is being received, including the SpaceX-required Pod Monitoring Telemetry. **Note that the Pod Monitoring Telemetry, plus the additional telemetry required in the Entry Criteria, must be functional in order to proceed with a powered-on Vacuum Test.**
- c. Exit criteria:
- i. All systems described above are safe and nominal
  - ii. Approval by Volunteer Advisers

#### 6. Vacuum Test

- a. This refers to the full Vacuum Test, where the Pod is fully functional in the Vacuum Chamber (as opposed to a sub-scale test, such as a battery-only test)
- b. Entry criteria
  - i. Approval by Volunteer Advisers of Pod Transport Procedure
  - ii. Approval by Volunteer Advisers of Pod Unloading Plan
  - iii. Approval by Volunteer Advisers of NAP fit and polarity
  - iv. Approval by Volunteer Advisers of Pod Health Check List
  - v. Successfully passing Structural Inspection
  - vi. Successfully passing Functional Test
    1. If portions of the Functional Test are passed, a limited Vacuum Test may be performed. Examples:
      - a. If a team passes all but the Power section, a power-off Vacuum Test could be performed.
      - b. If a team does not pass the Pressurized Systems portion, a power-on Vacuum Test can be performed
      - c. Pod Health Check list and Pod Monitoring Telemetry must be functional for all powered-on Vacuum Tests
- c. Test Logistics
  - i. When a team is called into Vacuum Test, Pod must be ready for transport
  - ii. Pod will be transported to Vacuum Chamber using Pod Transport Procedure
  - iii. NAP will be given to Pod either before transport or at Vacuum Chamber
  - iv. Pod will be placed into Vacuum Chamber and door will be closed
  - v. Vehicle telemetry connectivity will be checked before pump-down begins
  - vi. Pod Health Check will be performed before pump-down begins
  - vii. Vacuum Chamber will be depressurized to 10 torr in approximately 7 minutes, held for approximately 20 minutes, and then re-pressurized in approximately 5 minutes
  - viii. Pod Health Check will be performed before door is opened
  - ix. If the Pod is deemed safe, door is opened, and Pod is removed from Vacuum Chamber using its Pod Unloading procedures
- d. What will be tested?
  - i. Pod systems shall all be monitored and checked while at vacuum:
    1. This includes all moving parts: brake systems, linear actuators, and, if applicable, the levitation system.
  - ii. If possible, battery shall be discharged at maximum load
  - iii. Pod shall enter its software state diagram (even if it stays in the “Idle” mode for 20 minutes, this is a useful demonstration)
- e. Exit Criteria:

- i. Pod systems all function nominally, temperature changes are all within an expected range, Pod telemetry is consistent, and actuations are nominal.
- ii. Visual inspection of Pod reveals no damage, including electronics damage (e.g. bulging of pouch cells, exploded capacitors, etc.)

#### 7. Navigation Test

- a. This test can be combined with the External Subtrack Test or Open-Air Hyperloop Test. However, since those tests need to be scheduled and time will be limited, it is likely more efficient to perform the Navigation Test in the Competition Testing Lot, where it can be performed at any time.
- b. Entry criteria
  - i. Approval by Volunteer Advisers of Pod Transport Procedure
  - ii. Approval of Volunteer Advisers of all Navigation Tests to be run
  - iii. Successfully passing {relevant portions} of the Functional Test
- c. What will be tested?
  - i. Pod is placed in a safe and mobile state (i.e. on its own wheels or a supporting platform with wheels) and initiated to the same Software State as in an actual run.
  - ii. Team shows telemetry values of position and velocity via its GUI
  - iii. Pod is left stationary for five minutes, and the navigation drift, if any, is observed
  - iv. Team shows resultant telemetry values of position and velocity via its GUI
  - v. Test variations can be repeated as necessary, including:
    - 1. Repeating the test with a failed (e.g. unplugged) navigation sensor and ensuring the fault detection software works properly
    - 2. Using the optical tape fixture to see sensitivity of Pod's sensor
  - vi. Exit Criteria
    - 1. Approval from Volunteer Advisers

#### 8. State Diagram Transition Test

- a. This test examines all software state transitions, including verification that the software will not initiate braking while accelerating and that the software will initiate braking before the Pod reaches the end of the tube. In most cases, this comes down to verifying two critical items:
  - i. The clock cannot start running before acceleration has been initiated
  - ii. Minimum and maximum time thresholds are properly implemented that cannot be over-ridden by navigation sensors
- b. Entry criteria
  - i. Approval by Volunteer Advisers of Pod Transport Procedure
  - ii. Approval of Volunteer Advisers of all State Diagram Transition Tests to be run
  - iii. Successfully passing relevant portions (as determined by Volunteer Advisers) of the Functional Test
- c. Test Logistics
  - i. Test takes place in open space in Competition Week Lot
  - ii. Test will likely be repeated several times due to the multiple mode transitions; thus, it is wise for each team to be able to efficiently reset its State Diagrams
  - iii. Team provides list of Software State tests that was approved in the Safety Briefing. This list will again be evaluated before testing begins.
  - iv. Pod is placed in a safe and mobile state (i.e. on its own wheels or a supporting platform with wheels) and initiated to the same Software State as in an actual run.



- v. Team shows telemetry values of time and Software State via its GUI
- vi. Pod is manually moved in order to trigger the proper state transitions.
- vii. Example Test 1 (“Don’t Brake While Accelerating”)
  1. Accelerate Pod
  2. Stop Pod and then immediately move Pod in a way that would trigger braking
  3. Verify braking does not occur until acceleration mechanism has shut down
- viii. Example Test 2 (“Brake If Navigation System Has Failed”)
  1. Accelerate Pod
  2. Stop Pod
  3. Hold Pod still and verify that brakes eventually actuate
- ix. Example Test 3 (“Don’t Start Clock Too Early”)
  1. Place Pod in Pre-flight Mode
  2. Mildly shake the Pod
  3. Verify the clock does not start ticking
- d. Exit Criteria
  - i. Software behavior matches pre-approved State Diagrams in all cases
  - ii. Volunteer Advisers and Team all agree that premature braking (during acceleration) is non-credible

#### 9. External Subtrack Test

- a. This test takes place on the 150-foot External Subtrack in the Competition Week Lot
- b. Entry Criteria
  - i. Approval by Volunteer Advisers of Pod Transport Procedure
  - ii. Successfully passing {relevant portions} of the Functional Test
  - iii. Successful completion of State Diagram Transition Test
  - iv. For teams who plan on stationary levitation:
    1. Previous demonstration of stationary levitation (either in Vacuum Test or during Mechanical Fit Check)
    2. Verified duration of levitation which would result in aluminum plate damage
  - v. Approval of Pod Health Check list (a custom sub-set can be approved for this test if needed; the full list must be operational for future Hyperloop tests)
- c. Pre-Test Discussions
  - i. Communication of pre-approved Safe Distances and Clear Zones
  - ii. Communication on whether Pod will be levitating for this test, when levitation will begin (e.g. before acceleration begins), and at what speed levitation will occur
- d. Test Logistics
  - i. Implementation of Clear Zone
  - ii. Verification that Overrun Attenuator is in place
  - iii. NAP will be given to Pod either before transport or at External Subtrack
  - iv. Using Pod Transport Procedure, Pod shall be transported onto the External Subtrack
  - v. Customized speed profile will be reviewed:
    1. Initial profiles will be slow and short (e.g. 3 miles per hour for 3 seconds)
    2. Speeds/times will be ramped up accordingly
    3. Maximum speed is 25 miles per hour
  - vi. Team shall initialize its Pod into the pre-tested Pre-launch State
  - vii. Once both SpaceX and Team have verbally said “Go,” Team will launch the Pod

- viii. Once the run is over, Pod enters or is placed into a pre-approved safe state and performs the Pod Health Check
- ix. Following the test, both SpaceX and Team will review data, and then re-initialize the test and repeat
- e. Exit Criteria
  - i. Pod properly transitions through its state diagram
  - ii. Pod translates smoothly down subtrack
    - 1. Team shall review attitude data to look for biases and oscillations
    - 2. SpaceX shall examine subtrack rail to look for damage
  - iii. Pod Monitoring Telemetry is steady and accurate
  - iv. Pod properly brakes based on pre-programmed software condition
  - v. If applicable, Pod levitation system functions properly
  - vi. Test can be efficiently re-initialized and repeated

#### 10. Open-Air Hyperloop Test

- a. This is a test in the Hyperloop, except with the doors open and thus at atmospheric pressure. This test is similar to the External Subtrack Test, except it can support higher speeds, longer distances, and navigation with the optical tape.
- b. In this test, the Pod will likely come to a stop in the middle of the Hyperloop. Thus, this test can only be run with Pods that have efficient Service Propulsion Systems.
- c. Entry Criteria
  - i. Approval by Volunteer Advisers of Pod Transport Procedure
  - ii. Approval by Volunteer Advisers of Pod Unloading Plan
  - iii. Successful completion of full Functional Test
  - iv. Successful completion of Mechanical Fit Check
  - v. Successful completion of State Diagram Tests
  - vi. Approval of Pod Health Check list
  - vii. Approval to proceed from SpaceX Organizers
- d. Pre-Test Discussions
  - i. Agreement of Volunteer Advisers and Team on speed profile (capped at 50 mph).
  - ii. Agreement on whether Pod will be levitating for this test
  - iii. For teams with stationary levitation systems:
    - 1. Verification of maximum hovering duration
    - 2. Explanation of when levitation begins (e.g. before or after acceleration begins)
    - 3. Verified duration of levitation which would result in aluminum plate damage
- e. Test Logistics
  - i. NAP will be pre-installed on the Pod.
  - ii. Pod will be transported via road to the Hyperloop Staging Area.
  - iii. Pod will be lifted, via a SpaceX-provided forklift if necessary, onto the Staging Area (which is an open-air flat surface, 20 feet in length)
  - iv. Pod will be moved into the Hyperloop using the Pod's Service Propulsion System.
  - v. Pod will perform the pre-approved Pod Health Check in order to verify connectivity and Pod health. This must include the Pod Monitoring Telemetry
  - vi. Team shall initialize Pod into the pre-tested Pre-launch State
  - vii. Once both SpaceX and Team have verbally said "Go," Team will launch the Pod



- viii. Once the run is complete, Pod enters or is placed into a pre-approved safe state and performs the Pod Health Check
- ix. If the Pod is deemed safe, Pod is removed from Hyperloop using its Pod Unloading procedures
- f. Exit Criteria
  - i. Pod properly transitions through its state diagram
  - ii. Pod translates smoothly down subtrack
    - 1. Team shall review attitude data to look for biases and oscillations
    - 2. SpaceX shall examine subtrack rail to look for damage
  - iii. Pod Monitoring Telemetry is steady and accurate
  - iv. Pod properly brakes based on pre-programmed software condition
  - v. If applicable, Pod levitation system functions properly
  - vi. If applicable, Pod detected the optical tape

#### 11. Hyperloop Run

- a. This is the real deal!
- b. Entry Criteria
  - i. Successful completion of full Functional Test
  - ii. Successful completion of Vacuum Test (powered on and under load)
  - iii. Successful completion of Mechanical Fit Check
  - iv. Successful completion of Navigation Test
  - v. Successful completion of State Diagram Tests
  - vi. Successful Completion of External Subtrack Test and/or Open-Air Hyperloop Test
  - vii. Successful demonstration of levitation, whether in the Vacuum Chamber, the External Subtrack, or Open-Air Hyperloop
  - viii. Approval of Pod Health Check list
  - ix. Approval by Volunteer Advisers of Pod Unloading Plan
  - x. Approval to proceed from SpaceX Organizers
- c. Pre-Test Discussions
  - i. Agreement of Volunteer Advisers and Team on speed profile
  - ii. Verification that battery capacity is sufficient for entire test (40 minutes)
  - iii. For teams with air-based levitation systems:
    - 1. Verification of maximum hovering duration
    - 2. Explanation of whether levitation begins before or after acceleration begins
- d. Test Logistics
  - i. NAP will be pre-installed on the Pod.
  - ii. Pod will be transported via road to the Hyperloop Staging Area.
  - iii. Pods will be lifted, via a SpaceX-provided forklift if necessary, onto the Staging Area (which is an open-air flat surface, 20 feet in length)
  - iv. Pod will be moved into the Hyperloop using the Pod's Service Propulsion System.
  - v. Pod will perform pre-approved Pod Health Check in order to verify connectivity and Pod health. This must include the Pod Monitoring Telemetry
  - vi. The Hyperloop Door ("Gate 1") will then be closed and the Pod Health Check will be repeated. This includes the demonstration of a continuous communications link.
  - vii. The Hyperloop will be depressurized to operating pressure.
  - viii. At operating pressure, the Pod Health Check will be repeated.



- ix. Pod team shall initialize their Pod into the pre-tested Pre-launch State
- x. Once both SpaceX and Team have verbally said "Go," Team will launch the Pod
- xi. Once the run is complete, Pod enters or is placed into a pre-approved safe state and performs the Pod Health Check.
- xii. If the Pod is deemed safe, the Hyperloop Exit Door (Gate 2) is opened
- xiii. Team runs Pod Unloading procedure to place Pod onto Exit Staging area and then off of the Hyperloop Test Track
- e. Exit Criteria
  - i. Pod did not damage Hyperloop and did not crash.
  - ii. Pod successfully stopped within 100 feet of the Hyperloop Exit Door (Gate 2). If so, congratulations!
  - iii. Three sources of Pod data are available to evaluate Pod's trajectory:
    - 1. The NAP's data recorder
    - 2. The team's Pod Monitoring Telemetry
    - 3. External sensors placed by SpaceX in the Hyperloop

# Bibliography

- [1] E. Truckenbrodt H. Schlichting. *Aerodynamik Des Flugzeugs*. Springer, 2001.
- [2] W. Malalasekera H. Versteeg. *An introduction to Computational Fluid Dynamics*. SAE International, 1995.
- [3] D. Anderson J. Tannehill and R. Pletcher. *Computational Fluid Dynamics and Heat Transfer*. Taylor Francis, 2012.
- [4] Prof. Dr. P. Jenny. Turbulent flows lecture notes. 2018.
- [5] J. Katz. *Race Car Aerodynamics: Designing for Speed*. Robert Bentley, 1995.
- [6] Prof. Dr. L. Kleiser. Berechnungsmethoden der energie- und verfahrenstechnik. 2019.
- [7] Michele Mossi. *Simulation of Benchmark and industrial unsteady compressible turbulent fluid flows*. EPFL, 1999.
- [8] Elon Musk. Hyperloop alpha. page 6, 2013.
- [9] Prof. Dr. T. Roesgen Prof. Dr. P. Jenny. Fluidodynamik i/ii skript zur vorlesung. 2018.
- [10] S. Stolz. Lecture notes on advanced cfd methods. 2009.







Eidgenössische Technische Hochschule Zürich  
Swiss Federal Institute of Technology Zurich

**Title of work:**

Aerodynamic Design of a Hyperloop Pod by Computational  
Fluid Dynamics Analysis

**Thesis type and date:**

Bachelor Thesis, May 2019

**Supervision:**

Prof. Dr. Horst-Michael Prasser, ETH Zurich  
Dr. Bojan Niceno, Paul Scherrer Institute (PSI)  
Dr. Yohei Sato, Paul Scherrer Institute (PSI)

**Student:**

Name: Nathalie Nick  
E-mail: nickn@student.ethz.ch  
Legi-Nr.: 14-929-145  
Semester: 6

**Statement regarding plagiarism:**

By signing this statement, I affirm that I have read and signed the Declaration of Originality, independently produced this paper, and adhered to the general practice of source citation in this subject-area.

Declaration of Originality:

[http://www.ethz.ch/faculty/exams/plagiarism/confirmation\\_en.pdf](http://www.ethz.ch/faculty/exams/plagiarism/confirmation_en.pdf)

Zurich, 31.05.2019: \_\_\_\_\_